POLITECNICO
MILANO 1863

SCUOLA DI INGEGNERIA INDUSTRIALE
E DELL'INFORMAZIONE

Multi-input Lateral Dynamics Control of an Electric Vehicle

Tesi di Laurea Magistrale in
Mechanical Engineering - Ingegneria Meccanica

Author: **Divy Dhingra**

Student ID: 925353
Advisor: Dr. Michele Vignati
Co-advisors: Ing. Michele Asperti, Prof. Edoardo Sabbioni
Academic Year: 2020-21

Abstract

This thesis focuses on lateral dynamics control of an electric vehicle with 4 in-wheel motors (IWMs). The controller uses rear steering and torque vectoring as the active systems to improve vehicle lateral dynamics. The aim of the controller is to improve the yaw rate while reducing the vehicle sideslip angle. The controller should be able to handle non-linearity while being stable and able to run in real-time. We implement a feedforward controller and an integral terminal sliding mode controller (ITSMC). The actuator inputs are first derived using the linearised single track model (LSTM) and then tested with the nonlinear 14DOF model using VI-CarRealTime (VI-CRT) software.

The reference values for the controller are calculated using a logistic function. The parameters for the logistic function are fitted to the yaw rate-steering wheel angle curve of the passive vehicle. The fitted parameters are then scaled to obtain the desired improvement in the reference values as compared to the passive vehicle. The ITSMC is able to track the reference yaw rate while improving the sideslip angle response of the active vehicle. The ITSMC relies on real time knowledge of sideslip angle which cannot be measured in the real vehicle. The sideslip angle is thus estimated by adding an extended Kalman filter (EKF) to the control loop. The controller performance with and without EKF is found to be similar for moderate and high lateral accelerations.

Keywords: Sliding Mode Control, Integral, Terminal, Lateral Dynamics Control, Multi-Input Control, Extended Kalman Filter

Sommario

Questa tesi si concentra sul controllo della dinamica laterale di un veicolo elettrico con 4 motori posizionati all'interno delle singole ruote (IWM). Il controllore utilizza lo sterzo posteriore ed il torque vectoring come sistemi attivi per migliorare la dinamica laterale del veicolo. Lo scopo del controllore è quello di migliorare la risposta della velocità di imbardata in combinazione con la riduzione dell'angolo di assetto. Il controllore dovrebbe essere in grado di gestire la non linearità rimanendo stabile e funzionando in real-time. Nella tesi sono implementati un controllore feedforward ed un controllore sliding mode integrale terminale (ITSMC). Gli ingressi degli attuatori sono prima ottenuti utilizzando il modello di veicolo monotraccia linearizzato (LSTM) e poi testati con il modello non lineare a 14 gradi di libertà utilizzando VI-CarRealTime (VI-CRT).

Le quantità di riferimento per il controllore sono definite tramite una funzione logistica. I parametri di questa funzione logistica sono tarati sulla curva che lega velocità di imbardata ed angolo di sterzo per il veicolo passivo. Successivamente questi parametri vengono scalati per ottenere il miglioramento desiderato delle quantità di riferimento rispetto a quelle assunte dal veicolo passivo. Il controllore ITSMC è in grado di seguire il riferimento della velocità di imbardata e contemporaneamente migliorare la risposta dell'angolo di assetto per il veicolo attivo. Il controllore ITSMC si affida alla conoscenza in tempo reale dell'angolo di assetto, che non può essere misurato in un veicolo di serie. L'angolo di assetto è quindi stimato tramite l'aggiunta al circuito di controllo di un filtro di Kalman esteso (EKF). Le prestazioni del controllore con l'aggiunta dell'EKF sono simili a quelle del controllore senza EKF per accelerazioni laterali moderate o elevate.

Parole chiave: Controllo sliding mode, Integrale, Terminale, Controllo della dinamica laterale, Controllo multi-ingresso, Filtro di Kalman esteso

Contents

1 | Introduction

The automotive industry has started shifting its focus towards commercial production of electric vehicles. From vehicle dynamics point of view, this is beneficial since electric motors are easier to control and faster to respond when compared to internal combustion engines (ICE). Moreover in recent times, electric actuators, computational power and sensors have become cheaper and more easily accessible. All these factors have opened a lot of possibilities for vehicle lateral dynamics control which may not be available $30-40$ years ago.

The availability of fast actuators, powerful on-board computer and cheap sensors has allowed the implementation of complex controllers which are highly effective in controlling vehicle dynamics. More emphasis is being put on control strategies which are able to adapt to changing environmental conditions or are robust to these changes. The availability of detailed vehicle models and simulation software has made it easier to simulate and analyse the performance of these controllers before implementing them on a real vehicle.

Vehicle lateral dynamics mainly focuses on the cornering performance of the vehicle. This is determined by vehicle yaw rate ($\dot{\psi}$) i.e. vehicle angular velocity about the vertical axis passing through its centre of gravity and vehicle sideslip angle (β) i.e. inverse tangent of the ratio between lateral (V_y) and longitudinal (V_x) velocity of the vehicle defined in the moving reference system aligned with the vehicle as shown in Figure 1.1.

$$\beta = \arctan\left(\frac{V_y}{V_x}\right) \tag{1.1}$$

1.1. Problem Statement

The aim of this thesis is to develop a lateral dynamics controller for the vehicle equipped with active rear steering (ARS) and 4 in-wheel motors which allow torque vectoring (TV). The aim of the controller is to improve the yaw rate response while minimizing vehicle sideslip angle as compared to the passive vehicle.

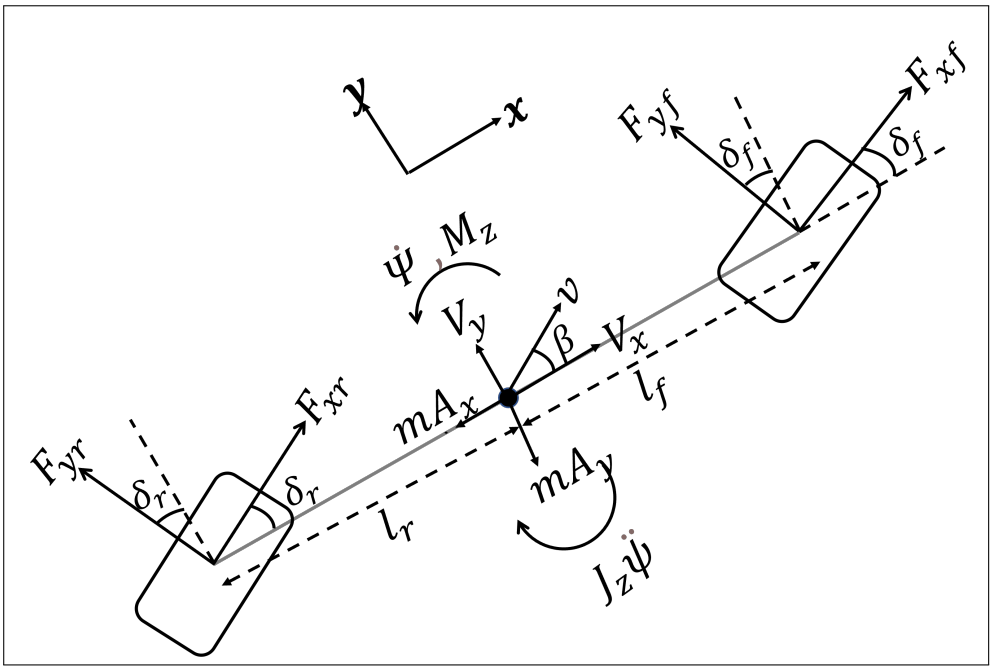

Figure 1.1: Single Track Model (STM) of a vehicle in curve with ARS and TV.

The lateral dynamics of a real vehicle is highly nonlinear. These nonlinearities arise mainly from nonlinear tyre forces, 3D effects like load transfer between left and right wheels during cornering and front and rear axles during acceleration or braking and due to suspension kinematics.

The control problem is further complicated by limited total force available at each wheel, difference in relaxation lengths for longitudinal and lateral forces, actuator dynamics, external disturbances, sensor noise, parameteric uncertainties and lack of sensors for measuring fundamental lateral dynamics quantities such as vehicle sideslip angle.

The controller should be fast, stable and be able to handle the nonlinear behaviour of the vehicle. It should be able to run in real time while relying only on easily available cost-effective sensors. The controller should also be robust in order to handle any external disturbances or change in environmental conditions such as tyre-road friction coefficient.

1.2. Thesis Outline and Structure

The thesis is structured into the following chapters:

- Chapter 2: The state of the art for the modelling and simulation of vehicle lateral dynamics, the controllers and vehicle state estimators is presented in this chapter.
- Chapter 3: The equations of motion for the linearised single track model (LSTM)

of a vehicle equipped with ARS and TV are derived in this chapter. The effect of each actuator on vehicle lateral dynamics is analysed by evaluating step response and frequency response of the transfer functions.

- Chapter 4: In this chapter two controllers: feedforward and integral terminal sliding mode controller are derived and tested using the LSTM. The chapter presents the method used for calculating reference yaw rate and sideslip angle. The chapter also presents the main highlights of extended Kalman filter (EKF) used to estimate the sideslip angle.
- Chapter 5: All the simulation results for steady state and transient maneuvers performed using the more realistic VI-CarRealTime model are presented in this chapter.
- Chapter 6: Concludes the thesis with an analysis of key results and comments on future work.

2 | State of the Art

In this chapter, the problem of vehicle lateral dynamics and control is presented in detail. The state of the art for modelling and simulation of vehicle lateral dynamics, controllers and observers for estimating unmeasurable physical quantities and parameters is presented and discussed.

2.1. Lateral Dynamics

The vehicle lateral dynamics focuses on the planar motion of a vehicle in a turn. The lateral dynamics involves the study of vehicle's response to steering inputs for different vehicle speeds and environmental conditions such as tyre-road friction coefficient and external disturbances. During a turn, the vehicle body experiences yaw rotation i.e. rotation about the vertical axis passing through its centre of gravity (CoG), roll rotation i.e. rotation about an axis passing through its CoG and aligned with the longitudinal direction of the vehicle, and longitudinal motion of the vehicle.

The vehicle CoG is located at a certain height above ground. This induces a load transfer proportional to lateral acceleration from inner to outer wheel while negotiating a turn. The roll motion of the vehicle also induces some steer of the wheels due to the presence of suspension. If the vehicle is accelerating or braking while turning, there will be load transfer between front and rear axle of the vehicle. These phenomena can affect the lateral force generated by the tyres.

The distribution of load transfers also depends on suspension characteristics of the vehicle. For example, a stiff anti-roll bar at the front axle will reduce body roll while decreasing the total lateral force generated at the front axle. Similarly, certain tuning of suspension parameters may produce more lateral forces while increasing body roll and sacrificing driver and passenger comfort. Thus, the lateral dynamics of the vehicle is indirectly affected by its vertical dynamics.

Vehicle lateral dynamics is also affected by its longitudinal dynamics. This is mainly due to the limited force that can be generated by each tyre. If the vehicle acceleration is high, the longitudinal forces at each tyre are also high. Since total force generated by each tyre

is limited by friction and vertical load, the available lateral force will reduce in comparison to a vehicle cruising at constant speed. This affects vehicle's response to steering inputs.

Tyres are the only contact point between the vehicle and the ground. The force generated by tyres is the only way a vehicle can move longitudinally or laterally. The force generated by tyre changes nonlinearly with tread temperature, tyre inner pressure, friction coefficient, frequency of excitation and many other factors. For most practical vehicle dynamics applications, only the relation between tyre deformation and developed force is important to understand lateral dynamics.

2.1.1. Lateral Dynamics Model

The lateral dynamics is quantified by yaw rate ($\dot{\psi}$) and sideslip angle (β) defined in the vehicle local reference system or lateral acceleration (a_Y) and yaw rate ($\dot{\psi}$) defined in the global reference system. The choice between the global or local reference system depends mainly on the type of maneuver that is being performed. For motion in curve, it is better to define the vehicle dynamics in local reference system using $\dot{\psi}$ and β as the state variables. This will be the reference system in the following chapters of this thesis.

There are several mathematical models available in literature for simulating the lateral dynamics of the passive vehicle. These models can then be modified to incorporate any active system present in the vehicle. Based on the number of degrees of freedom (DOF), there can be three levels of model available in literature:

1. Single Track Model (STM): 3DOF (v_x, $\dot{\psi}$ and β) [1]
2. Double Track Model: 14DOF i.e. 6DOF for chassis, vertical displacement and angular speed (2DOF) of each wheel [2]
3. Multibody Models: many degrees of freedom [3]

The models with a higher number of DOF are able to accurately predict the real vehicle's behaviour. This accuracy is achieved at the cost of modelling complexity and computational resources. Lateral dynamics controllers are required to be able to run in real time. Hence, relying on extremely complex models which require large computational resources may not be suitable for designing the controller. We choose to use the STM for calculating the actuator inputs as it will certainly allow real time running of the controller.

For any type of vehicle model, a model for tyre forces is required. The tyres generate lateral and longitudinal forces as a consequence of slip in the corresponding direction. The lateral slip is the angle between absolute and longitudinal velocity of the hub defined in the tyre local reference system. The lateral force generated at the axle depends nonlinearly on the

average lateral slip of the two tyres of the corresponding axle, as shown in Figure 2.1.

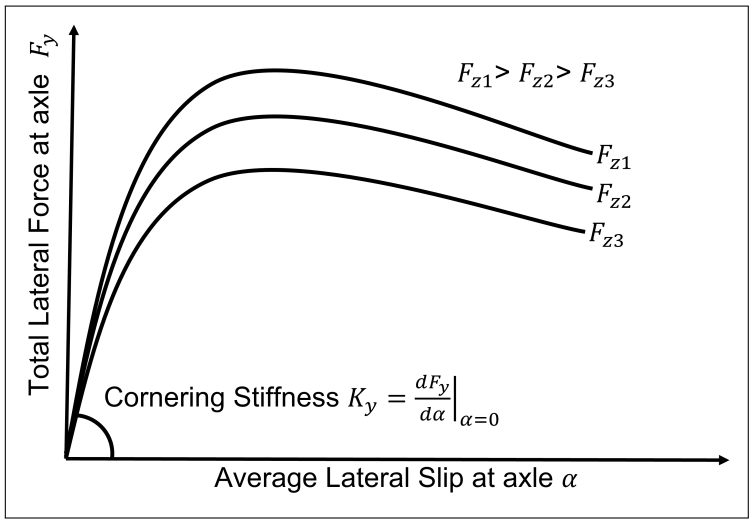

Figure 2.1: Lateral force vs slip curve for a generic tyre.

From Figure 2.1, we can see that for very small lateral slip angle (α), the lateral force increases linearly before reaching the peak value and then decreases. The slope of the force-slip curve at the origin is known as cornering stiffness (K_y). The correct estimation of the cornering stiffnesses allows us to develop a linearised model which is able to give good estimation of the real vehicle's lateral dynamics up to lateral acceleration of 4 m/s^2 [4].

An analytical approach incorporating all the dependencies of lateral force on various factors may be computationally expensive. Thus resulting in large simulation times. This problem is solved by using empirical formulas or models such as the those presented in [5] [6]. These detailed empirical formulas reliably reproduce steady state and transient tyre-force dynamics. The parameters for these formulae or models are fitted to experimental data by the tyre-maker and given to the car-maker for studying their effect on vehicle lateral dynamics.

2.1.2. Simulation

The components involved in vehicle dynamics such as suspension, engine/motor, brakes, driver models etc. can be modelled as initial value problems. The equations of motion for all these components are first or second order ordinary differential equations which can be solved in MATLAB© or Simulink© [2]. With the availability of reliable vehicle data, validated models can provide good qualitative and quantitative estimation of the real vehicle's lateral dynamics.

The model development and validation process can be a challenging task, especially when the number of DOFs is high. There are many commercial software which provide validated vehicle models which are defined in a high level of detail. These software packages are generally modular i.e. the model can be divided into independent sub-models such as steering system, powertrain, tyre characteristic curves, brakes and so on. The user can define each component by entering appropriate values in the pre-defined list of parameters.

In this thesis work, we use VI-CarRealTime [7] for simulating vehicle dynamics. VI-CarRealTime (VI-CRT) is essentially a 14DOF model which allows real time simulation of vehicle dynamics while incorporating detailed models of individual components such as suspensions, steering system, engine/motor, tyre models etc. VI-CarRealTime software allows easy communication with external models defined in Simulink by providing the vehicle model as "S-function" for "co-simulation".

The inputs and outputs of the "S-function" are selected by the user from the given list. The user is only required to connect the ports of the vehicle "S-function" with appropriate Simulink© blocks performing the necessary calculations. This avoids the need for writing complicated piece of code to pass the information between VI-CRT and Simulink models during the simulation. One such example of the co-simulation of VI-CRT model in Simulink is presented in Figure 2.2.

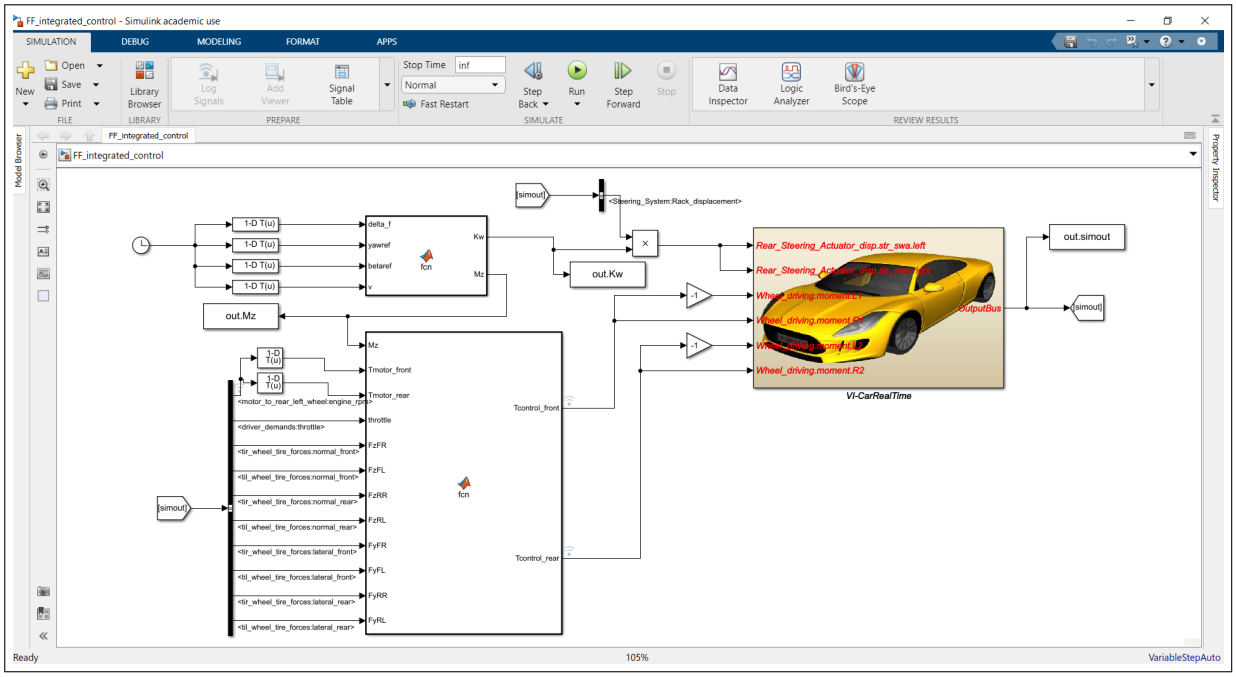

Figure 2.2: An example of VI-CRT co-simulation with Simulink.

2.2. Lateral Dynamics Controllers

There has been wide variety of algorithms/controllers available in the literature for controlling the vehicle lateral dynamics. These algorithms mostly rely on torque vectoring (TV), active rear steering (ARS) or both for controlling vehicle lateral dynamics. The controllers using TV as active system also require a lower level controller to convert the required yaw moment into driving or braking torque applied to the wheels while accounting for friction or actuator limits.

The effect of active rear steering system on lateral dynamics has been extensively studied in literature. In [8], the authors present two ARS system: steering wheel based and vehicle speed based system. In the past, due to lack of computational power and expensive electrical actuators and sensors, researchers used hydraulically actuated ARS using only steering wheel angle as input for the rear steering system. On one hand, this method is simple and easy to implement mechanically. On the other hand, a steering wheel based method is not flexible as the desired sideslip angle needs to be fixed *a priori*.

There are many mechanisms which can generate an additional yaw moment such as active differential, drive moments applied through In-Wheel Motors (IWMs) or braking one or more wheels. In this thesis work, we choose to work considering a vehicle equipped with 4 IWMs. Drive moments of equal magnitude and opposite sign are applied to left and right wheel of the same axle through IWMs to generate a yaw moment. This allows the opportunity to control vehicle lateral dynamics without drastically reducing vehicle speed during the maneuver. This layout performs well during both transient and steady state maneuvers [9].

In literature, a wide variety of controllers is available which control yaw rate, sideslip angle, both yaw rate and sidelsip angle or an index related to under/oversteering [10]. The most simple approach for lateral dynamics control is to design a Proportional Integral and Derivative (PID) controller. These controllers work well for the linear system or within the linear region (region near an equilibrium point) of a nonlinear system. Their performance is not predictable in the nonlinear region far away from the chosen equilibrium point. Thus limiting their applicability for nonlinear systems such as a vehicle.

Another type of controllers often shown in literature are Fuzzy Logic controllers. These controllers require a tricky tuning of controller parameters and a precise definition of the fuzzy logic. Thus tuning these controllers becomes a demanding task for the designer and needs a lot of experience and knowledge about the problem. Another possibility is to use Model Predictive Controllers (MPC). MPC optimises the sequence of inputs to minimize the predicted error for a finite time and then applies only the first input of the sequence.

The performance of these controllers is good as the input is continuously optimised to minimize the error. The major drawback of MPC is the high computational cost involved in the process.

There is also the possibility of implementing Model Matching Controller which relies on exact knowledge of the plant model. This again suffers from either high computational cost or inability to cope with system non-linearity. Thus, large computational cost, design complexity or inability to handle system non-linearity can be a major drawback for any controller. For commercial vehicles, a fast, simple and stable controller is desirable for running in real time during any maneuver.

2.2.1. Sliding Mode Controller

The Sliding Mode Controller (SMC) belongs to the variable structure family of control. SMC is capable of running online in real time while also handling system non-linearity [11]. SMC is also known to be robust against uncertainty in system parameters. Thus making it a suitable choice for controlling vehicle lateral dynamics. The design of SMC has three key parts. We explain each part by considering a generic system $\dot{\underline{x}}_{n\times 1} = \underline{f}(\underline{x}) + \underline{B}(\underline{u})$, where $\underline{x}$ is the state vector and $\underline{u}$ is the actuator input vector.

We can define m sliding surfaces ($m \leq n$) in the state space for such a system. The sliding surfaces are chosen as the conditions that are to be simultaneously satisfied by the state variables. Thus, the sliding surface can be algebraically defined as a function $\underline{S} = \underline{g}(\underline{x})_{m\times 1} = 0$. For example, $\underline{g}(\underline{x})$ can be defined as:

$$\underline{g}(\underline{x}) = \underline{x}_r - \underline{x}, \tag{2.1}$$

where $\underline{x}_r$ is the reference value for each state variable. This implies that on the sliding surface $\underline{S} = 0$, the state variables should achieve the desired value $\underline{x}_r$.

With the sliding surface defined, the next step is to calculate the actuator inputs $\underline{u}$. The input is calculated such that the system always converge to $\underline{S} = 0$ and then remains there. This can be guaranteed by considering a quadratic Lyapunov function (V) and its derivative ($\dot{V}$) such that:

$$V = \frac{1}{2}\underline{S}^T\underline{S} \implies \underline{S}^T\dot{\underline{S}} < 0 \tag{2.2}$$

In order to achieve the above inequality, we impose:

$$\dot{\underline{S}} = -[K]sign(\underline{S}). \tag{2.3}$$

Controller inputs are calculated such that the above condition is always satisfied [12].

In Equation 2.3, we use the $sign()$ as switching function. This can cause finite amplitude oscillations in the system response, known as chattering, which can be avoided by using a smoother switching function [13]. The chattering in the system response can also be caused by unmodelled dynamics. This problem can be avoided by adding an asymptotic observer to the control loop [13].

In [14], the author implemented a sliding mode control using direct yaw moment control (DYC) and ARS to control sideslip angle. In [15], the authors implemented and compared different feedback controllers. The integrated sliding mode controller appeared to be the more robust and better performing during transient conditions. In [12], the authors designed an integrated sideslip angle-yaw rate sliding mode controller using rear active differential and ARS. In [16], the author developed a sliding mode controller using rear steering to improve handling and driver comfort. In [17], the author developed a sliding mode controller for over-steering vehicle and compared the performance with a Linear Quadratic Regulator.

In [18], the authors implemented integrated sliding mode control with proportional-integral (PI) type error function using brake torque vectoring and rear steering as active systems. In [19], the authors proposed a non-singular terminal sliding mode controller which converges in finite time without causing any singularity. In [20], the authors developed an integral terminal sliding mode control for yaw rate using front steering as active system. In [21], an adaptive fast non-singular integral terminal sliding model control is developed for autonomous under-water vehicles.

In most sliding mode controller implementations for lateral dynamics control, the sliding surface is modelled as proportional error or proportional integral error. The errors are also left decoupled i.e. each sliding surface is constructed using only yaw rate or sideslip angle error. In most implementations, moreover the yaw moment is generated through brake torque vectoring which can result in considerable decrease in vehicle speed during the maneuver.

This reduction in speed due to braking forces also results in a considerable drop in vehicle sideslip angle. This may also lead the vehicle to instability. Thus we intend to use 4 IWMs which apply same magnitude of differential torques on both wheels of each axle so that the vehicle speed can be maintained.

2.2.2. Observer in the Loop

In any vehicle dynamics simulation environment, quantities like yaw rate and vehicle sideslip angle are exactly known. In a real vehicle, directly measuring some physical quantities like sideslip angle may not be feasible due to the need of expensive sensors

and special mounting apparatus. Thus, an observer which can estimate the sideslip angle exploiting signals coming from commonly available sensors is added to the control loop.

Moreover, sensors used to measure physical quantities are always noisy. This may affect the controller performance. Thus, the controller needs to be robust enough such that it is able to handle the sensor noise. Here, the observer can also be used to filter out the sensor data and reduce the noise levels in measured signals. With lower noise in the input signals, the controller performance will naturally improve.

An asymptotic observer added to the control loop also reduces chattering in the system response [11] [13]. Unlike other methods of removing chattering, the addition of an observer does not reduce controller robustness [11]. However, an observer is typically more effective in removing the chattering caused by the unmodelled dynamics rather than that due to finite switching frequency. On combining an asymptotic observer with a smooth switching function, we expect the controller to be more robust and not causing any chattering in the system response.

In this thesis work, we investigate a non-singular integral terminal sliding mode control to achieve desired yaw rate and sideslip angle while accounting for actuator limits. The "integral" part should help in achieving null steady state error. The "terminal" part should help in reaching the reference values in finite time i.e. better rate of convergence. We also implement an extended Kalman filter (EKF) [10] [22] to estimate sideslip angle and filter yaw rate signal.

3 | Active Rear Steering and Torque Vectoring

In this chapter, we analyse the effect of Active Rear Steering (ARS) and Torque Vectoring (TV) on vehicle lateral dynamics using the Linearized Single Track Model (LSTM) [1]. The LSTM can be analytically or numerically solved to analyze the steady state or the transient behaviour of the vehicle. The LSTM is an extremely simple model which provides good qualitative and quantitative estimation of vehicle lateral dynamics, particularly for lateral accelerations lower than 4 m/s^2 [4]. It should be noted that the lateral acceleration experienced during highway, town and country road driving stays mostly within $1 - 4\ m/s^2$ [16].

The LSTM developed in this chapter is a multi input (ARS and TV) and multi output (yaw rate and vehicle sideslip angle) system. The transfer functions of the multi-input multi-output (MIMO) model can provide information such as the static gain, step response and phase difference between input and output. The transfer functions are useful to investigate the effect of a parameter on the model dynamics. Even though the LSTM may not match the real vehicle dynamics, the qualitative and quantitative results are extremely helpful in understanding the real vehicle behaviour.

We start the analysis by deriving the equations of motion for the linearized single track model of a vehicle with ARS and TV. Then, we derive the analytical expressions of the transfer functions. Following this, we calculate the step response and frequency response function for different rear-to-front steering ratios at different vehicle speeds. Finally, the same calculations are done for yaw moment as well.

3.1. Linearized Single Track Model

The single track model of a vehicle can be considered as valid under the following assumptions:

1. 3D effects are neglected i.e. any load transfer, roll, pitch and vertical motion is neglected,

2. Aerodynamic forces or moments, rolling resistance and self-aligning torques are neglected,
3. Longitudinal slip and combined friction effect is neglected,
4. Vehicle is considered as a rigid body moving in a plane.

The forces, moments, velocities and inertial accelerations acting on the vehicle under these assumptions are presented in Figure 3.1. Since we are interested in studying the vehicle motion in curve, it is beneficial to write the equations of motion in the moving reference system aligned with the vehicle by appropriately resolving the tyre forces.

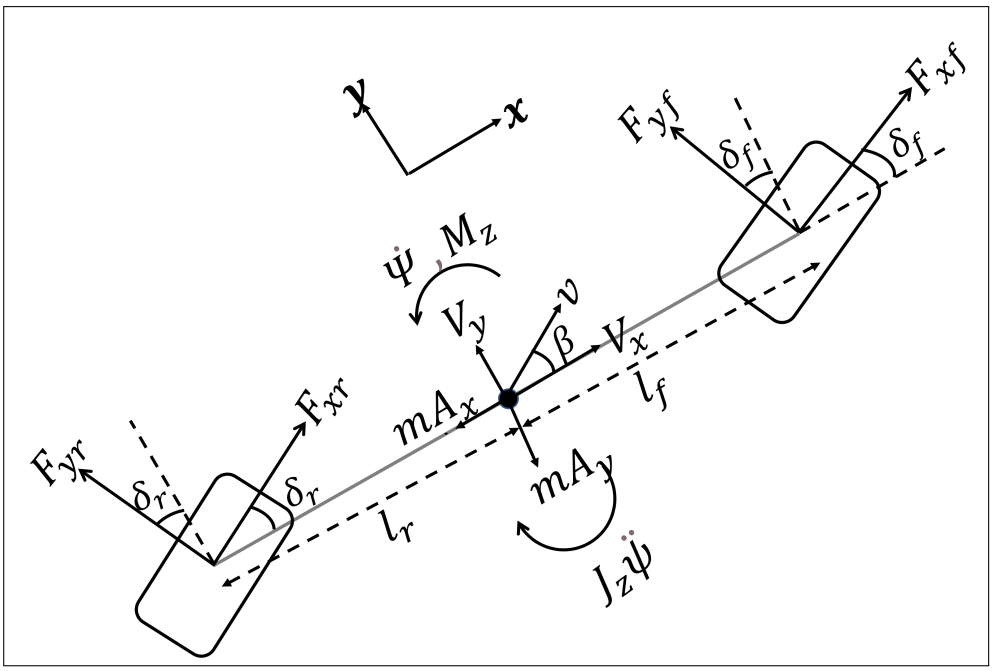

Figure 3.1: Single Track Model (STM) of a vehicle in curve with ARS and TV.

On balancing the forces and moments in the moving reference system aligned with the vehicle, we get the following equations:

$$mA_x = F_{xf}\cos\delta_f - F_{yf}\sin\delta_f + F_{xr}\cos\delta_r - F_{yr}\sin\delta_r \tag{3.1}$$

$$mA_y = F_{xf}\sin\delta_f + F_{yf}\cos\delta_f + F_{xr}\sin\delta_r + F_{yr}\cos\delta_r \tag{3.2}$$

$$J_z\ddot{\psi} = l_f(F_{xf}\sin\delta_f + F_{yf}\cos\delta_f) - l_r(F_{xr}\sin\delta_r + F_{yr}\cos\delta_r) + M_z \tag{3.3}$$

where, m is the vehicle mass, A_x is the inertial acceleration in the vehicle longitudinal direction, A_y is the inertial acceleration in the vehicle lateral direction, J_z is the yaw moment of inertia, l_f and l_r is the distance between vehicle centre of mass (CoM) and

front and rear axle respectively, $\ddot{\psi}$ is the inertial yaw acceleration, F_{xf} and F_{yf} is the longitudinal and lateral force generated at the front axle respectively, F_{xr} and F_{yr} is the longitudinal and lateral force generated at the rear axle respectively, δ_f and δ_r are the average front and rear wheel steering angles respectively and M_z is the yaw moment generated by TV.

The lateral forces ($F_{yf},\ F_{yr}$) depend on the lateral slip angles ($\alpha_f,\ \alpha_r$). The lateral slip angle is calculated by resolving the velocities in the reference system aligned with the wheel. For front wheels, the lateral slip angle (α_f) is calculated as:

$$\alpha_f = \arctan\left(\frac{-V_{yf}}{V_{xf}}\right) = \arctan\left(\frac{-(V_y + \dot{\psi} l_f)\cos\delta_f + V_x \sin\delta_f}{V_x \cos\delta_f + (V_y + \dot{\psi} l_f)\sin\delta_f}\right) \tag{3.4}$$

Similarly, the lateral slip angle for the rear wheels (α_r) is calculated as:

$$\alpha_r = \arctan\left(\frac{-V_{yr}}{V_{xr}}\right) = \arctan\left(\frac{-(V_y - \dot{\psi} l_r)\cos\delta_r + V_x \sin\delta_r}{V_x \cos\delta_f + (V_y - \dot{\psi} l_r)\sin\delta_r}\right) \tag{3.5}$$

Here, V_x is the vehicle longitudinal velocity, V_y is the vehicle lateral velocity and $\dot{\psi}$ is the vehicle yaw rate in the moving reference system aligned with the vehicle.

If V is the vehicle speed and β is the vehicle sideslip angle, then $V_y = V\sin\beta$ and $V_x = V\cos\beta$. Using the small angle approximations, the lateral slips are linearized as:

$$\alpha_f = \delta_f - \beta - \frac{\dot{\psi} l_f}{V}, \tag{3.6}$$

$$\alpha_r = \delta_r - \beta + \frac{\dot{\psi} l_r}{V}. \tag{3.7}$$

For small lateral slip angles, the lateral forces can be approximated using first order Taylor series approximation as follows:

$$F_{yf}(\alpha_f) \approx F_{yf_0} + \frac{\partial F_{yf}}{\partial \alpha_f}(\alpha_f - \alpha_{f_0}) \approx K_f \alpha_f = K_f\left(\delta_f - \beta - \frac{\dot{\psi} l_f}{V}\right), \tag{3.8}$$

$$F_{yr}(\alpha_r) \approx F_{yr_0} + \frac{\partial F_{yr}}{\partial \alpha_r}(\alpha_r - \alpha_{r_0}) \approx K_r \alpha_f = K_r\left(\delta_r - \beta + \frac{\dot{\psi} l_f}{V}\right), \tag{3.9}$$

where $K_f = \partial F_{yf}/\partial \alpha_f$ is the cornering stiffness for the front axle and $K_r = \partial F_{yr}/\partial \alpha_r$ is the cornering stiffness for the rear axle.

Since the chosen reference system is rotating with the vehicle, the lateral (A_y) and longitudinal acceleration (A_x) should also account for the vehicle yaw rate. First, the velocity

of the centre of mass ($\vec{V_G}$) is defined as:

$$\vec{V_G} = V_x\vec{i} + V_y\vec{j}. \tag{3.10}$$

Then, we calculate the acceleration of the CoM as:

$$\vec{A_G} = A_x\vec{i} + A_y\vec{j} = \dot{\vec{V}_G} = \dot{V_x}\vec{i} + \dot{V_y}\vec{j} + (\dot{\psi}\vec{k})\Lambda(\vec{V_G}) = (\dot{V_x} - \dot{\psi}V_y)\vec{i} + (\dot{V_y} + \dot{\psi}V_x)\vec{j} \tag{3.11}$$

By substituting the above expression in Equations 3.2 and 3.3, ignoring the terms related to longitudinal dynamics and using small angle approximations, we get:

$$mA_y \approx mV(\dot{\beta} + \dot{\psi}) \approx K_f\left(\delta_f - \beta - \frac{\dot{\psi}l_f}{V}\right) + K_r\left(\delta_r - \beta + \frac{\dot{\psi}l_f}{V}\right) \tag{3.12}$$

$$J_z\ddot{\psi} \approx K_f l_f\left(\delta_f - \beta - \frac{\dot{\psi}l_f}{V}\right) - K_r l_r\left(\delta_r - \beta + \frac{\dot{\psi}l_f}{V}\right) + M_z \tag{3.13}$$

This system of equations can be represented in matrix-vector form as:

$$\begin{bmatrix}\ddot{\psi}\\ \dot{\beta}\end{bmatrix} = \begin{bmatrix}\frac{-(K_f l_f^2 + K_r l_r^2)}{J_z v} & \frac{-(K_f l_f - K_r l_r)}{J_z}\\ \frac{K_r l_r - K_f l_f - mv^2}{mv^2} & \frac{-(K_f + K_r)}{mv}\end{bmatrix}\begin{bmatrix}\dot{\psi}\\ \beta\end{bmatrix} + \begin{bmatrix}\frac{K_f l_f}{J_z} & \frac{-K_r l_r}{J_z} & \frac{1}{J_z}\\ \frac{K_f}{mv} & \frac{K_r}{mv} & 0\end{bmatrix}\begin{bmatrix}\delta_f\\ \delta_r\\ M_z\end{bmatrix}. \tag{3.14}$$

This is known as linearized single track model (LSTM) for vehicle lateral dynamics.

3.2. Transfer Functions

The LSTM has 3 inputs ($\delta_r,\ M_z,\ \delta_f$) and 2 outputs ($\dot{\psi},\ \beta$). Of the 3 inputs, δ_f is either applied by the driver (closed loop maneuver) or fixed before the simulation (open loop maneuver). To study the effect of active rear steering (ARS), we substitute $\delta_r = K_w\delta_f$. Using this substitution, the system of equations becomes:

$$\begin{bmatrix}\ddot{\psi}\\ \dot{\beta}\end{bmatrix} = \begin{bmatrix}\frac{-(K_f l_f^2 + K_r l_r^2)}{J_z v} & \frac{-(K_f l_f - K_r l_r)}{J_z}\\ \frac{K_r l_r - K_f l_f - mv^2}{mv^2} & \frac{-(K_f + K_r)}{mv}\end{bmatrix}\begin{bmatrix}\dot{\psi}\\ \beta\end{bmatrix} + \begin{bmatrix}\frac{K_f l_f - K_w K_r l_r}{J_z} & \frac{1}{J_z}\\ \frac{K_f + K_w K_r}{mv} & 0\end{bmatrix}\begin{bmatrix}\delta_f\\ M_z\end{bmatrix} \tag{3.15}$$

The above system of equation can be represented in a more compact form as follows:

$$\dot{\underline{z}} = [A]\underline{z} + [C]\underline{u}, \quad \underline{z} = [\dot{\psi}\ \beta]^T,\ \underline{u} = [\delta_f\ M_z]^T. \tag{3.16}$$

Assuming all the parameters, including K_f and K_r to be constant, we apply the Laplace transform and re-arrange the terms to obtain the transfer functions as follows:

$$\underline{z}(s) = (s[I]_{2\times 2} - [A])^{-1}[C]\underline{u}(s) = \begin{bmatrix} G_{11} & G_{12} \\ G_{21} & G_{22} \end{bmatrix} \underline{u}(s) \tag{3.17}$$

On performing the symbolic calculations, the expression of the transfer functions (G_{ij}) is as follows:

$$G_{11}(s) = \frac{\dot{\psi}}{\delta_f} = \frac{\frac{vK_fK_r(1-K_w)l}{K_fK_rl^2+mv^2(K_rl_r-K_fl_f)}\left(\frac{(K_rK_wl_r-K_fl_f)mv}{K_fK_r(K_w-1)l}s+1\right)}{\frac{J_zmv^2}{K_fK_rl^2+mv^2(K_rl_r-K_fl_f)}s^2 + s\frac{v(m(K_fl_f^2+K_rl_r^2)+J_z(K_f+K_r))}{K_fK_rl^2+mv^2(K_rl_r-K_fl_f)}+1} \tag{3.18}$$

$$G_{12}(s) = \frac{\dot{\psi}}{M_z} = \frac{\frac{v(K_f+K_r)}{K_fK_rl^2+mv^2(K_rl_r-K_fl_f)}\left(\frac{mv}{K_f+K_r}s+1\right)}{\frac{J_zmv^2}{K_fK_rl^2+mv^2(K_rl_r-K_fl_f)}s^2 + s\frac{v(m(K_fl_f^2+K_rl_r^2)+J_z(K_f+K_r))}{K_fK_rl^2+mv^2(K_rl_r-K_fl_f)}+1} \tag{3.19}$$

$$G_{21}(s) = \frac{\beta}{\delta_f} = \frac{\frac{mv^2(K_rl_rK_w-K_fl_f)+K_fK_rl(K_wl_f+l_r)}{K_fK_rl^2+mv^2(K_rl_r-K_fl_f)}\left(\frac{J_zv(K_rK_w+K_f)}{mv^2(K_rl_rK_w-K_fl_f)+K_fK_r(K_wl_fl+l_rl)}s+1\right)}{\frac{J_zmv^2}{K_fK_rl^2+mv^2(K_rl_r-K_fl_f)}s^2 + s\frac{v(m(K_fl_f^2+K_rl_r^2)+J_z(K_f+K_r))}{K_fK_rl^2+mv^2(K_rl_r-K_fl_f)}+1} \tag{3.20}$$

$$G_{22}(s) = \frac{\beta}{M_z} = \frac{\frac{-mv^2-K_fl_f+K_rl_r}{K_fK_rl^2+mv^2(K_rl_r-K_fl_f)}}{\frac{J_zmv^2}{K_fK_rl^2+mv^2(K_rl_r-K_fl_f)}s^2 + s\frac{v(m(K_fl_f^2+K_rl_r^2)+J_z(K_f+K_r))}{K_fK_rl^2+mv^2(K_rl_r-K_fl_f)}+1}, \tag{3.21}$$

where, $l = l_f + l_r$.

The poles of these transfer functions represent the poles of the mechanical system. The rear-to-front steering ratio (K_w) affects only the zeros and the static gains of the transfer functions of yaw rate and sideslip angle against front steering wheel angle i.e. G_{11} and G_{21}. It does not affect the transfer functions for M_z i.e. G_{12} and G_{22} in any way.

Assuming the inputs δ_f and M_z to be constant, the steady state values of the above transfer functions is calculated by substituting $s = 0$ in the Equations 3.18-3.21. To further simplify the expressions of static gains, the understeering coefficient k is defined as:

$$k = \frac{m(K_rl_r - K_fl_f)}{l^2K_fK_r}. \tag{3.22}$$

If $k < 0$, the vehicle is oversteering with $\alpha_f < \alpha_r$. If $k > 0$, the vehicle is understeering with $\alpha_f > \alpha_r$. If $k = 0$, the vehicle is neutral with $\alpha_f = \alpha_r$.

On substituting the above expression of k and $s = 0$ in the Equations 3.18-3.21, the static

gain of the four transfer functions becomes:

$$G_{11}(0) = \left(\frac{\dot{\psi}}{\delta_f}\right)_{SS} = \frac{v(1-K_w)}{l(1+kv^2)}, \tag{3.23}$$

$$G_{12}(0) = \left(\frac{\dot{\psi}}{M_z}\right)_{SS} = \frac{v(K_f+K_r)}{K_f K_r l^2(1+kv^2)}, \tag{3.24}$$

$$G_{21}(0) = \left(\frac{\beta}{\delta_f}\right)_{SS} = \frac{mv^2 l_r(K_w-1)}{K_f l^2(1+kv^2)} + \frac{kv^2}{1+kv^2} + \frac{K_w l_f + l_r}{l(1+kv^2)}, \tag{3.25}$$

$$G_{22}(0) = \left(\frac{\beta}{M_z}\right)_{SS} = \frac{-mv^2}{K_f K_r l^2(1+kv^2)} + \frac{k}{m(1+kv^2)}, \tag{3.26}$$

where the subscript $()_{SS}$ denotes steady state value of the corresponding transfer function.

From the above equations, we can observe that negative K_w will increase the static gain for G_{11}. At the same time, negative K_w would decrease the magnitude of $G_{21}(0)$ for understeering vehicle ($k > 0$) as first and third fraction in Equation 3.25 would decrease in value if K_w is negative in comparison to the passive vehicle ($K_w = 0$). The static gains for torque vectoring (M_z) depend on vehicle speed, cornering stiffnesses, wheelbase and understeering coefficient.

3.3. Step Response and Frequency Response

To study the effect of K_w or M_z on vehicle dynamics, we generate and analyse the step response and the frequency response plots for the four transfer functions. We use the relevant parameters of the `CityCar_FullElectric` model of VI-CarRealTime (VI-CRT). These parameters are listed in Table 3.1. The value of understeering coefficient k for this vehicle is $5.276 \times 10^{-4}\ s^2 rad/m^2$.

Table 3.1: Parameters for `CityCar_FullElectric` model.

Parameter	Meaning	Value [Unit]
m	Total Mass	1153.141 $[kg]$
J_z	Yaw moment of inertia	965.6842 $[kgm^2]$
l_f	Distance between CoG and front axle	0.8618 $[m]$
l_r	Distance between CoG and rear axle	1.2898 $[m]$
l	Wheelbase	2.1516 $[m]$
c_f	Front track width	1.3787 $[m]$
c_r	Rear track width	1.3691 $[m]$
K_f	Front axle cornering stiffness	136000 $[N/rad]$
K_r	Rear axle cornering stiffness	117000 $[N/rad]$

The cornering stiffnesses of a real vehicle change with slip angle, camber angle, lateral load transfer, vertical load etc. In order to maintain the correlation between LSTM and VI-CRT vehicle model, we simulate the constant radius curve maneuver with the VI-CRT model for low lateral accelerations ($\leq 2\ m/s^2$). This ensures that the total lateral forces at the axle vary linearly with respect to slip angle. The cornering stiffnesses are then calculated as the slope of total force at the axle against average lateral slip at the axle.

We calculate the slope as $\Delta F_{yj}/\Delta\alpha_j$ $(j = f, r)$. The slope for different ranges of α_j is presented in Table 3.2. The K_f and K_r values presented in Table 3.1 are calculated by averaging the corresponding values for $\alpha = [1.9 - 2]\ mrad$ (low speed CRC maneuver) and $[2 - 2.1]\ mrad$ (high speed CRC maneuver) in Table 3.2.

Table 3.2: Front and rear cornering stiffness calculated for different α values in the linear range of tyres. Unit for cornering stiffness (K_f, K_r): $[kN/rad]$.

CRC: $v = 5m/s$, $R = 50; m$			CRC: $v = 25m/s$, $R = 500\ m$		
$\alpha\ [mrad]$	K_f	K_r	$\alpha\ [mrad]$	K_f	K_r
[0.5-0.51]	134.84	118.08	[.1-.11]	137.32	118.88
[0.6-0.61]	136.51	118.16	[.5-.51]	131.07	117.98
[1.0-1.10]	136.93	121.13	[1.0-1.1]	132.44	117.29
[1.5-1.51]	138.15	113.80	[2.0-2.1]	132.31	116.78
[1.9-2.00]	140.94	116.61	[4.0-4.1]	131.92	115.89

3.3.1. Effect of K_w

The rear-to-front steering ratio affects only the transfer functions relating the two model outputs: $\dot{\psi}$ and β to the model input δ_f. We calculate the frequency response functions (FRF) and step response for 4 different values of K_w $(-1, -1/3, 1/3, 1)$ and 2 different speeds (10 km/h and 90 km/h). This choice of values will allow us to analyse the effect of active rear steering at low and high speed. Here, negative K_w implies that the rear wheels are steered in the opposite direction of the front wheels.

When $K_w = 1$, it implies both front and rear wheels are steered by the same angle in same direction. In this case, the vehicle will move on a diagonal line whose slope (with respect to longitudinal direction) is equal to δ_f without yaw motion. Thus, the step response for $\dot{\psi}$ would achieve a steady state value of 0 and for β it would achieve a steady state value of 1, for any vehicle speed.

These observations are verified by the plots presented in Figures 3.2, 3.3, 3.4 and 3.5. In Figures 3.2 and 3.3, the FRF for $\dot{\psi}$ increases with the magnitude of negative K_w, for both vehicle speeds. For low vehicle speed, the magnitude of FRF for β is lower for negative

K_w whereas for high vehicle speed it may be lower for a positive K_w depending on the excitation frequency.

Thus, if the vehicle speed is low, a higher $\dot{\psi}$ can be achieved with respect to passive vehicle while also minimizing β by steering the rear wheels in the direction opposite to front wheels. At higher vehicle speed, increasing yaw rate by counter steering the rear wheels may considerably increase the magnitude of β, especially during low frequency excitation. Such an increase may result in unstable behaviour of the vehicle due to high slip angles at the wheels.

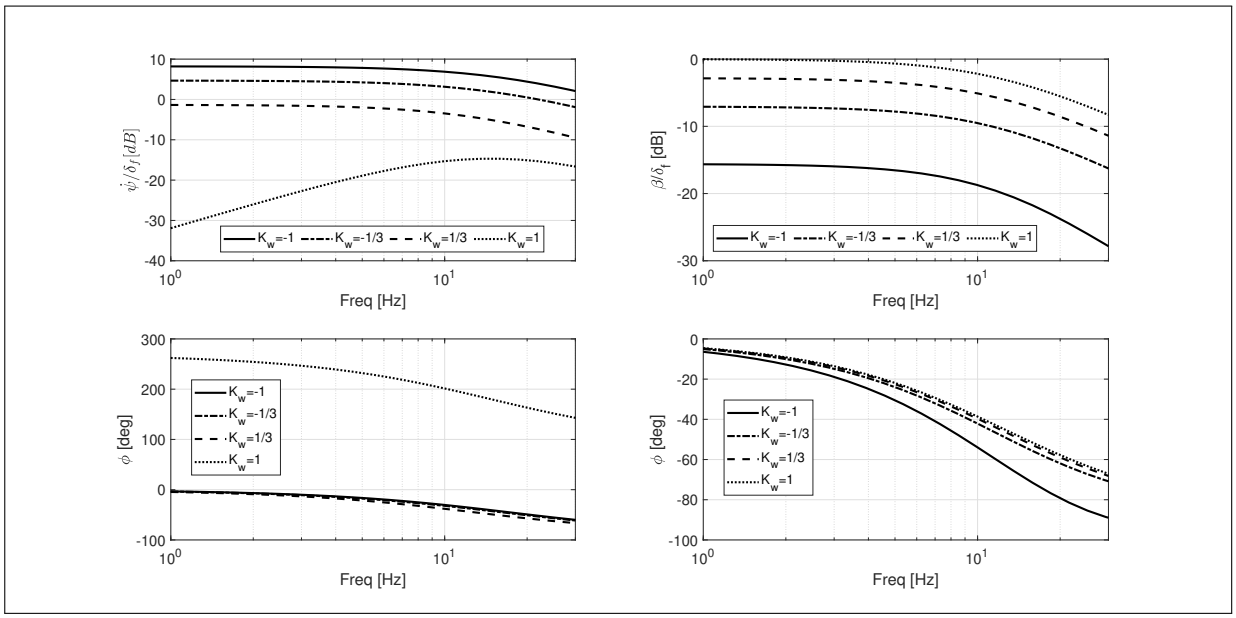

Figure 3.2: Effect of K_w on FRFs at vehicle speed 10 km/h.

These observations are further verified by analysing the step response of the two relevant transfer functions. In Figures 3.4 and 3.5, we can observe that the steady state value achieved by the yaw rate increases with vehicle speed for all K_w except for $K_w = 1$. At low vehicle speed, negative K_w has the lowest magnitude of steady state value of β. At high vehicle speed, positive K_w value ($K_w = 1/3$) results in the lowest magnitude of the steady state value of β. For this positive K_w value, the steady state value of yaw rate is lowest when compared to other K_w values, not including the special case of $K_w = 1$ in the comparison.

These observations indicate that active rear steering alone is not able to improve the yaw rate while also minimizing the sideslip angle, especially at high speed. Also, fixing the magnitude of K_w for all the vehicle speeds may be counter productive. This is because β is minimum for different magnitudes and signs of K_w for different vehicle speeds.

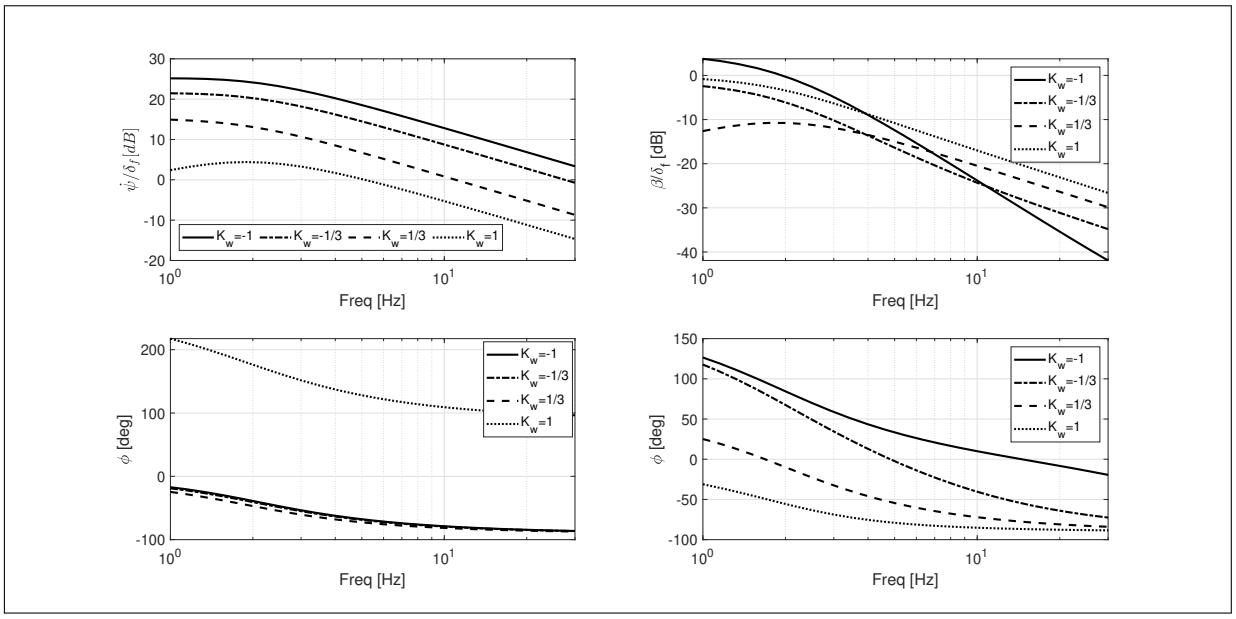

Figure 3.3: Effect of K_w on FRFs at vehicle speed 90 km/h.

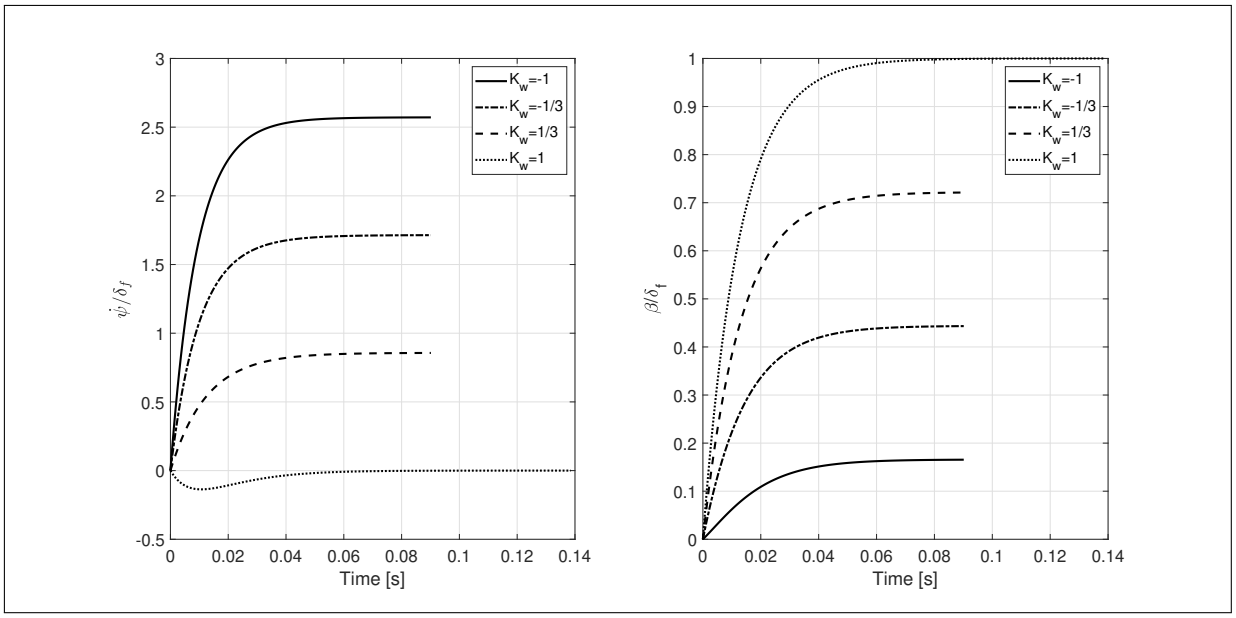

Figure 3.4: Effect of K_w on step response of the transfer functions at vehicle speed 10 km/h.

3.3.2. Effect of M_z

Next we analyse the effect of yaw moment M_z on vehicle lateral dynamics. For the City Car model, we calculate the frequency response function and step response for the same two vehicle speeds i.e. 10 and 90 km/h. From the previously calculated expressions, we can observe that the transfer functions relating model output with M_z are not affected

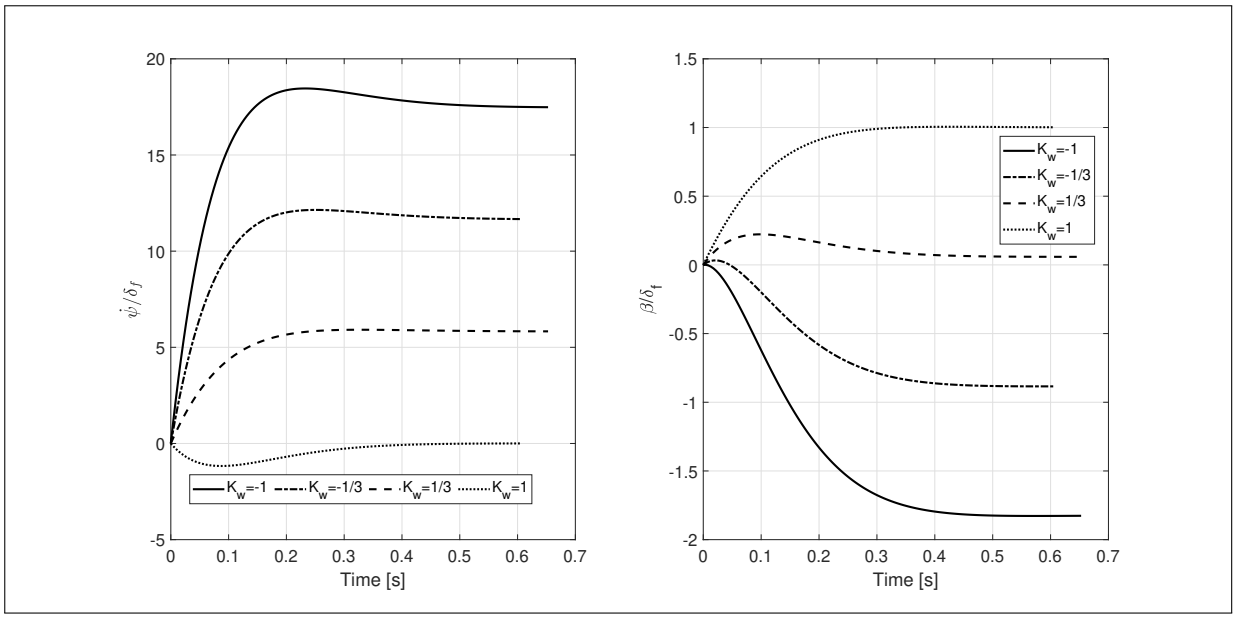

Figure 3.5: Effect of K_w on step response of the transfer functions at vehicle speed 90 km/h.

by K_w.

In Figure 3.6, we can see that the magnitude of the FRF increases with vehicle speed for both $\dot{\psi}$ and β for excitation frequencies lower than 10 Hz. At higher excitation frequency, the FRF for low vehicle speed is higher. For low vehicle speed, the initial phase between M_z and β is 0° i.e. positive M_z will result in positive β. For high speed, the initial phase between M_z and β is 180° i.e. positive M_z will result in negative β.

The above observations are further verified by the step responses presented in Figure 3.7. The magnitude of the steady state value of $\dot{\psi}$ and β is higher for high speed. At the same time, the sign of the steady state value of β changes from low to high speed. Also, the steady state value of β is one order of magnitude lower than that of $\dot{\psi}$. Thus, for same M_z, the gain for $\dot{\psi}$ will always be 1 order of magnitude higher than that for β. This difference is further increased at lower speeds.

In Figures 3.4, 3.5 and 3.7, we can see that the combination of active rear steering and torque vectoring can obtain the desired yaw rate while minimizing the sideslip angle, especially at high vehicle speed. At high speed, we need to implement positive K_w in order to minimize β. This would reduce the steady state value for $\dot{\psi}$. The yaw moment generated by TV can increase the yaw rate steady state value without significantly affecting the steady state value of β. Hence, a combination of the two inputs becomes necessary to achieve the target β and $\dot{\psi}$, particularly at high speed.

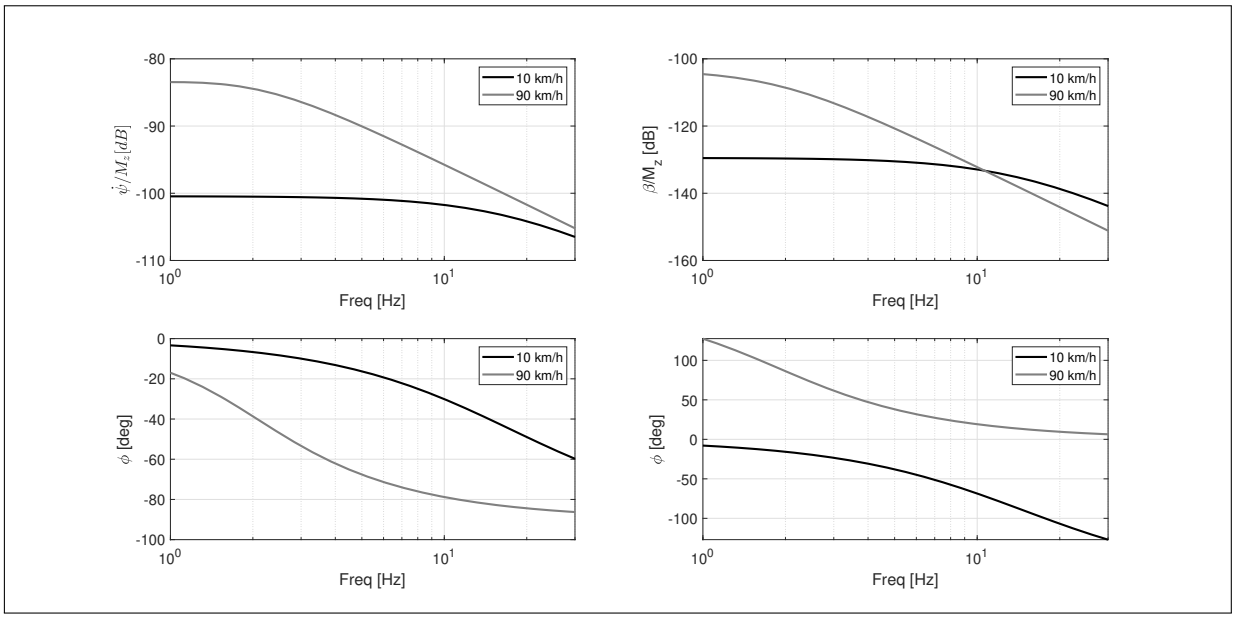

Figure 3.6: Effect of M_z on FRFs at 10 km/h and 90 km/h.

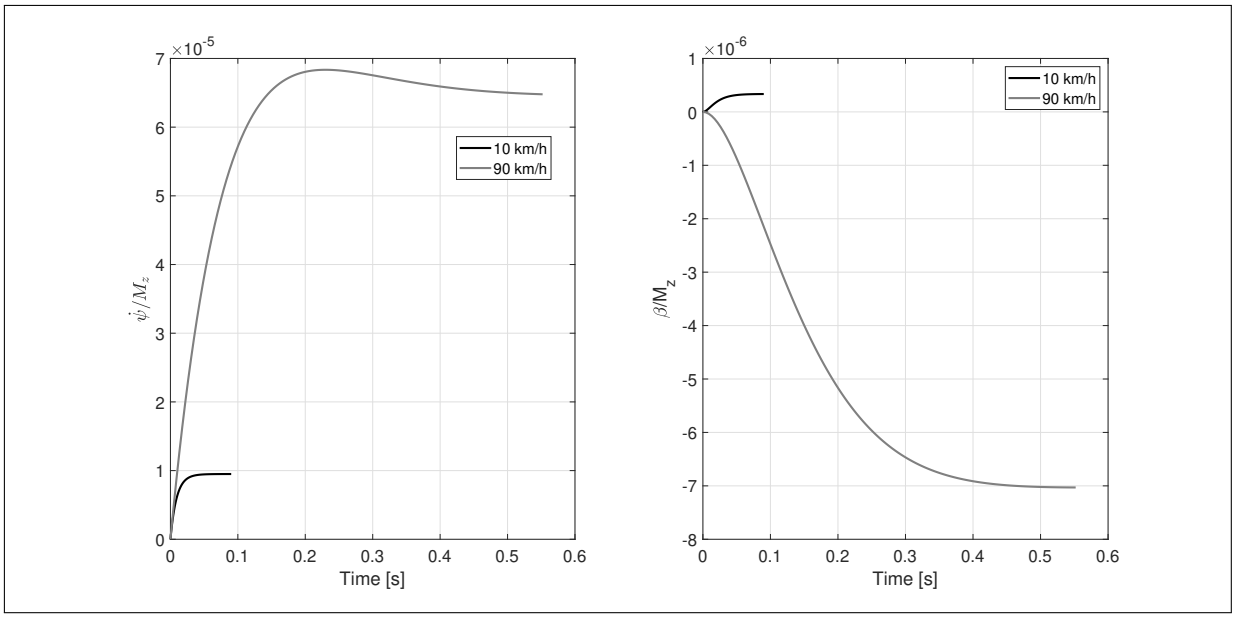

Figure 3.7: Effect of M_z on step response of the transfer functions for 10 km/h and 90 km/h.

3.4. Conclusion

The linearized single track model for a vehicle with active rear steering and torque vectoring has been derived. The transfer functions relating the two model outputs $\dot{\psi}$ and β with the two inputs δ_f and M_z are derived and analyzed through frequency response function and step response. Active rear steering alone is not capable of minimizing β

while increasing $\dot{\psi}$ as compared to the passive vehicle, especially at high speed. On the other hand, torque vectoring alone can only influence $\dot{\psi}$ significantly, especially at low speed. Thus, a carefully chosen combination of the two inputs can improve the yaw rate while also minimizing the vehicle sideslip angle as compared to the passive vehicle.

4 | Controllers

In this chapter, we design and implement the integrated control of $\dot{\psi}$ and β using the linearized single track model (LSTM) derived in the previous chapter. In the previous chapter, we could conclude that active rear steering (ARS) or torque vectoring (TV) alone cannot minimize β while also improving $\dot{\psi}$, particularly at high speed. Hence, a combination of TV and ARS is necessary to improve $\dot{\psi}$ while minimizing β.

We test two controllers: a feedforward controller and an integral terminal sliding mode controller. Both these controllers are tested with the LSTM without imposing any limits on the actuator inputs or considering the actuator dynamics. This way we can get a first estimation of a reasonable actuator sizing for the real vehicle. The feedforward control law provides a simple approach with the aim to improve the steady state dynamics. The sliding mode control aims to improve both steady state and transient dynamics of the vehicle.

The sliding mode controllers are known to suffer from chattering problem i.e. finite amplitude finite frequency oscillations in the system response. There can be two sources for chattering: finite sampling rate or unmodelled dynamics [13]. The chattering arising due to finite sampling rate is avoided by using a smooth switching function. The chattering arising due to unmodelled dynamics is avoided by using an asymptotic observer [13]. Here, we use an extended Kalman filter as the state observer for the system.

First, we derive a feedforward controller based on the transfer functions derived in the previous chapter. Next, we derive a non-singular integral terminal sliding mode control law for the LSTM. The control input calculated by both the control law is also analysed qualitatively to predict if it may cause unstable behaviour of the real vehicle. Following this, we present a method for calculating reference values using the logistic function. Finally, we present the extended Kalman filter (EKF) used to estimate sideslip angle and filter noisy yaw rate signal.

4.1. Feedforward Control

The feedforward (FF) control relies on the precise knowledge of plant model and its parameters. This precise knowledge is then used to calculate the exact input required to achieve the reference signal. This results in no steady state error which may not be the case with feedback controllers.

There is one drawback of FF controllers. Since there is no feedback loop, the control system cannot detect any deviation from the reference signal. The FF controller always works under the assumption that the model and its parameters are exactly known and there are no disturbances acting on the system. However, this significant drawback can be eliminated by combining the FF controller with a feedback control loop. The feedback loop ensures robustness against external disturbances and unforeseen changes in the plant model or its parameters.

The LSTM is a simple model of the real vehicle, which ignores any external disturbances acting on the vehicle. Thus, we derive and test only the FF part of the controller for the LSTM. We start the derivation of the FF control law by recalling the equations of motion presented in Equation 3.15:

$$\begin{bmatrix} \ddot{\psi} \\ \dot{\beta} \end{bmatrix} = \begin{bmatrix} \frac{-(K_f l_f^2 + K_r l_r^2)}{J_z v} & \frac{-(K_f l_f - K_r l_r)}{J_z} \\ \frac{K_r l_r - K_f l_f - m v^2}{m v^2} & \frac{-(K_f + K_r)}{m v} \end{bmatrix} \begin{bmatrix} \dot{\psi} \\ \beta \end{bmatrix} + \begin{bmatrix} \frac{K_f l_f - K_w K_r l_r}{J_z} & \frac{1}{J_z} \\ \frac{K_f + K_w K_r}{m v} & 0 \end{bmatrix} \begin{bmatrix} \delta_f \\ M_z \end{bmatrix}. \tag{4.1}$$

The above system of equation can be written as follows:

$$\dot{\underline{z}} = [A]\underline{z} + [B]\underline{u}, \;\; \underline{z} = [\dot{\psi} \; \beta]^T, \; \underline{u} = [\delta_f \; M_z]^T. \tag{4.2}$$

The steady state solution ($\underline{z}_{SS}$) for the above dynamical system is calculated as follows:

$$\dot{\underline{z}} = 0 \implies [A]\underline{z}_{SS} + [B]\underline{u} = 0 \implies \underline{z}_{SS} = -[A]^{-}[B]\underline{u}. \tag{4.3}$$

Since δ_f is either defined by the driver or fixed *a priori*, the above system of equations can be rearranged and written as:

$$\begin{bmatrix} \dot{\psi}_{SS} \\ \beta_{SS} \end{bmatrix} = \begin{bmatrix} \frac{v K_r K_f l}{D} \\ \frac{K_f(-l_f m v^2 + K_r l_r l)}{D} \end{bmatrix} \delta_f + \begin{bmatrix} \frac{-v K_r K_f l \delta_f}{D} & \frac{v(K_f + K_r)}{D} \\ \frac{K_r \delta_f (l_r m v^2 + K_f l_f l)}{D} & \frac{K_r l_r - K_f l_f - m v^2}{D} \end{bmatrix} \begin{bmatrix} K_w \\ M_z \end{bmatrix} \tag{4.4}$$

where, $l = l_f + l_r$ and $D = m v^2 (K_r l_r - K_f l_f) + K_f K_r l^2$. Solving the above system of

equation for K_w and M_z, we get the following:

$$K_w = \frac{mv^2\dot{\psi}_{SS} - K_f\delta_f v - (K_r l_r - K_f l_f)\dot{\psi}_{SS} + (K_f + K_r)v\beta_{SS}}{\delta_f v K_r}, \tag{4.5}$$

$$M_z = \frac{l_r m v^2\dot{\psi}_{SS} - K_f\delta_f l v + K_f l_f l\dot{\psi}_{SS} + K_f l v\beta_{SS}}{v}. \tag{4.6}$$

Thus the actuator inputs required to achieve the desired $\dot{\psi}_{SS}$ and β_{SS} can be calculated using the above expressions.

Next, we simulate the LSTM with K_w and M_z calculated using these expressions. During the simulation, we impose a limit on yaw rate achieved by the model i.e. $\dot{\psi} < \mu g/v$, where $\mu = 1$ and $g = 9.81\ m/s^2$. Once this limit is crossed, we impose $\ddot{\psi} = 0$ and continue the simulation.

The simulations are performed for $v = 10\ km/h$ and $90\ km/h$ with $\delta_f = 1°$. The reference $\dot{\psi}$ is set to 10% higher than the steady state $\dot{\psi}$ of the passive vehicle. The limit on $\dot{\psi}$ is also imposed on the reference value $\dot{\psi}_{SS}$. For each vehicle speed, the reference β_r is either set to 0 or a nonzero value in order to compare its effect on the two model inputs.

The results for low speed simulation with both sideslip angle references of $\beta_r = 0°$ and $0.4°$ are presented in Figure 4.1. In Figure 4.1, we can observe that the required input changes significantly as the reference β value is changed. To achieve exactly 0 sideslip angle, the actuator inputs are significantly higher as compared to achieving a non-zero β value. Similar observations can be drawn from the high speed simulation result presented in Figure 4.2.

For the same desired steady state yaw rate ($\dot{\psi}_{SS}$), the actuator inputs are proportional to the desired steady state (β_{SS}) value (Equations 4.5 and 4.6). Therefore, the actuator inputs can be reduced by choosing the desired β_{SS} value which is lower than that of the passive vehicle. At low vehicle speed the magnitude of reference β value should be lower than the steady state sideslip angle for the passive LSTM, which is positive for positive steering input. At high vehicle speed the magnitude of reference β value should be higher than the steady state value of the passive vehicle, which is negative for positive steering input. The choice of reference β value may also depend on driver and passenger comfort.

A rough estimation of the actuator size can be obtained using Equations 4.5 and 4.6. We define a sampling space using 4 parameters: $\eta_{\dot{\psi}} \in [1.01, 1.1]$, $\eta_\beta \in [0.5, 1.5]$, $v \in [10, 90]\ km/h$ and $\delta_f \in [0.1°, 5°]$. Here $\eta_{\dot{\psi}}$ is the ratio between target steady state $\dot{\psi}$ and the steady state $\dot{\psi}$ of the passive vehicle for given v and δ_f. Similarly, η_β is the ratio

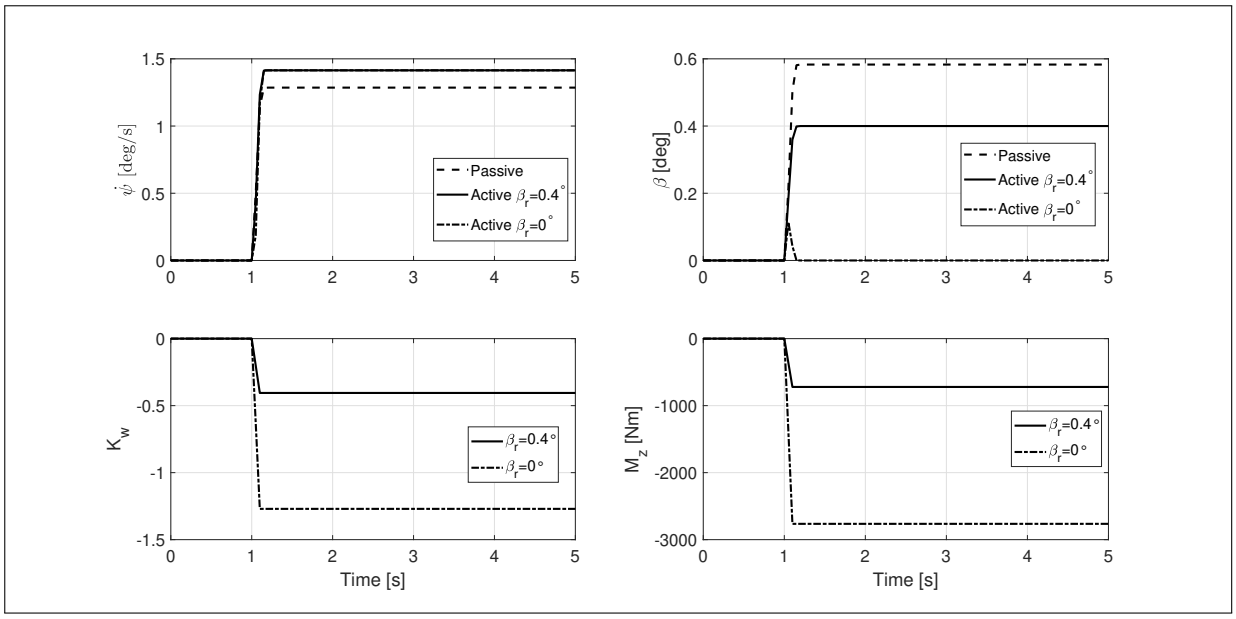

Figure 4.1: Feedforward control of LSTM ($v = 10\ km/h,\ \delta_f = 1°$) to obtain 10% higher $\dot{\psi}$ with 2 different β_r values.

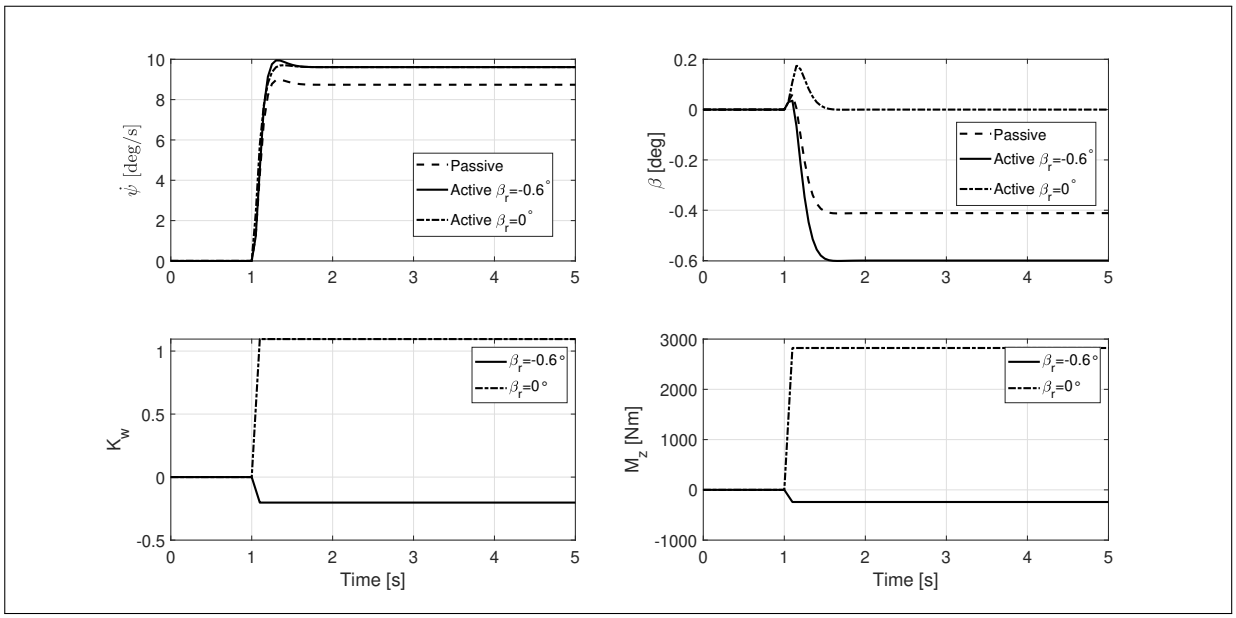

Figure 4.2: Feedforward control of LSTM ($v = 90\ km/h,\ \delta_f = 1°$) to obtain 10% higher $\dot{\psi}$ with 2 different β_r values.

between target steady state β and the steady state β of the passive vehicle for the same v and δ_f.

We generate 1000 uniformly distributed samples from this sampling space using Latin Hypercube Sampling method [23]. A sample point defines the desired gain in $\dot{\psi}$ ($\eta_{\dot{\psi}}$) and

β (η_β) for a given combination of v and δ_f. The steady state values for passive LSTM are calculated using Equations 3.23 ($\dot{\psi}_{pas}$) and 3.25 (β_{pas}) by substituting $K_w = 0$. The target yaw rate reads $\dot{\psi}_{SS} = \eta_{\dot{\psi}}\dot{\psi}_{pas}$ and the target sideslip angle reads $\beta_{SS} = \eta_\beta\beta_{pas}$.

Before calculating the required actuator inputs for LSTM, we place an upper limit on the target yaw rate i.e. $\dot{\psi}_{SS} \leq \mu g/v$. This allows for realistic sizing of the actuators while also accounting for the friction limit. The target yaw rate $\dot{\psi}_{SS}$ and the target β_{SS} are then substituted in Equations 4.5 and 4.6 to obtain the required $\delta_r = K_w\delta_f$ and M_z for each parameter sample.

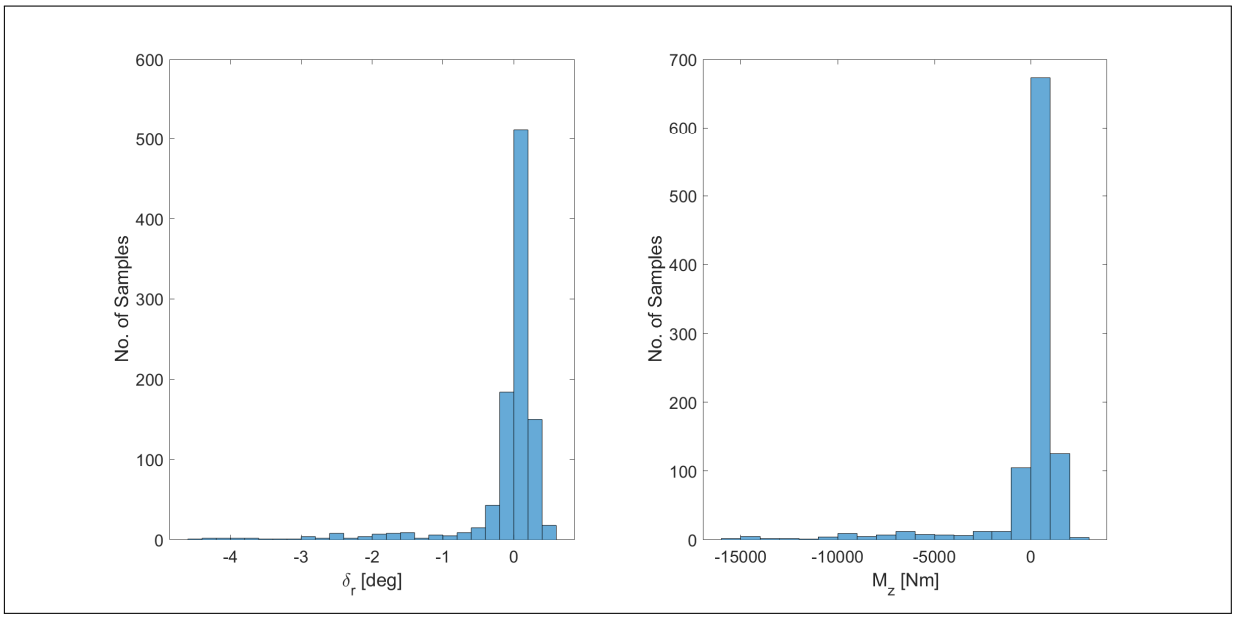

Figure 4.3: Histograms of the required actuator inputs for 1000 uniformly distributed samples.

For easier visualization, we present the histograms for the two inputs in Figure 4.3. In Figure 4.3, we can observe that most combinations of $\dot{\psi}_{SS}$ and β_{SS} can be achieved by $-1° \leq \delta_r \leq 0.6°$ and $-3000\ Nm \leq M_z \leq 3000\ Nm$. These values may be useful for designing the rear steering system and the mechanical characteristics of the motors used for TV actuation.

4.2. Integral Terminal Sliding Mode Control

The Sliding Mode Control (SMC) belongs to the variable structure family of controllers. The actuators inputs are calculated such that the system first moves towards the sliding surface and then stays on that surface. This requires multiple control structures. The sliding surface is defined as a function of state variables. The actuators inputs are then

calculated using the mathematical definition of the sliding surface, the system model and its parameters.

The sliding mode controllers are known to suffer from chattering problem [13]. This happens when the system experiences small disturbances once it reaches the sliding surface and the controller uses large inputs to keep the system on sliding surface. This results in "bang-bang" type input from the actuators which may lead to undesired finite amplitude finite frequency vibrations during the maneuver. This can be solved by using a smoother switching function, as will be discussed during the derivation of control law. The chattering problem may also occur due to unmodelled dynamics. This is avoided by adding an asymptotic observer in the control loop [13].

We start the derivation of the sliding mode control law for LSTM by recalling the equations of motion derived in Equation 3.14:

$$\dot{\underline{z}} = \begin{bmatrix} \ddot{\psi} \\ \dot{\beta} \end{bmatrix} = \begin{bmatrix} \frac{-(K_f l_f^2 + K_r l_r^2)}{J_z v} & \frac{-(K_f l_f - K_r l_r)}{J_z} \\ \frac{K_r l_r - K_f l_f - mv^2}{mv^2} & \frac{-(K_f + K_r)}{mv} \end{bmatrix} \begin{bmatrix} \dot{\psi} \\ \beta \end{bmatrix} + \begin{bmatrix} \frac{K_f l_f}{J_z} & \frac{-K_r l_r}{J_z} & \frac{1}{J_z} \\ \frac{K_f}{mv} & \frac{K_r}{mv} & 0 \end{bmatrix} \begin{bmatrix} \delta_f \\ \delta_r \\ M_z \end{bmatrix}. \tag{4.7}$$

The above equation can be written in a more compact form as follows:

$$\dot{\underline{z}} = [A]\underline{z} + [C]\delta_F + [B]\underline{u},\ \underline{u} = [\delta_r, M_z]^T \tag{4.8}$$

where

$$[A] = \begin{bmatrix} \frac{-(K_f l_f^2 + K_r l_r^2)}{J_z v} & \frac{-(K_f l_f - K_r l_r)}{J_z} \\ \frac{K_r l_r - K_f l_f - mv^2}{mv^2} & \frac{-(K_f + K_r)}{mv} \end{bmatrix},\ [C] = \begin{bmatrix} \frac{K_f l_f}{J_z} \\ \frac{K_f}{mv} \end{bmatrix},\ [B] = \begin{bmatrix} \frac{-K_r l_r}{J_z} & \frac{1}{J_z} \\ \frac{K_r}{mv} & 0 \end{bmatrix}. \tag{4.9}$$

In order to achieve fast non-singular finite-time convergence to the target yaw rate and sideslip angle, the error is defined as [24]:

$$\underline{\mathrm{Er}} = \begin{bmatrix} a(\int_0^t (\dot{\psi}_r - \dot{\psi}) d\tau)^p + b(\int_0^t (\dot{\psi}_r - \dot{\psi}) d\tau)^g + (\dot{\psi}_r - \dot{\psi}) \\ a(\int_0^t (\beta_r - \beta) d\tau)^p + b(\int_0^t (\beta_r - \beta) d\tau)^g + (\beta_r - \beta) \end{bmatrix} \tag{4.10}$$

where $a > 0,\ b > 0,\ \dot{\psi}_r$ is the reference yaw rate and β_r is the reference sideslip angle. Here, we use two integral terms so that the convergence rate is reasonably high even if the error is low [24]. The sliding surface is then defined as:

$$\underline{\mathrm{S}} = \begin{bmatrix} S_1 \\ S_2 \end{bmatrix} = [K_e]\underline{\mathrm{Er}}, \tag{4.11}$$

where, $[K_e]$ is a 2×2 constant matrix.

The error dynamics at the sliding surface ($\underline{\mathrm{S}} = 0 \implies \underline{\mathrm{Er}} = 0$) is as follows:

$$a\left(\int_0^t e d\tau\right)^p + b\left(\int_0^t e d\tau\right)^g + e = 0 \implies \dot{e}_I = -a e_I^p - b e_I^g, \tag{4.12}$$

where $e_I = \int_0^t e d\tau$ and e is the error. From the above expression, we can observe that the sign of $\dot{e}_I$ is always opposite to e_I implying that the integral error will always be decreasing. In [24], it is suggested to use $1 < p < 2$ and $g > p$. When the integral error is high, $\dot{e}_I$ is high due to e_I^g term. As we get close to the target values, e_I will reduce. In this case, $\dot{e}_I$ is still reasonably high due to e_I^p term. Thus, using two integral terms results in faster decay of integral error and thus achieving higher convergence rate [24].

Also, $b \geq a$ will further help in increasing the magnitude of $\dot{e}_I$ when e_I is low. These conditions on $a,\ b,\ g$ and p ensures that $\dot{e}_I$ is reasonably high even if the error is extremely small. This in turn results in a faster convergence to the reference values.

It should be noted that in the above definition of the sliding surfaces, the exponents $(p,\ g)$ are positive. It is possible that e_I takes negative values during the maneuver and will result in imaginary values when raised to the positive powers p and g. This is physically incorrect. The imaginary values arising from the integral terms will create problem while calculating the actuator inputs during the maneuver. To avoid this, the above error functions are re-defined as:

$$\underline{\mathrm{Er}} = \begin{bmatrix} a \times sign(e_{I,\dot{\psi}})(|e_{I,\dot{\psi}}|)^p + b \times sign(e_{I,\dot{\psi}})(|e_{I,\dot{\psi}}|)^g + (\dot{\psi}_r - \dot{\psi}) \\ a \times sign(e_{I,\beta})(|e_{I,\beta}|)^p + b \times sign(e_{I,\beta})(|e_{I,\beta}|)^g + (\beta_r - \beta) \end{bmatrix}, \tag{4.13}$$

where $e_{I,\dot{\psi}} = \int_0^t (\dot{\psi}_r - \dot{\psi}) d\tau$ and $e_{I,\beta} = \int_0^t (\beta_r - \beta) d\tau$. As stated above, the parameter p is a fraction between 1 and 2 and $g > p$. We choose p and g from their feasible ranges such that their numerator and denominator are odd numbers. This will be helpful in the following calculations.

To obtain the actuator inputs, we start by calculating the derivative of the error function ($\dot{\underline{\mathrm{Er}}}$) as follows:

$$\dot{\underline{\mathrm{Er}}} = \begin{bmatrix} Er_{\dot{\psi}} \\ Er_{\beta} \end{bmatrix} = \begin{bmatrix} ap(e_{I,\dot{\psi}})^{p-1}(\dot{\psi}_r - \dot{\psi}) + bg(e_{I,\dot{\psi}})^{g-1}(\dot{\psi}_r - \dot{\psi}) + (\ddot{\psi}_r - \ddot{\psi}) \\ ap(e_{I,\beta})^{p-1}(\beta_r - \beta) + bg(e_{I,\beta})^{g-1}(\beta_r - \beta) + (\dot{\beta}_r - \dot{\beta}) \end{bmatrix}. \tag{4.14}$$

By choosing the numerator and denominator of p and g as odd numbers, the numerator of $p-1$ and $g-1$ will be an even number. This way negative $e_{I,\dot{\psi}}$ or $e_{I,\beta}$ raised to $p-1$ and $g-1$ respectively will not result in an imaginary number. This allows us to omit the

use of the $sign()$ function in the following steps.

As $[K_e]$ is constant, the sliding surface derivatives are calculated as follows:

$$\dot{\underline{S}} = [K_e]\dot{\underline{Er}} = [K_e][(\dot{\underline{z}}_r - \dot{\underline{z}}) + [E_1](\underline{z}_r - \underline{z})] \tag{4.15}$$

where

$$[E_1] = \begin{bmatrix} ap(e_{I,\dot{\psi}})^{p-1} + bg(e_{I,\dot{\psi}})^{g-1} & 0 \\ 0 & ap(e_{I,\beta})^{p-1} + bg(e_{I,\beta})^{g-1} \end{bmatrix}. \tag{4.16}$$

On substituting $\dot{\underline{z}} = [A]\underline{z} + [C]\delta_f + [B]\underline{u}$ in Equation 4.15, we get:

$$\dot{\underline{S}} = [K_e]\big(\dot{\underline{z}}_r - [A]\underline{z} - [C]\delta_f - [B]\underline{u} + [E_1](\underline{z} - \underline{z}_r)\big) \tag{4.17}$$

The convergence and stability of the controller is ensured if the following condition is satisfied [11] [12]

$$\underline{S}^T\dot{\underline{S}} < 0. \tag{4.18}$$

Therefore, we impose:

$$\dot{\underline{S}} = -\begin{bmatrix} \frac{K_1 S_1}{|S_1|+K_3} \\ \frac{K_2 S_2}{|S_2|+K_4} \end{bmatrix}, \tag{4.19}$$

where K_1, K_2, K_3 and K_4 are positive constants. Such a definition helps in avoiding the chattering problem due to finite sampling rate. On substituting Equation 4.19 in Equation 4.17 and solving for $\underline{u}$, we get:

$$\underline{u} = [B]^{-1}\big(\underbrace{\dot{\underline{z}}_r - [A]\underline{z} - [C]\delta_f}_{Feedforward} + \underbrace{[E_1](\underline{z}_r - \underline{z})}_{PI} + \underbrace{\underline{N}_{2\times 1}}_{Sliding\ Surface}\big), \tag{4.20}$$

where $\underline{N}$ is defined as:

$$\underline{N} = [K_e]^{-1}\begin{bmatrix} \frac{K_1 S_1}{|S_1|+K_3} \\ \frac{K_2 S_2}{|S_2|+K_4} \end{bmatrix}. \tag{4.21}$$

Here, the matrices $[B]$ and $[K_e]$ are being inverted while calculating the controller input. On observing the structure of $[B]$ in Equation 4.9, we can conclude that the inverse of $[B]$ always exists as long as $K_r \neq 0$ and $J_z \neq \infty$. These conditions are satisfied for all real vehicles. The elements of $[K_e]$ should be chosen such that its is invertible. This ensures that the controller is non-singular.

To summarise, the following parameters need to be tuned for implementing the fast non-singular integral terminal sliding mode controller:

1. Constants for error function: $a,\ b,\ p$ and g,
2. Elements of coupling matrix: $[K_e]$ such that it is invertible
3. Constants for saturation function: $K_1,\ K_2,\ K_3$ and K_4

We choose $a = 10,\ b = 1,\ p = 5/3,\ g = 3,\ [K_e] = I_{2\times2},\ K_1 = 6,\ K_2 = 2.2,\ K_3 = 0.1047$ and $K_4 = 0.0384$ using the trial and error approach. Similar to previous section, the model is simulated for two vehicle speeds (10 and 90 km/h) and fixed front steering angle ($\delta_f = 1°$) with the model parameters defined in the previous chapter. The reference values for $\dot{\psi}$ and β are set to the same values used in the previous section. The controller calculates the required value for δ_r and not K_w. So, we calculate $K_w = \delta_r/\delta_f$ in order to have an easier comparison with the actuator inputs calculated by the feedforward algorithm.

In Figure 4.4, we can observe that the yaw rate achieved by the active vehicle during both maneuvers is improved by 10%. The actuator inputs are higher when reference $\beta_r = 0$ as compared to the maneuver where reference $\beta_r \neq 0$. The initial increase or the slight delay in β observed in Figure 4.1 (FF controller) are absent in Figure 4.4 (SMC). The steady state values of the input calculated by the SMC are the same as those calculated by the feedforward controller. Similar observations can be drawn from Figure 4.5.

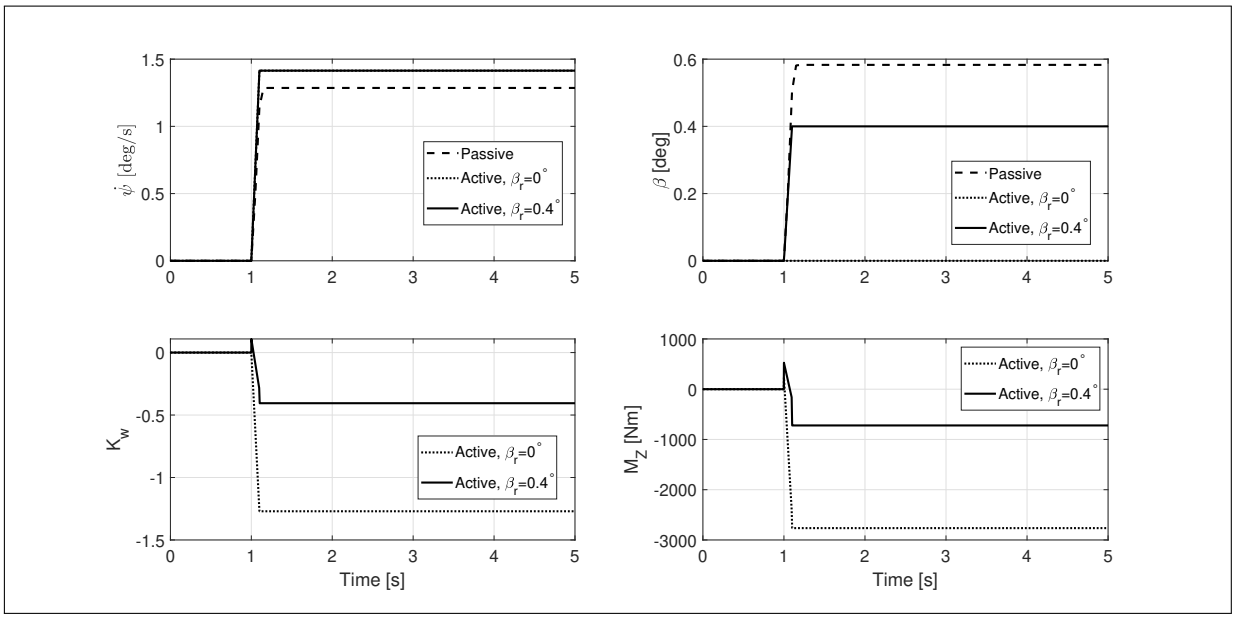

Figure 4.4: Sliding Mode Control (SMC) of LSTM ($v = 10\ km/h,\ \delta_f = 1°$) to obtain 10% higher $\dot{\psi}$ with 2 different β_r values.

The integral terminal sliding mode controller has improved the transient response of the system while maintaining the steady state accuracy similar to the feedforward controller.

However, the inputs calculated by the sliding mode controller during the transient phase of the maneuver change abruptly. This may introduce some undesired oscillations when testing the controller with the more realistic 14DOF model.

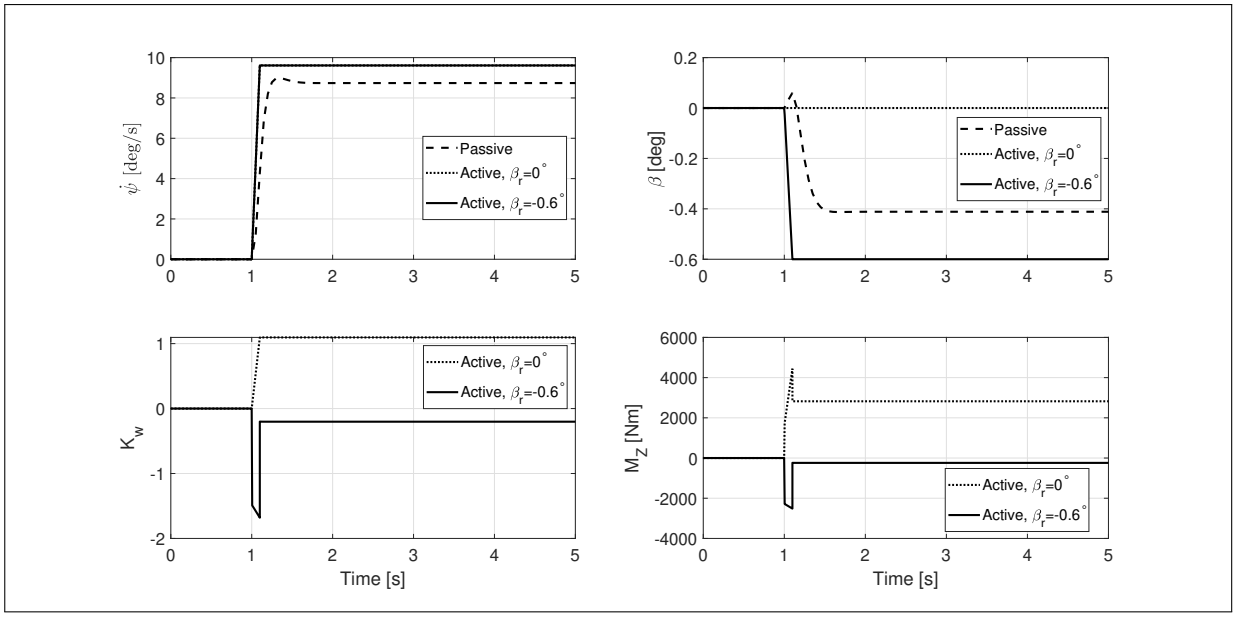

Figure 4.5: Sliding Mode Control (SMC) of LSTM ($v = 90\ km/h,\ \delta_f = 1°$) to obtain 10% higher $\dot{\psi}$ with 2 different β_r values.

The force and actuator dynamics become even more important when simulating the real vehicle behaviour. Typically, the effect of M_z on yaw rate is faster as compared to δ_r in the physical model. This is because the relaxation length for longitudinal force is smaller than that for the lateral force and therefore allows for a faster dynamics in the corresponding direction.

At the beginning of the maneuver in Figure 4.5 (Active, $\beta_r = -0.6°$), K_w and M_z are both negative. This means that, in absence of longitudinal and lateral force dynamics, the yaw rate will increase rapidly (due to $K_w < 0$) and will be balanced by the negative yaw moment in real time. In reality the relaxation length for longitudinal forces is smaller and the effect of applying negative yaw moment will be faster. This means that the yaw rate will start decreasing due to negative M_z before negative K_w can increase it.

4.3. Reference $\dot{\psi}_r$ and β_r

An appropriate definition of reference $\dot{\psi}_r$ and β_r is important while testing the controller with the 14DOF model. We define the reference $\dot{\psi}_r$ and β_r with respect to steering wheel angle (δ_{SW}). For any type of maneuver, we start by simulating the passive vehicle model

and collecting $\delta_{SW} - \dot{\psi}$ data. Then we fit a logistic function to the passive vehicle data obtained from the simulations. The fitted function is then scaled by the desired amount to obtain the reference values for the active vehicle.

The logistic function asymptotically approaches a finite value for high values of their arguments. This is helpful in incorporating friction limit while calculating the reference yaw rate. The logistic function is defined as follows [25] (Case 2*b*):

$$y = \frac{K}{1 + Ce^{-rx}} + d, \tag{4.22}$$

where K is the distance between the two asymptotic values of y (the dependent variable), C is the integration constant usually set to 1, r is the desired rate of change, x is the independent variable and d is an adjusting parameter. Following the notes for Case 2*b* in [25], at $x = 0$, $y = 0.5K + d$. For us, x is the steering wheel angle (δ_{SW}). Thus, to obtain $\dot{\psi}_r = 0$ when $\delta_{SW} = 0$, we set $d = -0.5K$.

The steps involved in generating the reference values for the active vehicle are as follows:

1. Obtain $\delta_{SW} - \dot{\psi}$ curve for the maneuver performed with passive vehicle
2. Define the logistic function as:

$$\dot{\psi}_{pas} = \frac{K}{1 + e^{-r\delta_{SW}}} - 0.5K,\ r = \frac{hv}{l(1 + kv^2)} \tag{4.23}$$

   where h and K are the parameters that need to be identified using the passive vehicle data.

3. Fit the logistic function ($\dot{\psi}_{pas}$) to passive vehicle data obtained in Step 1 and identify h and K
4. Calculate the reference yaw rate for the active vehicle as:

$$\dot{\psi}_r = \frac{K}{1 + e^{-r'\delta_{SW}}} - 0.5K,\ r' = \frac{\eta_{\dot{\psi}} hv}{l(1 + kv^2)} \tag{4.24}$$

   where $\eta_{\dot{\psi}}$ is the desired scaling factor for yaw rate. We set $\eta_{\dot{\psi}} = 1.1$ to achieve 10% improvement in yaw rate

5. β_r can be set to either 0 or to a non-zero value calculated as:

$$\beta_r = \begin{cases} \left(\frac{l_r}{v} - \frac{ml_f v}{lK_r}\right)\eta_\beta \dot{\psi}_{pas} & \left(\frac{l_r}{v} - \frac{ml_f v}{lK_r}\right) > 0 \\ \left(\frac{l_r}{v} - \frac{ml_f v}{lK_r}\right)(2 - \eta_\beta)\dot{\psi}_{pas} & \left(\frac{l_r}{v} - \frac{ml_f v}{lK_r}\right) \leq 0 \end{cases} \tag{4.25}$$

where η_β is the desired scaling factor for sideslip angle. Here, $\eta_\beta \in (0, 1)$. We set $\eta_\beta = 0.5$ to obtain 50% scaling.

The nonzero β_r values are calculated such that β_r for the active vehicle is always lower than that of passive vehicle for same steering input. As observed in the previous sections, this can reduce the required actuator inputs for achieving desired yaw rate. This is beneficial especially if the actuators are undersized for the given vehicle.

4.4. Extended Kalman Filter

In this section, we present the Extended Kalman Filter with the augmented state vector which also includes friction coefficient [10][22]. The EKF uses the nonlinear lateral dynamics model derived in Equations 3.2 and 3.3:

$$m(\dot{v}_y + \dot{\psi} v_x) = F_{xf} \sin\delta_f + F_{yf} \cos\delta_f + F_{xr} \sin\delta_r + F_{yr} \cos\delta_r \tag{4.26}$$

$$J_z \ddot{\psi} = l_f(F_{xf} \sin\delta_f + F_{yf} \cos\delta_f) - l_r(F_{xr} \sin\delta_r + F_{yr} \cos\delta_r) + M_z \tag{4.27}$$

Unlike in previous chapter, the lateral forces are calculated using the nonlinear three parameter Pacejka tyre model:

$$F_{yj} = D_j \sin[C_j \arctan(B_j \alpha_j)],\ D_j = \mu F_{zj} d_j,\ B_j = \frac{b_j}{\mu}, \qquad j = f, r, \tag{4.28}$$

where μ is the friction coefficient. Here, the parameters C_j, d_j and b_j are calculated by fitting the above equation to the normalised lateral force-average lateral slip curves generated by steady state ramp steer maneuver at 90 km/h. The lateral force is normalised dividing it by the static vertical load at the corresponding axle.

The calculation of lateral forces requires the knowledge of friction coefficient between tyre and road surface. This also cannot be measured directly and is estimated by the EKF. The augmented state vector then becomes:

$$\underline{z} = \begin{bmatrix} \underline{x} \\ \mu \end{bmatrix} = \begin{bmatrix} v_y \\ \dot{\psi} \\ \mu \end{bmatrix}, \tag{4.29}$$

where $\underline{x}$ is the state vector of the system. The system of equations then becomes:

$$\dot{\underline{z}} = \begin{bmatrix} \dot{v}_y \\ \ddot{\psi} \\ \dot{\mu} \end{bmatrix} = \begin{bmatrix} \underline{g}(\underline{z}, \underline{u}) \\ 0 \end{bmatrix} + \begin{bmatrix} \underline{w} \\ w_\mu \end{bmatrix} \tag{4.30}$$

where $\underline{g}$ is the nonlinear function defined in Equations 4.26 and 4.27, $\underline{u}$ is the input vector, $\underline{w}$ and w_μ are the process noise.

A lot of vehicles equipped with the Electronic Stability Controller (ESC) use sensors that measure yaw rate ($\dot{\psi}$) and lateral acceleration (a_Y). Thus we construct the measurement vector ($\underline{y}$) as:

$$\underline{y} = \left[\frac{a_y}{g}, \dot{\psi}, \frac{\hat{F}_{yf}}{F_{zf0}}, \frac{\hat{F}_{yr}}{F_{zr0}} \right]^T, \; \hat{F}_{yf} = m a_y \frac{l_r}{l}, \hat{F}_{yr} = m a_y \frac{l_f}{l} \tag{4.31}$$

where F_{zf0} and F_{zr0} is the static vertical load at the front and rear axle respectively. Here, introducing estimated lateral forces ($\hat{F}_{yj}$) in the measurement vector speeds up the estimation of friction coefficient [22].

The discrete EKF is then written as:

$$\dot{\hat{\underline{z}}}_{k+1} = \underline{f}(\hat{\underline{z}}_k, \underline{u}_k) + [G](\underline{y} - \hat{\underline{y}}_k) \tag{4.32}$$

$$\hat{\underline{y}}_{k+1} = \underline{h}(\hat{\underline{z}}_{k+1}, \underline{u}) \tag{4.33}$$

where $\underline{f}$ includes the equations of motion and $[G]$ is the gain matrix obtained by solving the Differential Riccati Equation [10]. The algorithm has been presented in detail in [10] and [22].

The EKF estimates β and filters the noisy signal of $\dot{\psi}$. These quantities are passed to the integral terminal sliding mode controller (ITSMC) to calculate the actuator inputs. The calculated inputs are then forwarded to the VI-CRT model which simulates vehicle dynamics and generates the clean signals for $\dot{\psi}$, a_y and other quantities. The noise is added to these clean signals before passing them to the EKF for estimation.

4.5. Conclusion

The two controllers: a feedforward controller and a integral terminal sliding mode controller are able to achieve the desired improvement in yaw rate while also achieving the desired sideslip angle for the LSTM. We investigated the effect of reference β_r value on the actuator inputs. If the reference $\beta_r = 0$, higher actuator inputs are required as compared

to the inputs required when β_r is set to a carefully chosen non-zero value.

Of the two controllers, the sliding mode control (SMC) resulted in better transient and steady state response of the LSTM. However, during transient conditions, the actuator inputs change abruptly before achieving the steady state. This may create some undesired oscillations during the maneuvers, especially when vehicle speed is high. Also, considering the lag due to different relaxation lengths for longitudinal and lateral forces, the SMC may cause some oscillations and overshoots in $\dot{\psi}$ and β.

The reference yaw rate and sideslip angles are generated by using a logistic function. The parameters of the logistic function are obtained by fitting it to the passive vehicle data. These parameters are then scaled to obtain the reference values for the active vehicle. We also present the extended Kalman filter used to estimate the vehicle sideslip angle. The filter also estimates the friction coefficient which is required to calculate the lateral forces.

The LSTM used in this chapter is a simple model with no uncertainties or external disturbances added to it. This allowed easier tuning of the SMC as the FF part of controller input (Equation 4.20) is able to exactly match the model dynamics. Further tuning may be required when implementing the SMC for 14DOF model or the actual vehicle where the FF may not match the actual dynamics. The actuator limits and its dynamics also need to be accounted for.

5 | Simulation Results

In this chapter, we test the two controllers: feedforward and sliding mode controller (SMC) using a more realistic 14DOF vehicle model. We use the VI-CarRealTime (VI-CRT) software and the predefined `CityCar_FullElectric` model to test the controller performance. The chosen model is a lightweight compact vehicle with relatively small electric motors attached to it. Some changes are made to the electric powertrain of the vehicle model and a rear steering system is also added to it.

We also test the SMC with an asymptotic observer added to the control loop. The controller developed in the previous chapters requires real time value of β. The sideslip angle cannot be directly measured using on-board sensors available in commercial vehicles. Thus, we use the observer to estimate the vehicle sideslip angle using a physical model and some measurable quantities like vehicle yaw rate and lateral acceleration. The observer can also prevent any chattering arising due to unmodelled dynamics [13].

We use the Extended Kalman Filter (EKF) as vehicle state observer to estimate sideslip angle and filter yaw rate sensor noise. We replicate the real sensor by adding zero-mean noise to the signals generated by the VI-CRT model. The EKF is added to the control loop and the controller is tested by performing steady-state and transient maneuvers.

In the following section, we highlight the performed steps to setup the actuators for the City Car VI-CRT model. Next, we test the feedforward controller using step steer maneuver. This will allows us to test the relevance of the parameter values, especially K_f and K_r, and also understand whether the actuators are properly sized. Following this, we test the integral terminal sliding mode controller (ITSMC) using several open and closed loop maneuvers performed at different vehicle speeds. We also test controller performance with EKF added to the control loop. Finally, we compare the ITSMC with EKF and a controller from the literature.

5.1. Actuators

The `CityCar_FullElectric` model is originally defined as a front wheel drive (FWD) vehicle with front steering only. The standard model does not have rear steering system

added to it, so it has been added in VI-CRT through following workflow:

1. Load the `CityCar_FullElectric` model
2. In the `Build Mode->CityCar_Steering->Steering System->Kinematics`, export all the kinematic data such as `Steer At Ground vs. Input Steer` of `Front Left Wheel` and `Front Right Wheel` with `Use Steer input and Jounce` option selected
3. In the `Build Mode->CityCar_FullElectric`, select the `Auxilliary #2` and add the rear steering system from the registered databases `mdids://carrealtime_shared/` by selecting the file `Auxilliary_rear_steering.xml`
4. In the `Build Mode->CityCar_FullElectric->Auxilliary_rear_steering->Kinematics`, import all the kinematic data exported in Step 2. For example, import the data to `Front Left Wheel` and `Front Right Wheel` with `Use Steer input and Jounce` option selected in `Steer At Ground vs. Input Steer` section

This establishes a kinematic equivalence with respect to front steering system.

There are various possibilities to generate yaw moment by Torque Vectoring (TV) such as braking one of the wheels, active differential and in-wheel motors (IWMs). In this thesis work, we use 4 IWMs with driving torques partitioned between the front and rear axle according to the static weight distribution. To simulate the actuator limits, we first modify the `CityCar_electric_powertrain` to replace the FWD-differential system with 4 IWMs.

The mechanical characteristics of the 4 IWMs are calculated such that the new powertrain is equivalent to the previous FWD-differential system in terms of the total torque (or longitudinal force) generated at the wheels. The transmission ratio of the motor is 1.35 and the drive ratio for the differential is 8.82. Therefore, in the existing powertrain, the torque transmitted to each of the front wheel is $8.82 \times 1.35/2 = 5.95$ times the torque generated by the motor (T_m).

Since the driving torque in the new powertrain is to be partitioned according to the static weight distribution, the mechanical characteristic of the front and rear IWM is calculated as:

$$\omega_{IWM} = \frac{\omega_{motor}}{8.82 \times 1.35},\ T_{front} = \frac{l_r \times 5.95 \times T_m}{l},\ T_{rear} = \frac{l_f \times 5.95 \times T_m}{l} \tag{5.1}$$

where, T_m is the motor torque, ω_{motor} is the FWD motor RPM, ω_{IWM} is the IWM motor RPM, T_{front} is torque at wheel by the front IWMs and T_{rear} is the torque at wheel by the rear IWMs. The mechanical characteristic of the FWD and the front and rear IWMs is presented in Figure 5.1.

The use of IWMs allows greater flexibility in generating driving or braking torques at the

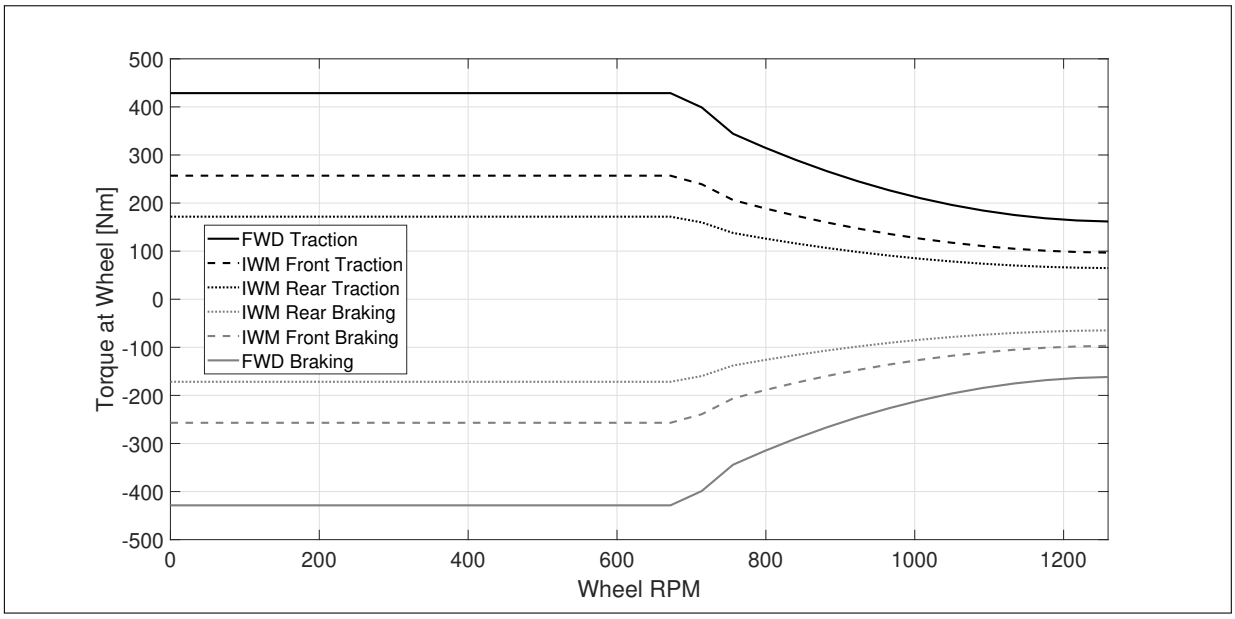

Figure 5.1: Mechanical characteristics of the FWD and IWMs vehicle.

4 wheels. By using IWMs, we can apply the same magnitude of driving torque to the left and right wheels of each axle in opposite direction to generate a yaw moment. This allows the vehicle to maintain its speed during the maneuver. However during the maneuver, the driving torques for generating the yaw moment should be carefully calculated such that no wheel gets saturated and locks or spins.

To apply a yaw moment M_z through TV, we start by calculating the torque demanded by the driver at front or rear wheels ($T_{driver,f/r}$) as:

$$T_{driver,f} = T_{m,f}(RPM) \times \frac{throttle}{100},\ T_{driver,r} = T_{m,r}(RPM) \times \frac{throttle}{100} \tag{5.2}$$

where $T_{m,f/r}$ is the maximum torque that can be applied by the corresponding IWM at the instantaneous RPM and $throttle$ is the amount of throttle in % used by the driver. Then, we calculate the drive moments required at the four wheels ($T_{M_z,ij}$) for generating the yaw moment M_z as shown below:

$$T_{M_z,FR} = \frac{l_r}{l}\frac{r_w}{c_f}M_z,\ T_{M_z,FL} = -T_{M_z,FR},\ T_{M_z,RR} = \frac{l_f}{l}\frac{r_w}{c_r}M_z,\ T_{M_z,RL} = -T_{M_z,RR} \tag{5.3}$$

where, r_w is the undeformed wheel radius, c_f is the front track width and c_r is the rear track width. Here, the magnitude of torque applied to left and right wheels is the same and the direction is opposite.

To avoid wheel locking and account for actuator limits, at the wheel with lower vertical

load of each axle, the following check and correction is performed:

if $|\mu F_{z,i}| < |F_{y,i}|$ **then**
  $T_{M_z,iR} = T_{M_z,iL} = 0$
else
  if $|T_{M_z,iR}| > \min(r_w\sqrt{(\mu F_{z,i})^2 - F_{y,i}^2}, (T_{m,iR} - T_{driver,i}))$ **then**
    $T_{M_z,iR} = \frac{T_{M_z,iR}}{|T_{M_z,iR}|} \times \min(r_w\sqrt{(\mu F_{z,i})^2 - F_{y,i}^2}, (T_{m,iR} - T_{driver,i}))$
  end if
end if

Here, the residual amount of tyre force $\left(\sqrt{(\mu F_{z,i})^2 - F_{y,i}^2}\right)$ is calculated by neglecting the presence of longitudinal forces. The drive moment for the left wheel of the axle is modified accordingly.

If the controller detects that the lateral force at the wheel exceeds its vertical load, then an anti-windup logic is activated which stops accumulating the integral error for both yaw rate and sideslip angle. If the controller detects that the driving torque required to generate M_z exceeds the available torque or friction limit, then the anti-windup logic only stops accumulating the integral β error. In this way, rear steering angle can still be controlled to achieve no steady state error in the yaw rate response.

5.2. Feedforward Control

In this section, we test the feedforward (FF) controller using the VI-CRT model. There are three key benefits of testing the FF controller first. The simulations can verify that the chosen parameters (especially K_f and K_r) are correct and physically relevant. The controller can also highlight whether the actuators, particularly the IWMs, are appropriately sized. The controller also serves as a simple method to check all the subsystems/functions are working as they should. If the actuators are adequate, the FF controller should reach the target values at least for low lateral accelerations $< 4\ m/s^2$ [4].

We test the feedforward controller by performing step steer maneuver at low and high speed. For both maneuvers, the steering angle starts to increase at 5 s and reaches the maximum value within 0.1 s. For low speed maneuver, the vehicle speed is set to 5 m/s and the steering wheel angle is increased from 0° to 60°. The high speed maneuver is performed at the vehicle speed of 25 m/s with the steering wheel angle increased from 0° to 20°. For both the maneuvers, $\eta_{\dot{\psi}} = 1.1$ and $\eta_\beta = 0.5$. The vehicle response and actuator inputs are presented in Figures 5.2, 5.3, 5.4 and 5.5.

In Figures 5.2 and 5.3, we can observe that the FF controller is able to reach the reference

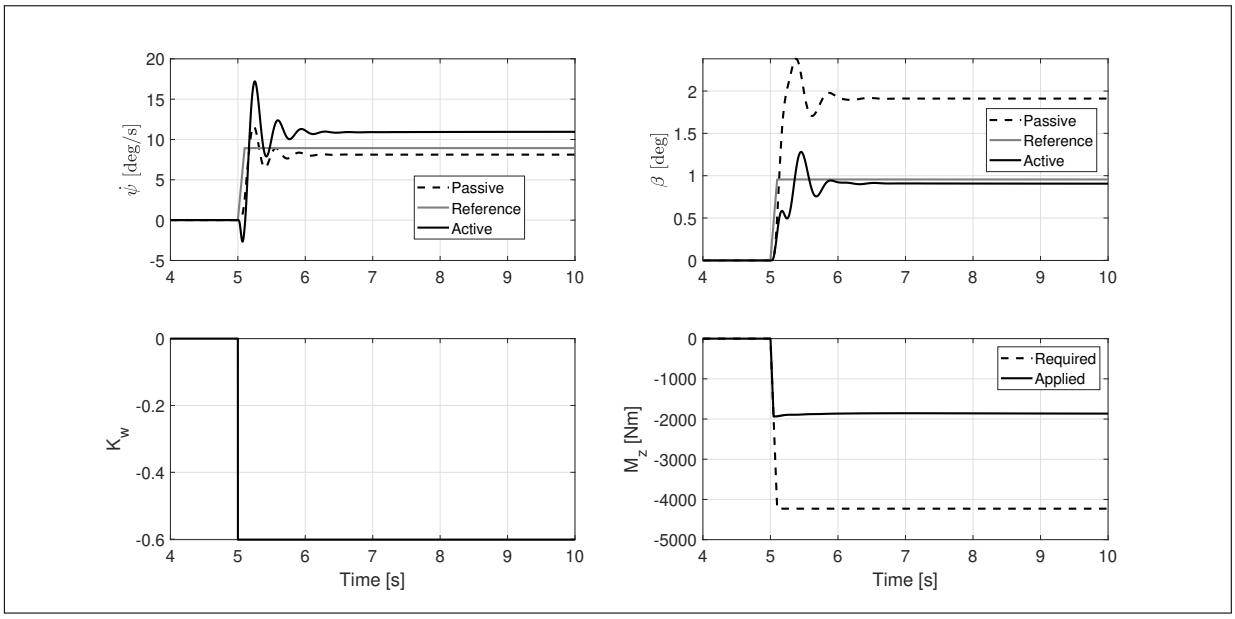

Figure 5.2: Low speed step steer maneuver performed with FF controller with $\beta_r \neq 0$.

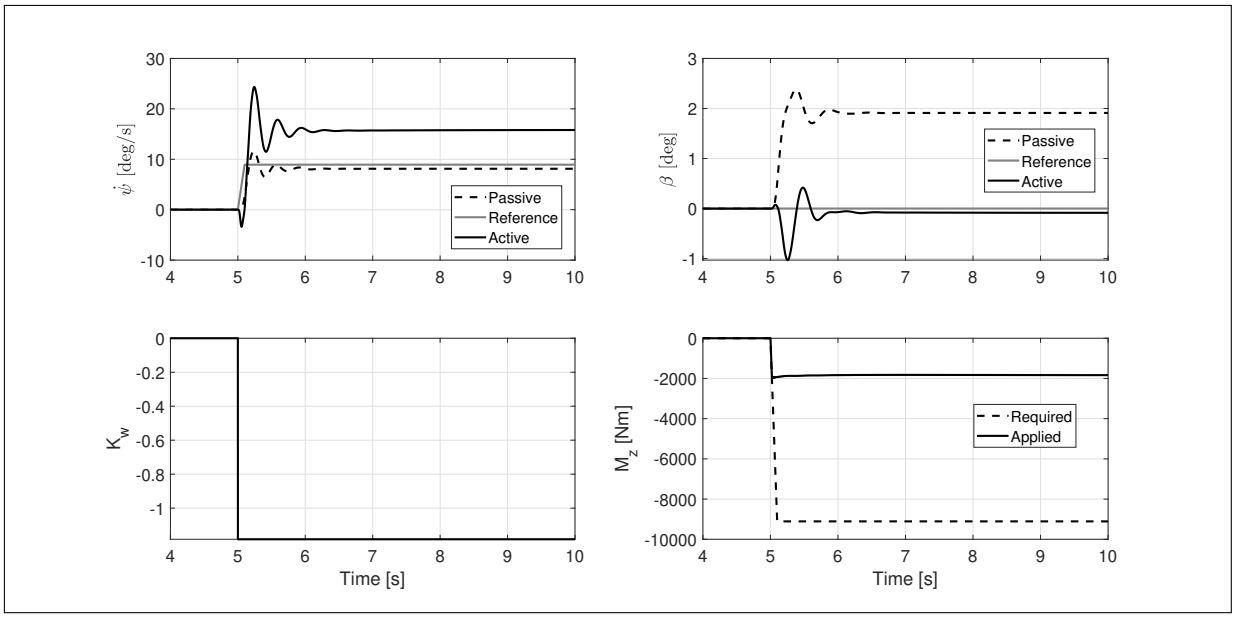

Figure 5.3: Low speed step steer maneuver performed with FF controller with $\beta_r = 0$.

β_r value with minimal steady state error. The controller is not able to achieve the desired yaw rate as the IWMs cannot generate the required yaw moment. This indicates that the IWMs are not adequately sized to maintain both vehicle speed and provide the yaw moment. In Figures 5.4 and 5.5, the vehicle is not able to track both reference yaw rate and sideslip angle. This is because the desired lateral acceleration exceeds 4 m/s^2 (LSTM assumptions are not valid) and the IWMs are again not able to generate the desired torques.

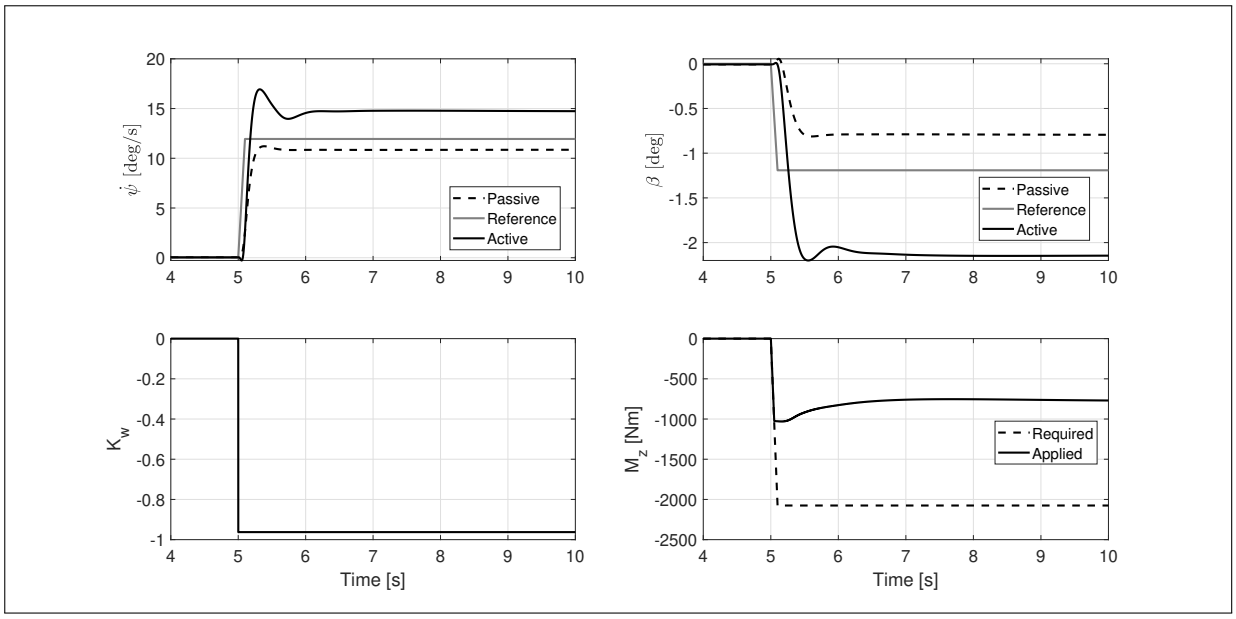

Figure 5.4: High speed step steer maneuver performed with FF controller with $\beta_r \neq 0$.

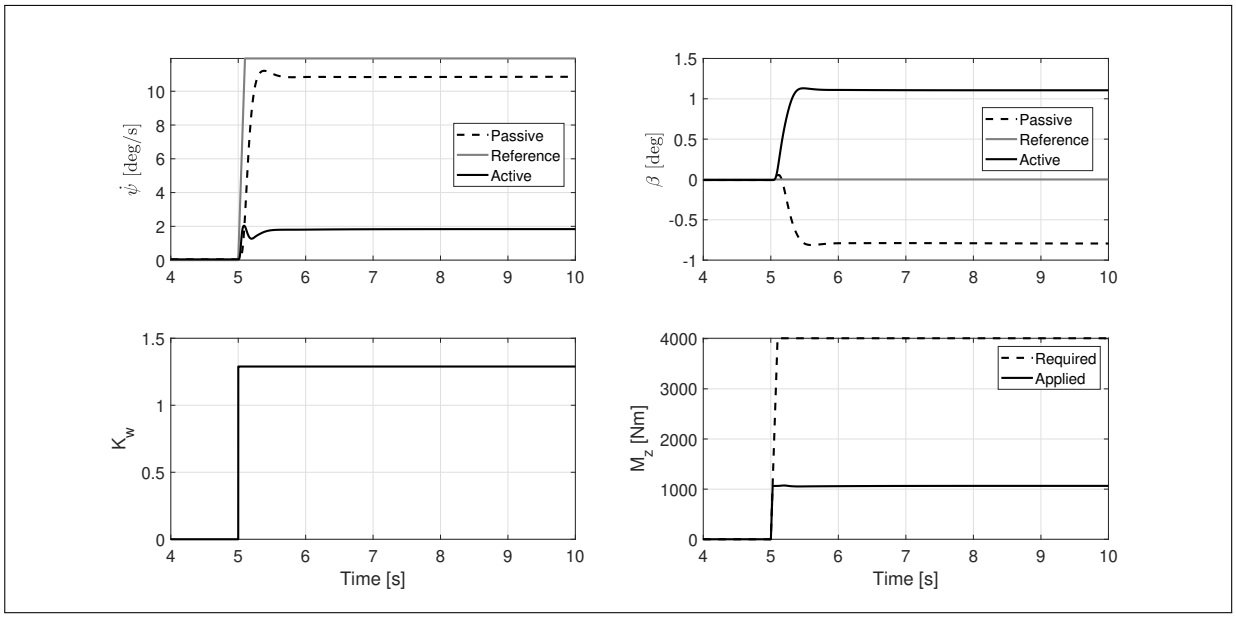

Figure 5.5: High speed step steer maneuver performed with FF controller with $\beta_r = 0$.

5.3. Integral Terminal Sliding Mode Control

In the previous section, we observed that the FF controller alone is not sufficient to achieve the target values, even in ideal conditions without any sensor noise. The yaw moment generated by IWMs is also limited and often gets saturated. Thus we focus on developing a feedback controller which can take advantage of ARS if IWMs get saturated.

In order to take advantage of ARS when IWMs are saturated, we test the controllers with two sets of sliding surfaces: one with each sliding surface made of either yaw rate or sideslip angle error function i.e. off-diagonal elements of $[K_e]$ are 0 and other with at least one sliding surface defined as linear combination of the two error functions i.e. at least one off-diagonal element of $[K_e]$ is not 0. In order to decided whether both or only one of the surface needs to be defined as linear combination of the two error functions, we recall the controller input derived in the previous chapter (Equation 4.20):

$$\underline{\mathrm{u}} = [B]^{-1}\big(\underbrace{\dot{\underline{\mathrm{z}}}_r - [A]\underline{\mathrm{z}} - [C]\delta_f}_{Feedforward} + \underbrace{[E_1](\underline{\mathrm{z}}_r - \underline{\mathrm{z}})}_{PI} + \underbrace{\underline{\mathrm{N}}_{2\times 1}}_{Sliding\ Surface}\big). \tag{5.4}$$

In the above equation defining actuators input, the only term affected by the sliding surface definition is $[B]^{-1}\underline{\mathrm{N}}$ which is defined as:

$$[B]^{-1}\underline{\mathrm{N}} = \begin{bmatrix} \frac{-mvK_{e_{21}}K_1S_1}{K_r(|S_1|+K_3)} + \frac{mvK_{e_{11}}K_2S_2}{K_r(|S_2|+K_4)} \\ \frac{(J_zK_{e_{22}}-l_rmvK_{e_{21}})K_1S_1}{|S_1|+K_3} + \frac{(-J_zK_{e_{12}}+l_rmvK_{e_{11}})K_2S_2}{|S_2|+K_4} \end{bmatrix} /det([K_e]), \tag{5.5}$$

where $K_{e_{ij}}$ are the elements of $[K_e]$ matrix. The first row of the above matrix will contribute to the calculation of δ_r while the second row will contribute to the calculation of M_z.

On observing the two rows, we can conclude that $K_{e_{12}} \leq 0$ and $K_{e_{21}} \leq 0$ in order for the actuator inputs to be always proportional to the sliding surfaces. We choose to define only the second sliding surface as linear combination of yaw rate and sideslip angle error functions i.e. impose $K_{e_{12}} = 0$. This will ensure that $det(K_e) \neq 0$ and the controller will be non-singular.

The set of parameters tested with the VI-CRT vehicle model are as follows:

1. Constants for error function: $a = 10,\ b = 1,\ p = 9/7$ and $g = 3$,
2. Elements of coupling matrix: $[K_e] = \begin{bmatrix} 3 & 0 \\ -0.008 & 1 \end{bmatrix}$ ($[K_e]$ is invertible),
3. Constants for saturation function: $K_1 = 30,\ K_2 = 9,\ K_3 = 1.571$ and $K_4 = 1.833$,
4. Reference scale: $\eta_{\dot{\psi}} = 1.1,\ \eta_\beta = 0.5$.

The above set of values are obtained through trial-and-error method such that vehicle response during low and high speed maneuvers is smooth and stable. The result for low speed ($5\ m/s$) ramp steer maneuver is presented in Figure 5.6.

In Figure 5.6, we observe a bump in yaw rate and sideslip angle which can be attributed to

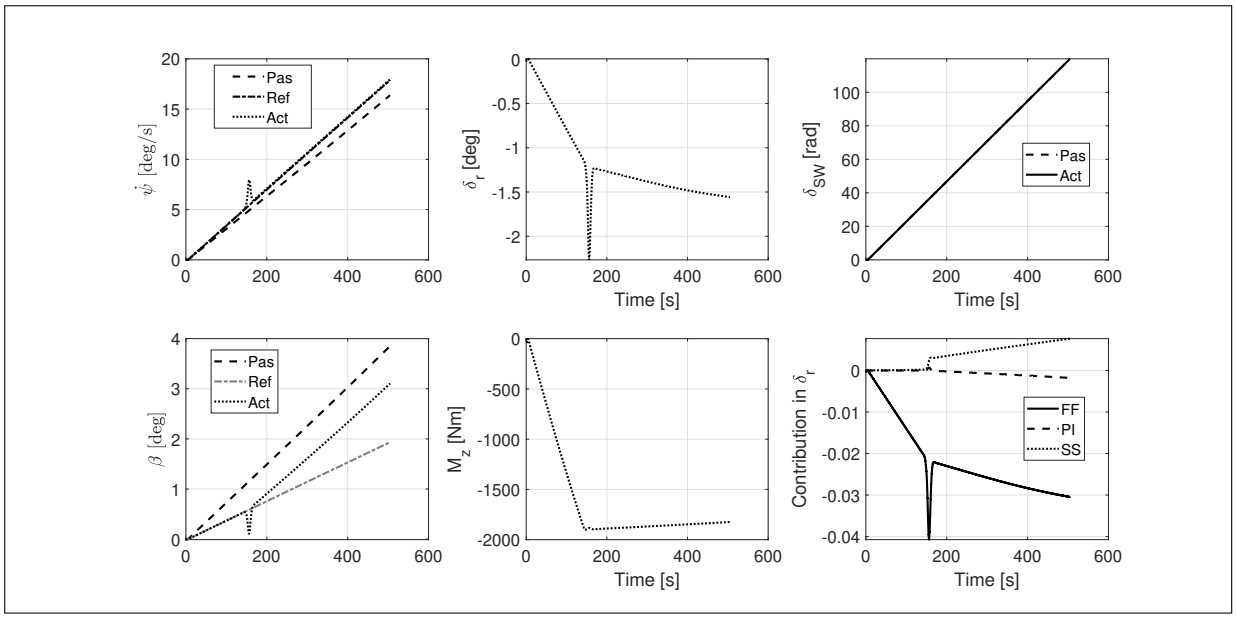

Figure 5.6: Vehicle response during low speed ramp steer maneuver with FF part included.

the feedforward part of Equation 5.4. This bump is exaggerated during high speed ramp steer maneuver, especially at high lateral accelerations. In order to avoid such bumps, we decide to remove the feedforward part of the controller and re-tune the parameters in order to obtain smoother vehicle response during both steady state and transient maneuvers. The controller input is now calculated as follows:

$$\underline{u} = [B]^{-1}\Big(\underbrace{[E_1](\underline{z}_r - \underline{z})}_{PI} + \underbrace{\underline{N}_{2\times 1}}_{Sliding\ Surface}\Big). \tag{5.6}$$

After trial-and-error, the following parameter values are used for further simulations:

1. Constants for error function: $a = 1,\ b = 1,\ p = 9/7$ and $g = 3$,
2. Elements of coupling matrix: $[K_e] = \begin{bmatrix} 2 & 0 \\ 0 & 1 \end{bmatrix}$ ($[K_e]$ is invertible)
3. Constants for saturation function: $K_1 = 2400,\ K_2 = 180,\ K_3 = 78.54$ and $K_4 = 104.72$,
4. Reference scale: $\eta_{\dot{\psi}} = 1.1,\ \eta_\beta = 0.5$.

The controller was tested with ramp steer and step steer maneuvers performed at low ($5\ m/s$) and high ($25\ m/s$) speeds and with a close loop constant radius curve maneuver.

We present the low speed ramp steer maneuver results in Figures 5.7 and 5.8. The vehicle speed is set to $5\ m/s$ and the steering wheel is increased from $0°$ to $120°$ in $500\ s$. The

maneuver is started at $t = 5\ s$ so that the vehicle can achieve a steady state condition before starting the maneuver. In Figure 5.7, we can observe that the reference yaw rate is achieved while also reducing the vehicle sideslip angle. In Figure 5.8, we can observe that the active vehicle shows an improvement in all the plots while also maintaining the vehicle speed.

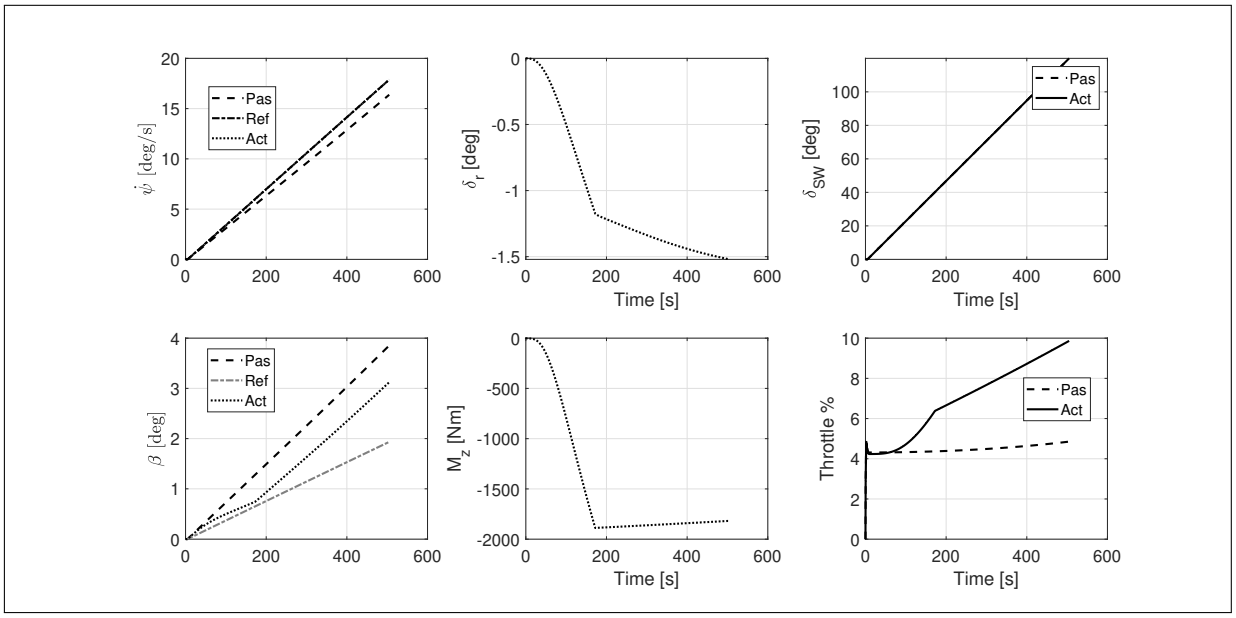

Figure 5.7: Low speed ramp steer maneuver: 10% improvement in $\dot{\psi}$ and $\eta_\beta = 0.5$.

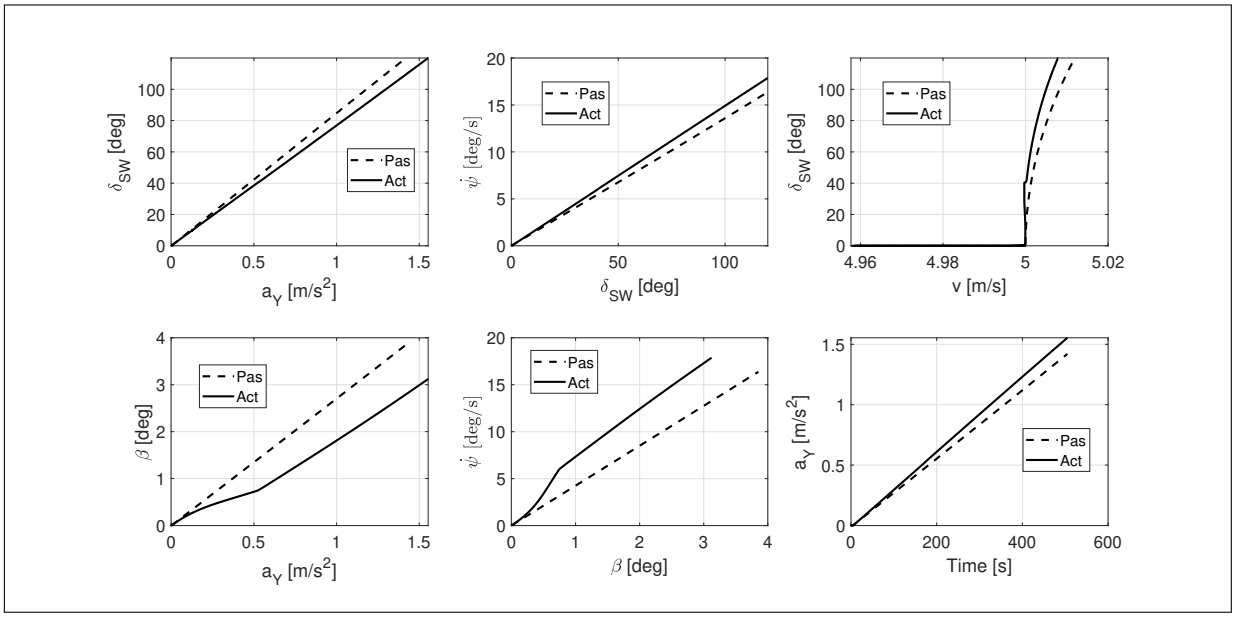

Figure 5.8: Relevant lateral dynamics quantities for low speed ramp steer maneuver.

The results for high speed ramp steer maneuver are presented in Figures 5.9 and 5.10.

The vehicle speed is set to 25 m/s while other settings are kept the same as those used for the low speed ramp steer maneuver. In Figure 5.9, we can see that the controller is able to track the reference yaw rate and sideslip angle up to 200 s ($a_Y \approx 8\ m/s^2$). After that, the controller is only able to track the reference yaw rate.

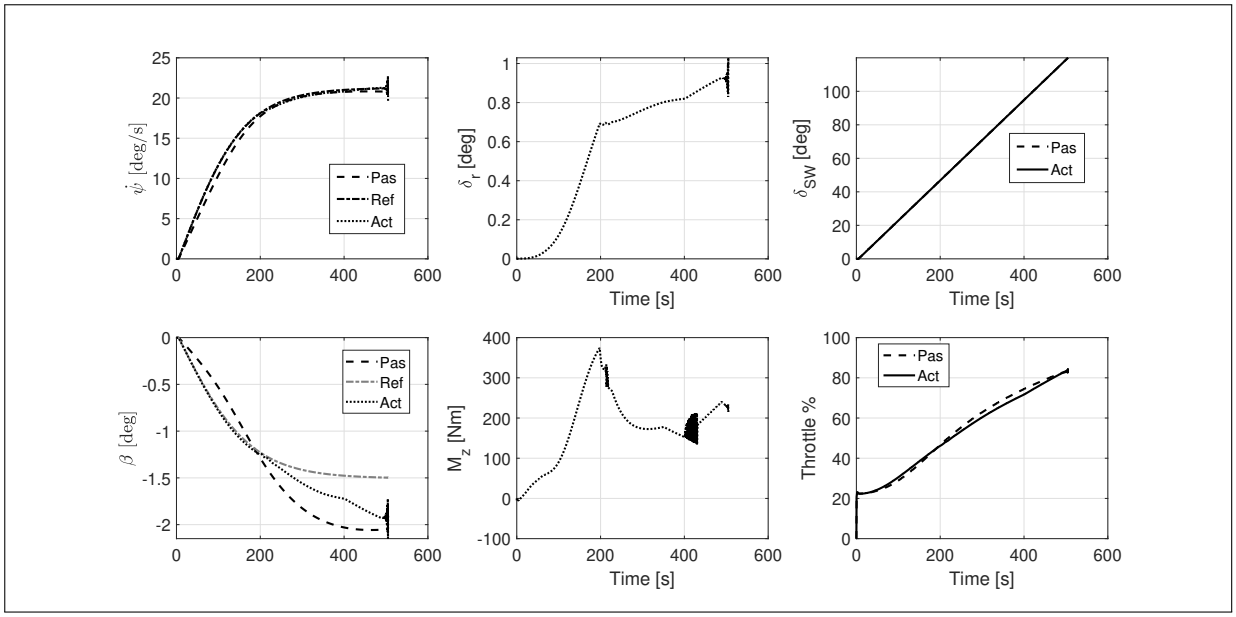

Figure 5.9: High speed ramp steer maneuver: 10% improvement in $\dot{\psi}$ and $\eta_\beta = 0.5$.

For very high steering input, we observe some oscillations in both yaw rate and sideslip angle. We suspect that these are caused due to presence of an unstable spiral equilibrium point near the friction limit as can be seen in Figure 5.10 ($\beta - \dot{\psi}$ plot). These oscillations occur at high lateral accelerations near the friction limit which a normal driver may not reach in common road driving conditions.

We also test the controller with a close loop steady state maneuver. The vehicle is run in straight line for 5 s and then the speed is increased from 5 m/s to 25 m/s in 55 s while maintaining the turn radius of 70 m. The results are presented in Figures 5.11 and 5.12. In Figure 5.11, we can observe that the active vehicle can achieve the same yaw rate with a lower steering wheel angle input and negligible difference in throttle input during low lateral accelerations. At high lateral acceleration, the steering wheel angle required to achieve the same yaw rate is only marginally higher as compared to the passive vehicle.

In Figure 5.12, we can observe that the magnitude of the sideslip angle of the active vehicle is lower in comparison to that of passive vehicle. Some minor oscillations can be observed in all the plots for low lateral accelerations. These oscillations do not affect the driver inputs significantly and the driver is able to steer the vehicle on the desired path.

Finally, we tested the controller's transient performance using step steer maneuver. The

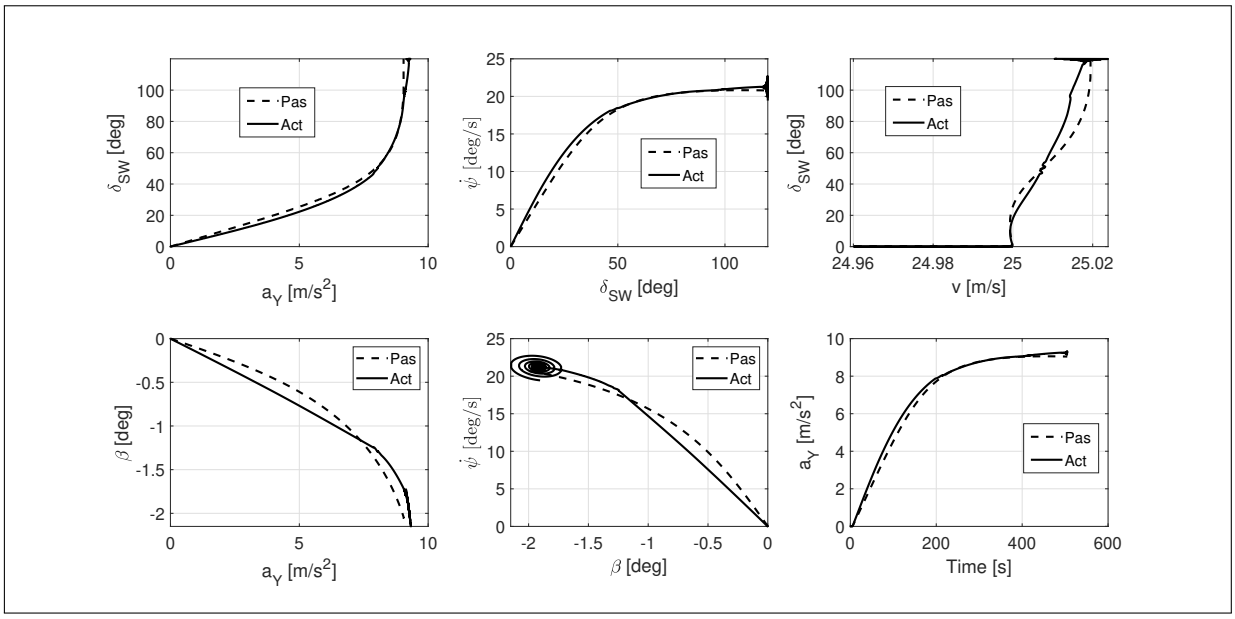

Figure 5.10: Relevant lateral dynamics quantities for high speed ramp steer maneuver.

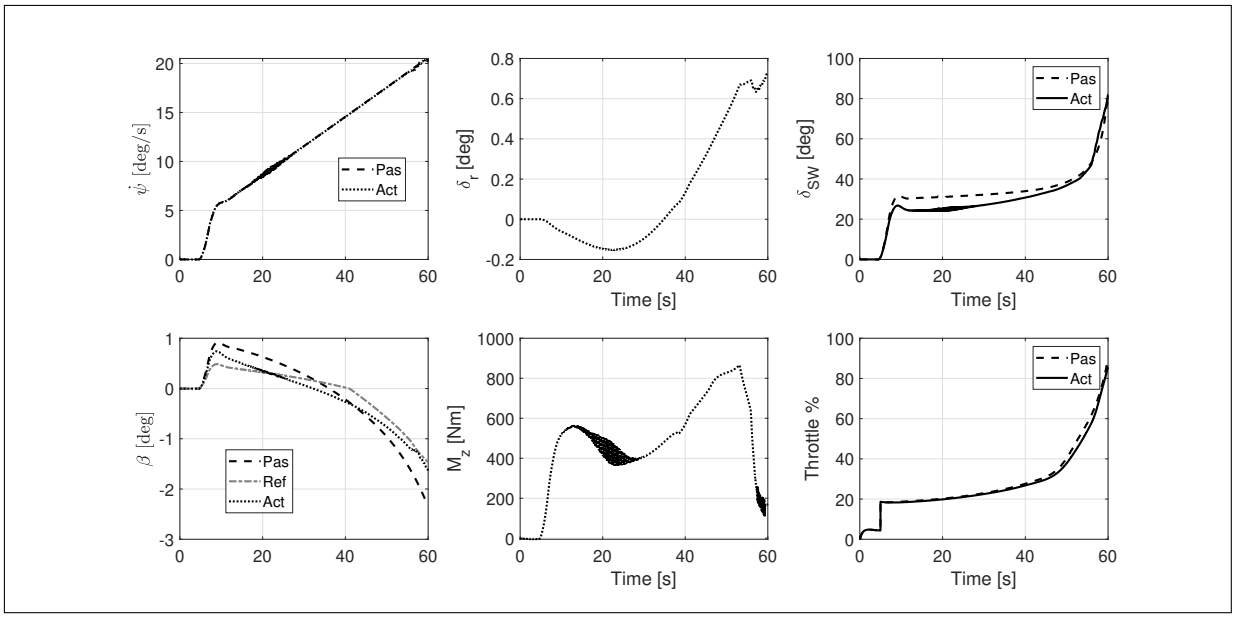

Figure 5.11: CRC maneuver with 10% improvement in yawrate and non-zero β_r values.

vehicle is run in straight line for 5 s and then the steering angle is increased and reaches the maximum value in 0.1 s. For the low speed maneuver, the vehicle speed is set to 5 m/s and δ_{SW} is increased from 0° to 60°. For the high speed maneuver, the vehicle speed is set to 25 m/s and δ_{SW} is increased from 0° to 20°. Here, we present the system response starting from 4 s to highlight that the vehicle has achieved a steady state before the start of maneuver.

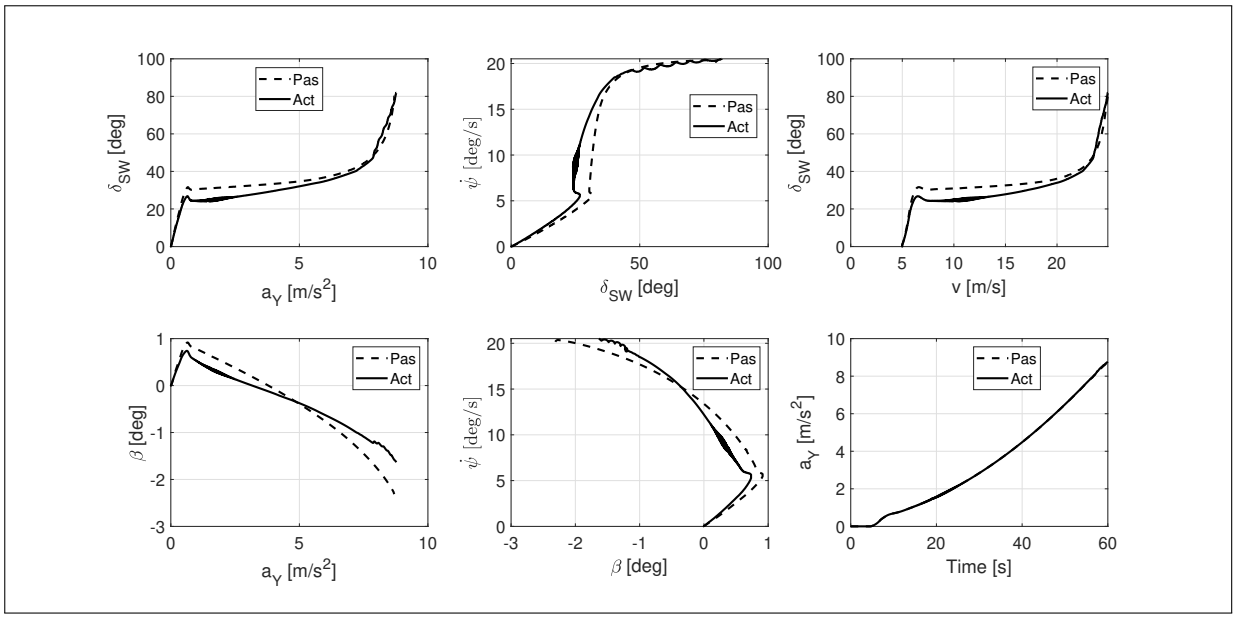

Figure 5.12: Relevant lateral dynamics quantities for CRC maneuver.

The results for low speed step steer maneuver are presented in Figures 5.13 and 5.14. In Figure 5.13, we can observe that the controller tracks the reference signal slowly. By tuning the controller, we could speed up the tracking of the reference signal. This however resulted in significant oscillations during high speed steady state maneuvers. The active vehicle shows minor improvement in vehicle sideslip angle. In Figure 5.14, the active vehicle show only minor improvement when compared to the passive vehicle.

We present the results for high speed step steer maneuver in Figures 5.15 and 5.16. In Figure 5.15, we can see that the controller converges to the reference yaw rate within 1 s after beginning of the maneuver with minimal oscillations thereafter. The magnitude of the sideslip angle of the active vehicle is approximately 12% higher in comparison to the passive vehicle. Therefore, the active vehicle is able to achieve the desired 10% improvement in yawrate without excessively increasing the magnitude of the sideslip angle.

In all the maneuvers, the IWM gets saturated first. Even with the IWM saturated, the sliding mode controller is able to achieve the target yaw rate in almost all the cases. The controller prioritises yaw rate tracking over sideslip angle tracking. This results in less than desired improvement in sideslip angle in comparison to the passive vehicle.

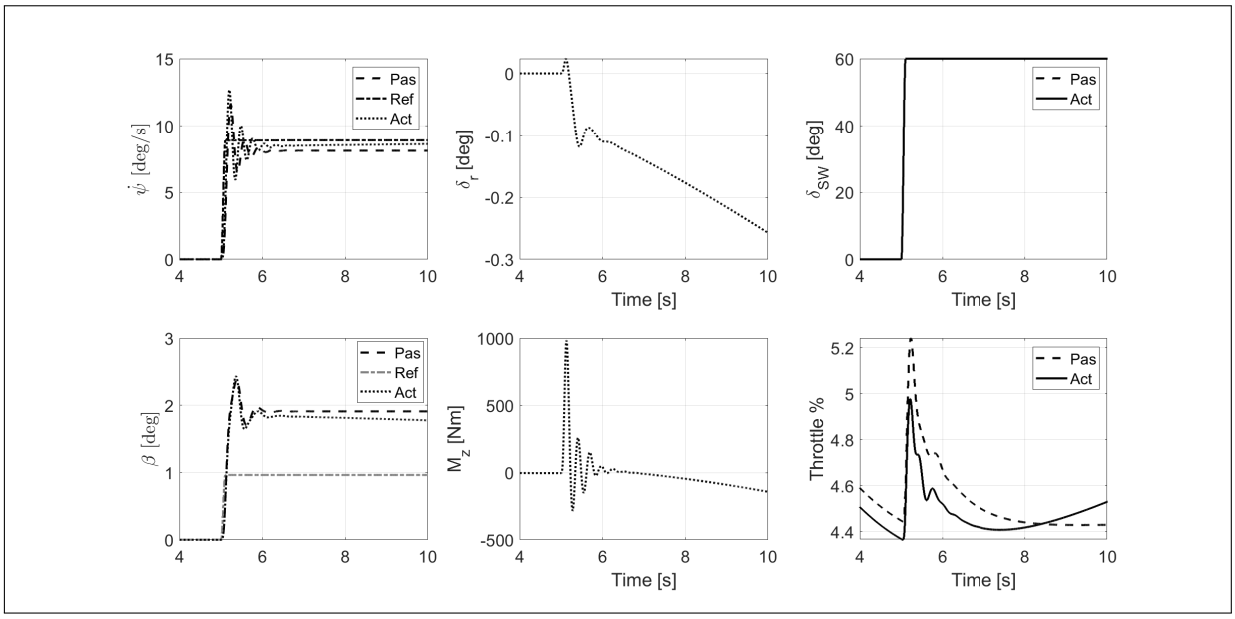

Figure 5.13: Low speed step steer maneuver with 10% improvement in yawrate and $\eta_\beta = 0.5$.

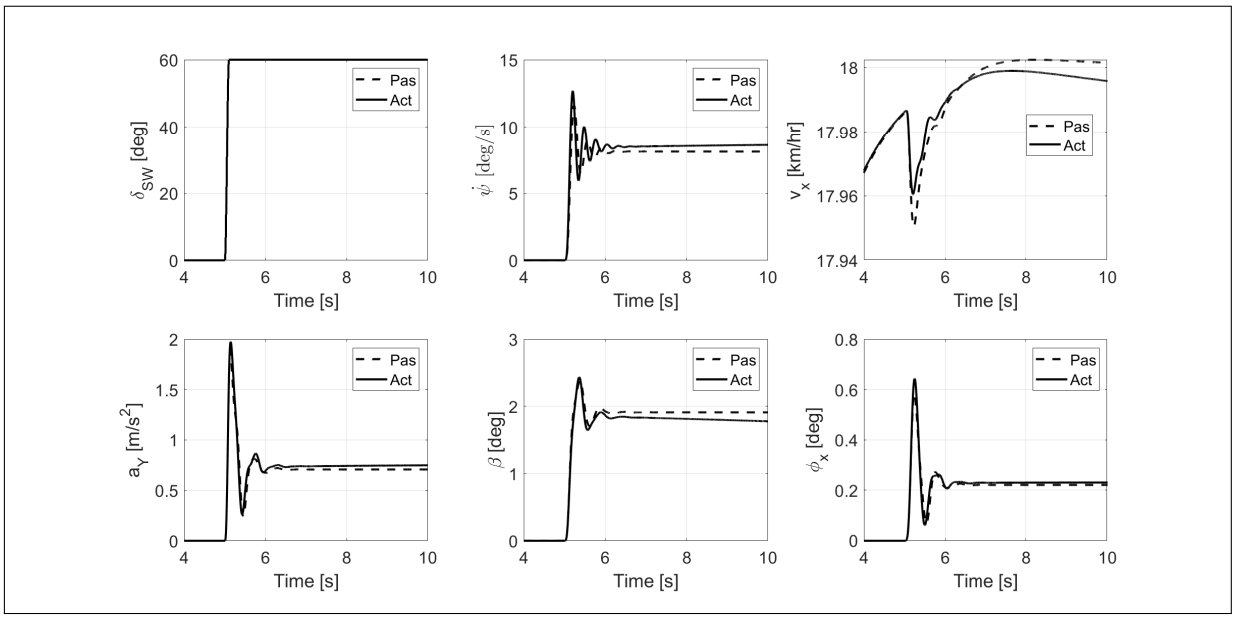

Figure 5.14: Relevant lateral dynamics quantities for low speed step steer maneuver.

5.4. Observer in the Loop

We re-tune the controller parameters with EKF added to the control loop because oscillations are observed in high speed ramp steer maneuver simulation performed with the

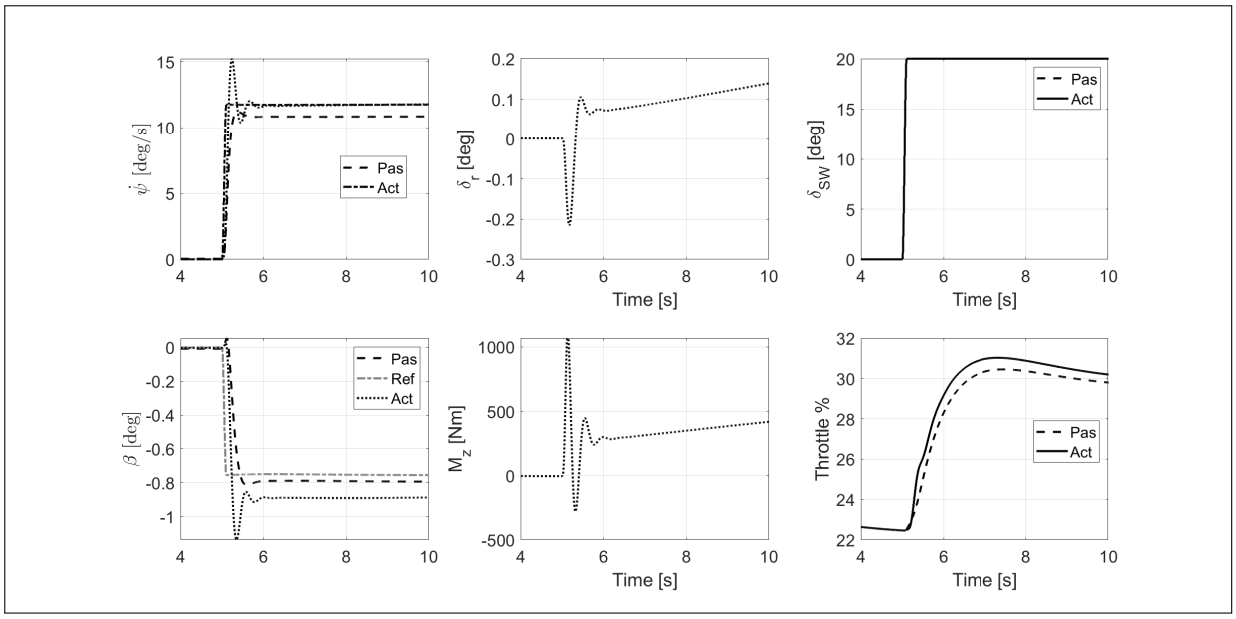

Figure 5.15: High speed step steer maneuver with 10% improvement in yawrate and $\eta_\beta = 0.5$.

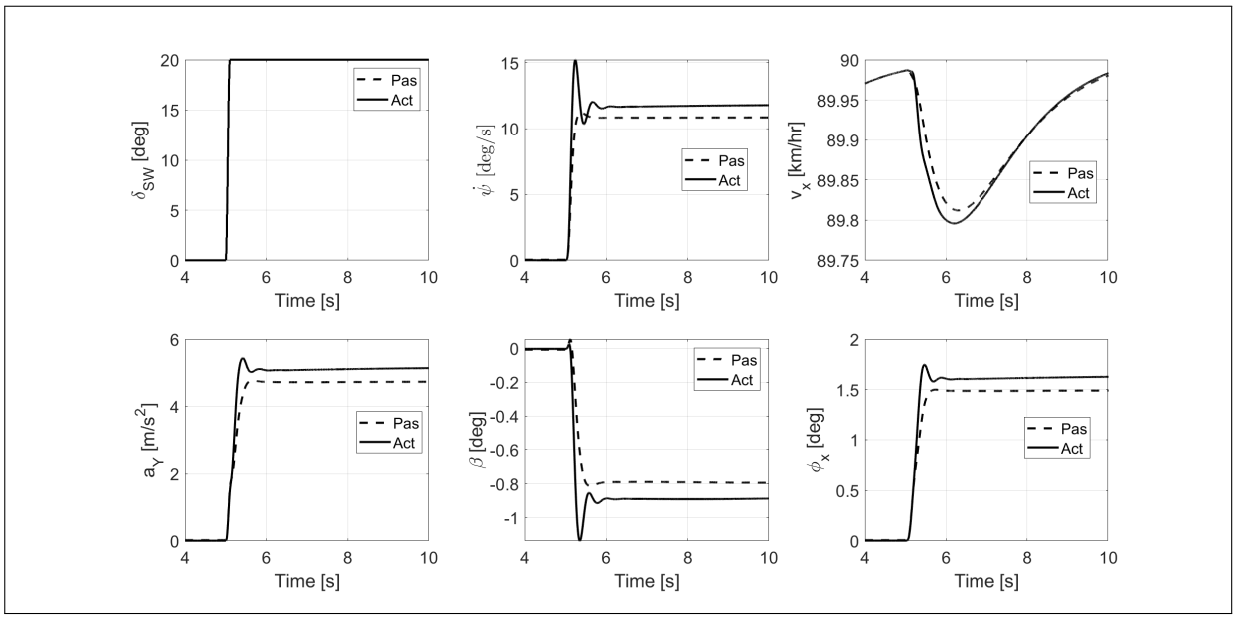

Figure 5.16: Relevant lateral dynamics quantities for high speed step steer maneuver.

previous set of parameters. The following parameter values are changed:

$$K_1 = 2100,\ K_3 = 349.0659,\ K_4 = 209.4395. \tag{5.7}$$

The maneuvers used to test the controller with EKF are same as those used in the previous section. A direct comparison of system response between the controller with and without

EKF is unfair as the controller parameters had to be changed. Thus we present and compare true, estimated and reference values of vehicle states only for the system with EKF added to the control loop.

We present the high speed ramp steer maneuver results in Figure 5.17. The EKF is able to accurately estimate β up to lateral acceleration of approximately 8 m/s^2. For high lateral accelerations, the estimated value of β is lower than the true value of β. For such high lateral accelerations, the controller is able to track the reference yaw rate and not the reference sideslip angle. The friction coefficient (μ) estimation is poor initially and improves as the lateral acceleration increases. This is expected as friction coefficient is non-observable for low lateral acceleration [22].

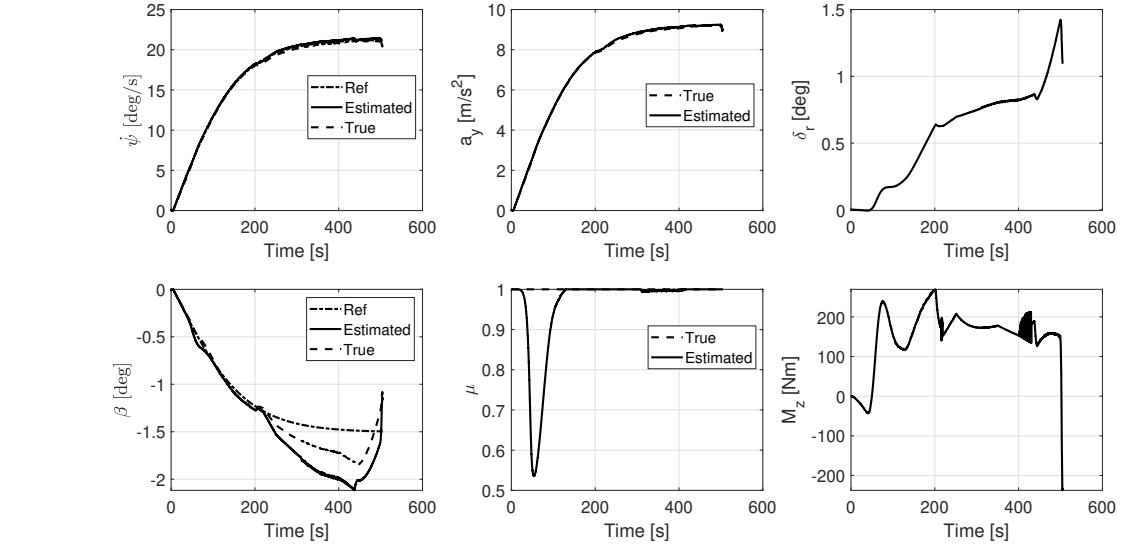

Figure 5.17: System response during high speed ramp steer maneuver with EKF added to the loop.

The close loop constant radius curve (CRC) maneuver results are presented in Figure 5.18. In Figure 5.18, we can observe that the driver of vehicle with EKF is able to negotiate the curve similar to the passive vehicle. The vehicle with EKF does not exhibit small amplitude oscillations which can be observed in the yaw rate response of the vehicle without EKF between $20 - 30$ s (Figure 5.11). The sideslip angle performance of the vehicle with EKF is slightly better as compared to the passive vehicle for moderate and high lateral accelerations.

In Figure 5.19, we present the low speed ramp steer maneuver results. The true yaw rate and vehicle sideslip angle with EKF are higher than the estimated value. The controller is able to track the reference yaw rate and sideslip angle for estimated values. In [22], the

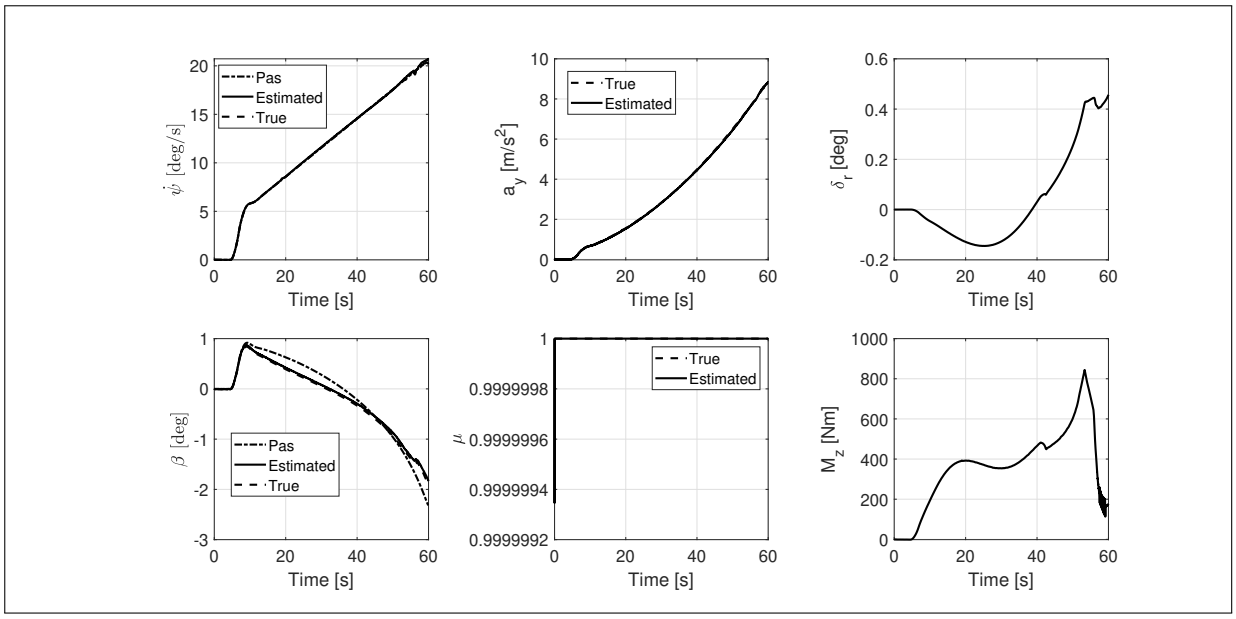

Figure 5.18: System response during CRC maneuver with EKF added to the loop.

author highlight that convergence may be poor for extremely low lateral accelerations. This is because for such low lateral accelerations, the friction coefficient becomes non-observable as cornering stiffness does not depend on it. This can lead to poor convergence of the filter.

At low vehicle speed, the vehicle dynamics is relatively stable and slow. Even if the true yaw rate is higher than estimated, it increases linearly with time and steering input. Thus, the vehicle response to steering input at low speed is consistent and qualitatively similar to that of active vehicle without EKF. This may not require the driver to make any abrupt changes in steering wheel input during low lateral acceleration maneuvers.

Next, we present the results for high speed step steer maneuver in Figure 5.20. The vehicle with EKF does not show large overshoots in yaw rate and sideslip angle when compared to the system response of vehicle without EKF (Figure 5.15). The yaw rate response of the controller with EKF converges slower than the controller without EKF. The sideslip angle response with EKF added to the control loop appear to be diverging. The poorer transient performance of the controller with EKF when compared to the controller without EKF is due to difference in controller parameters. Similar observations can be made from the low speed step steer maneuver results presented in Figure 5.21.

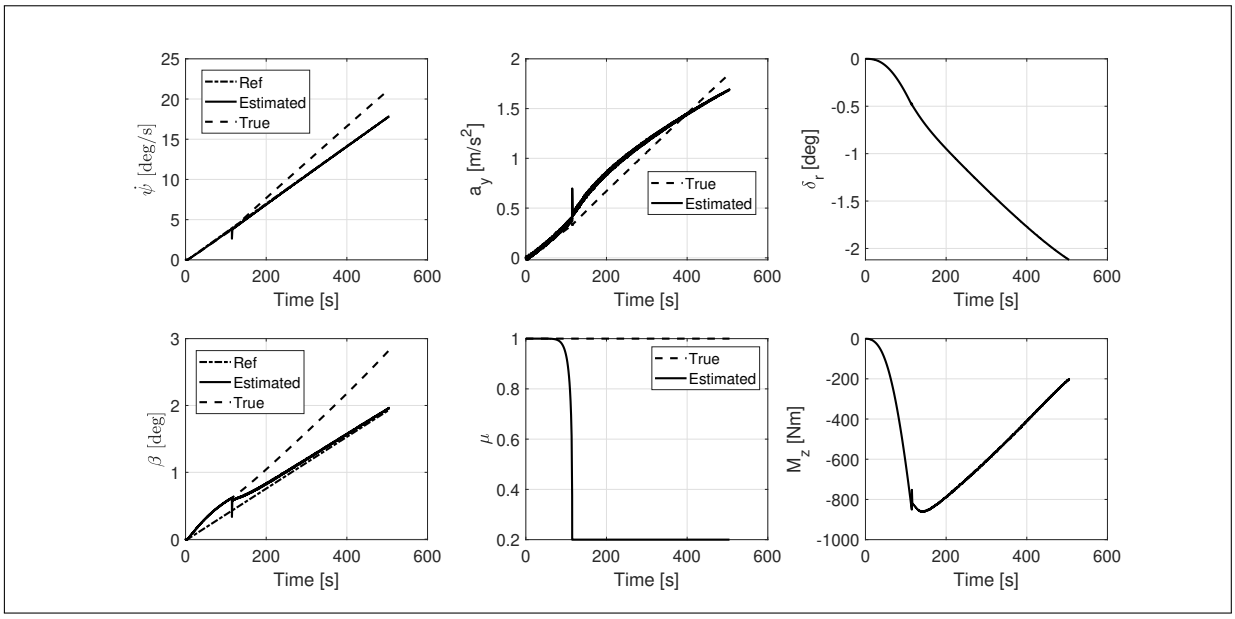

Figure 5.19: System response during low speed ramp steer maneuver with EKF added to the loop.

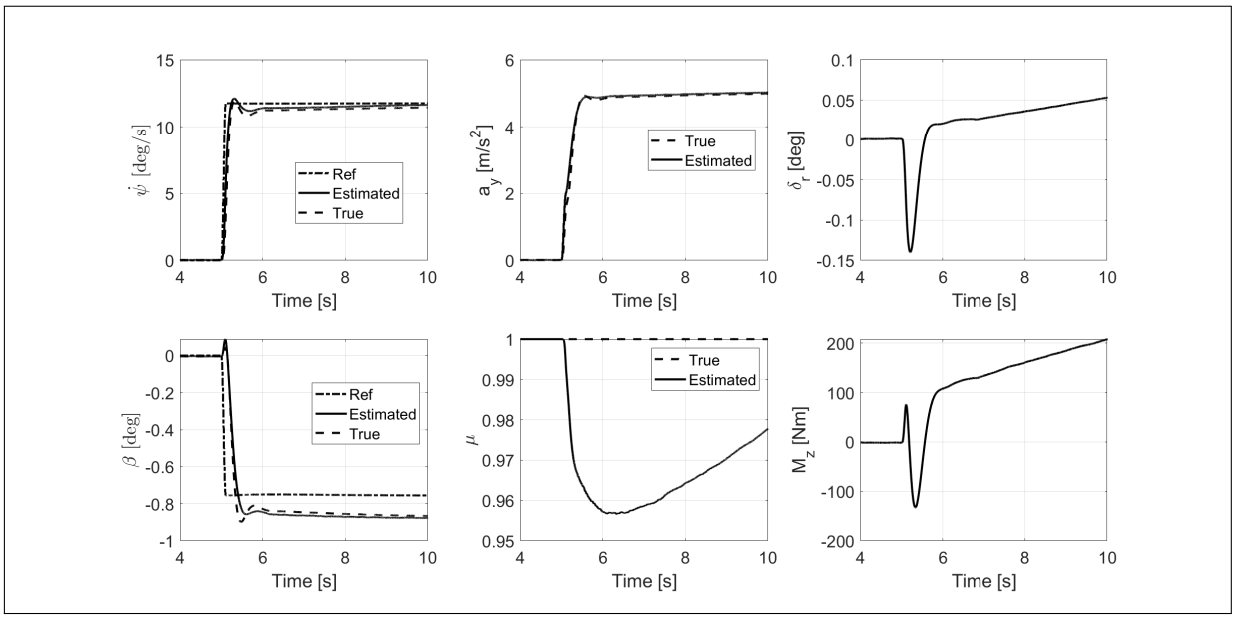

Figure 5.20: System response during high speed step steer maneuver with EKF added to the loop.

5.5. Comparison with an existing controller

In this section, we compare the integral terminal sliding mode controller (with EKF) with another controller from the literature. We choose the sliding mode controller presented in [12]. The authors used yaw rate and sideslip angle error as the two sliding surfaces

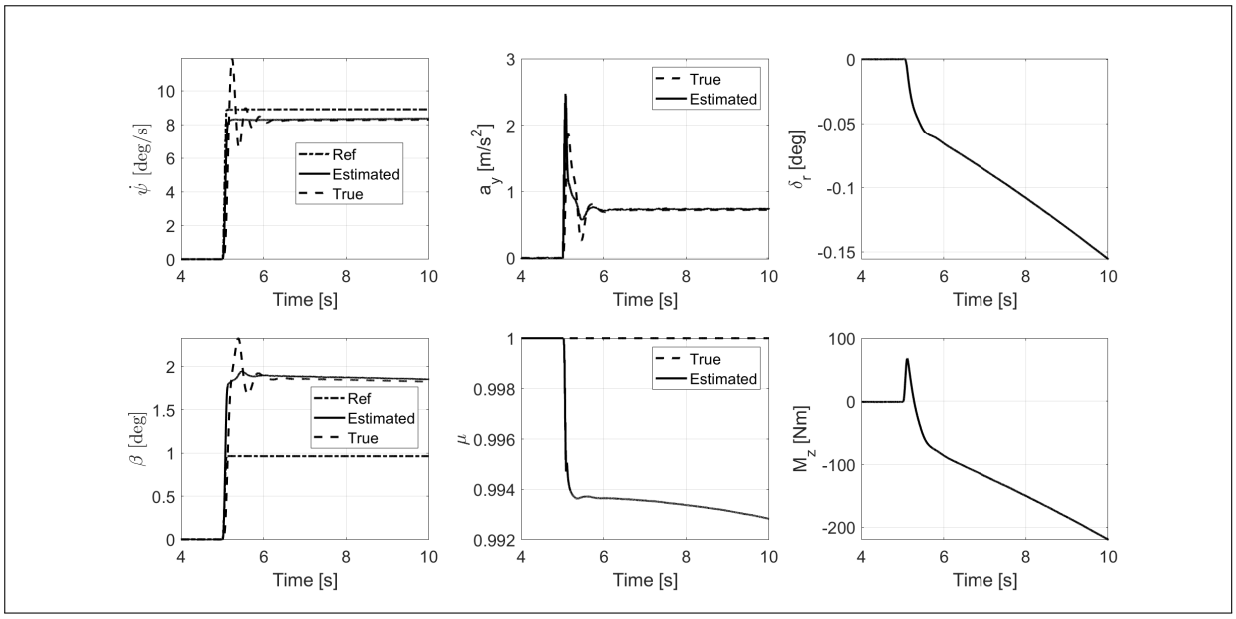

Figure 5.21: System response during low speed step steer maneuver with EKF added to the loop.

and derived the control law. In the paper, the control law is derived while accounting for parametric uncertainty and modelling imprecision of a prototype vehicle. In this thesis work, the controller works with a virtual vehicle whose relevant parameters are precisely known. Thus, we do not follow the exact approach used in [12].

The major difference between the two controllers is the choice of sliding surfaces. We implement the approach in [12] by switching off the integral terms of the ITSMC with EKF and re-tuning the controller parameters such that the vehicle response to the steering input is smooth, especially at high speed. The tracking performance of the two controllers is then compared by performing steady state and transient maneuvers with VI-CRT model. The maneuver details are same as those used in the previous sections. Here, we compare only the true and the reference vehicle states ($\dot{\psi},\ \beta$) and the actuator inputs ($\delta_r,\ M_z$).

The system response and actuator inputs during the high speed ramp steer maneuver are presented in Figure 5.22. We can observe that the two controllers generate similar yaw rate response. The controller from literature without integral terms generates higher magnitude of sideslip angle as compared to the ITSMC with EKF. The actuator inputs required by the existing controller is also lower than the ITSMC even if high controller gains are used for the controller from literature. Any further increase in gains would cause undesired oscillations in the system response for high steering inputs at high vehicle speed.

The results for low speed ramp steer maneuver are presented in Figure 5.23. Here, the

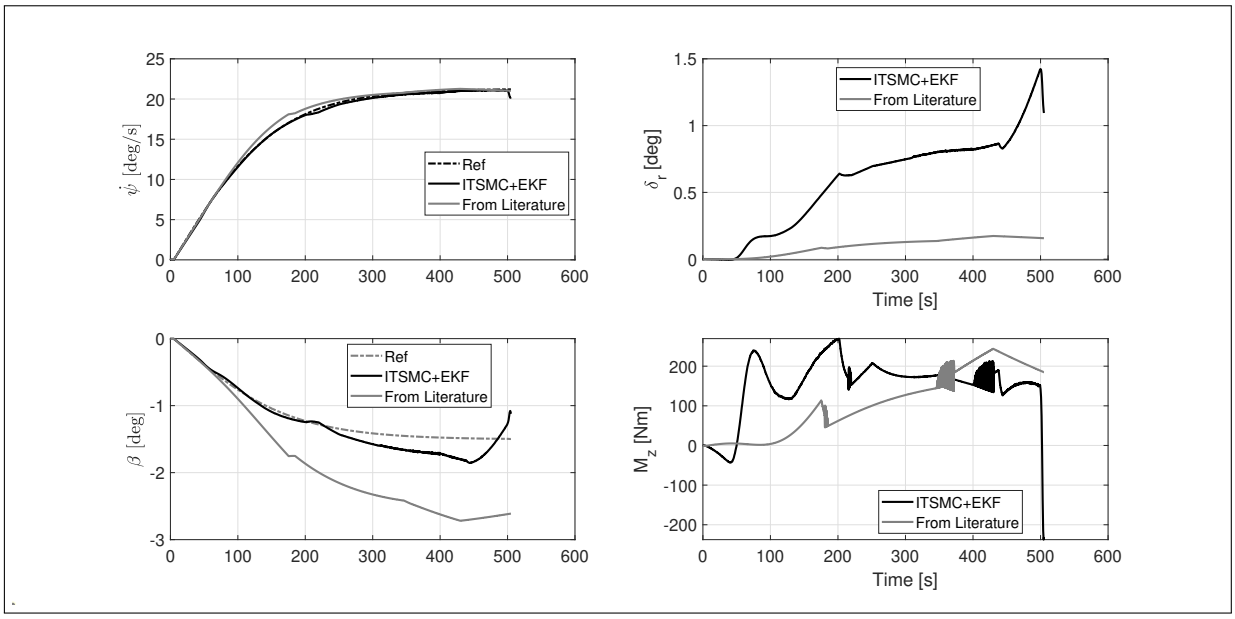

Figure 5.22: Comparison between a controller from literature and ITSMC with EKF for high speed ramp steer maneuver.

controller from literature generates lower yaw rate and higher sideslip angle for same steering input. Thus, performing worse than the ITSMC (with EKF) developed in this thesis. The actuator inputs required by the existing controller are much lower as compared to ITSMC which contributes to poorer tracking performance. As mentioned before, any attempts to increase the actuator inputs would result in oscillations in the system response for high steering inputs during the high speed ramp steer maneuver.

The close loop CRC maneuver results are presented in Figure 5.24. For CRC manuever, the driver is able to negotiate the curve with both the controllers. Similar to previous maneuvers, the sideslip angle performance of the controller from literature is slightly worse than the ITSMC with EKF.

The results for step steer maneuver performed at high and low vehicle speed are presented in Figures 5.25 and 5.26 respectively. During both the maneuvers, the controller without integral terms generates marginally lower yaw rate response as compared to the ITSMC with EKF. The ITSMC with EKF generates marginally higher magnitude of β as compared to the existing controller. The actuator inputs for the controller with ITSMC do not achieve steady state value whereas the inputs for controller without the integral term seem to achieve a steady state value. Thus, the ITSMC with EKF would eventually converge to the reference values whereas the controller from the literature may not.

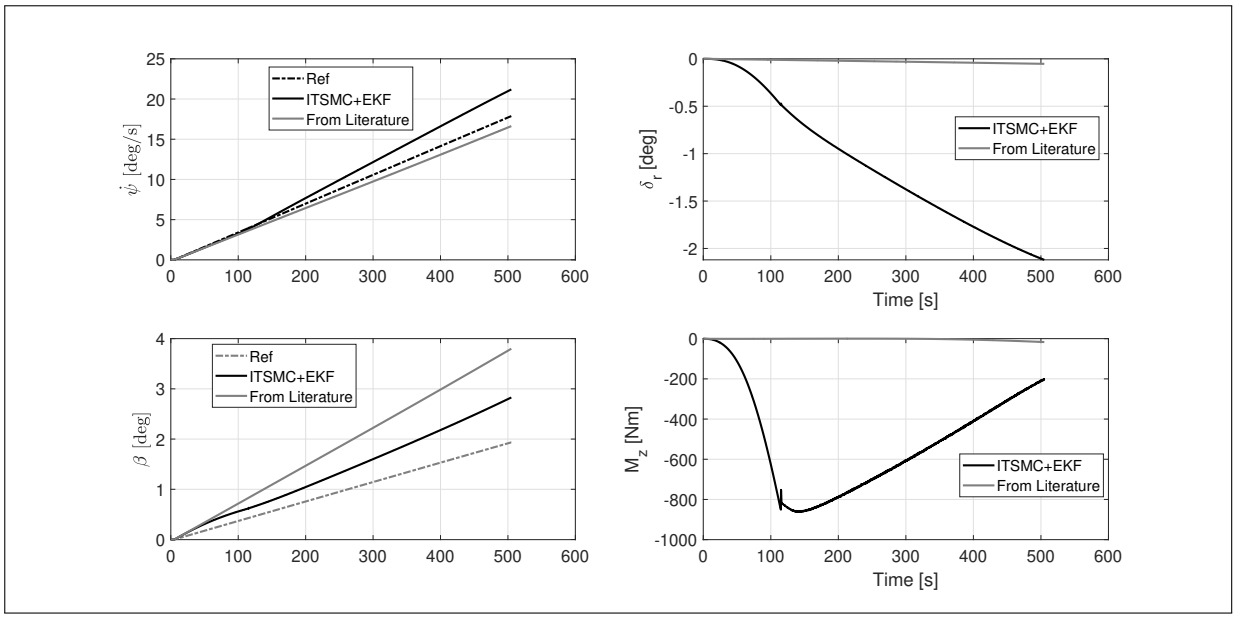

Figure 5.23: Comparison between a controller from literature and ITSMC with EKF for low speed ramp steer maneuver.

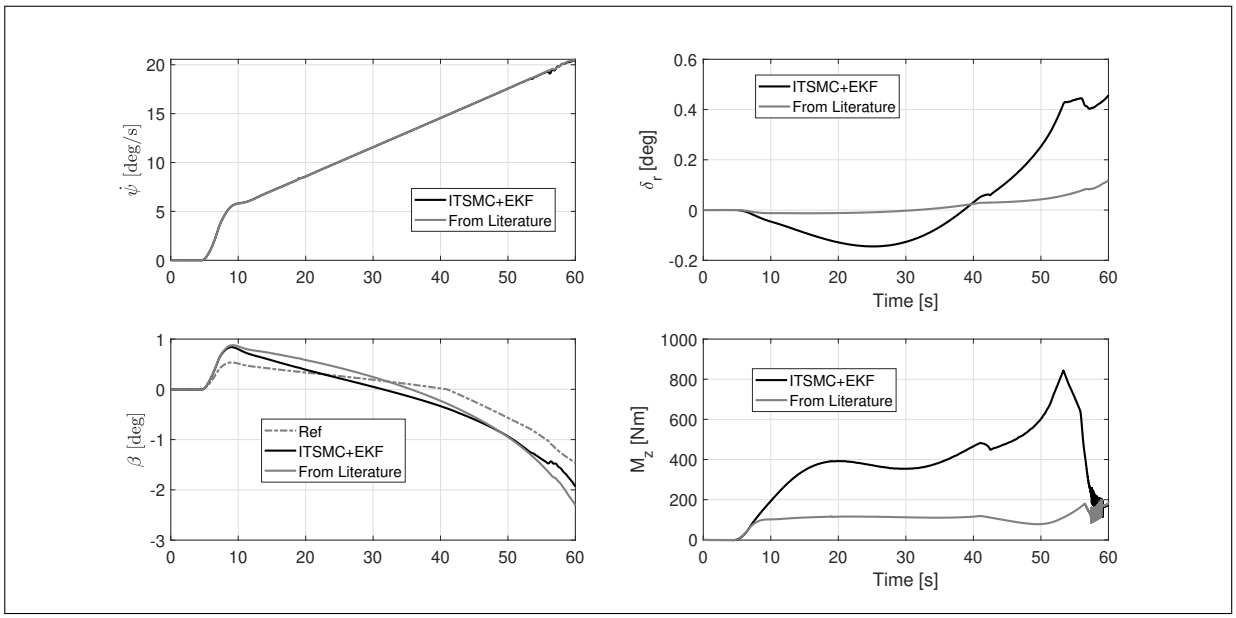

Figure 5.24: Comparison between a controller from literature and ITSMC with EKF for CRC maneuver.

5.6. Conclusion

The feedforward and the integral terminal sliding mode controller (ITSMC) are tested using the VI-CRT model by simulating steady state and transient maneuvers. The feedforward controller can not track the reference signals due to saturation of IWMs. With

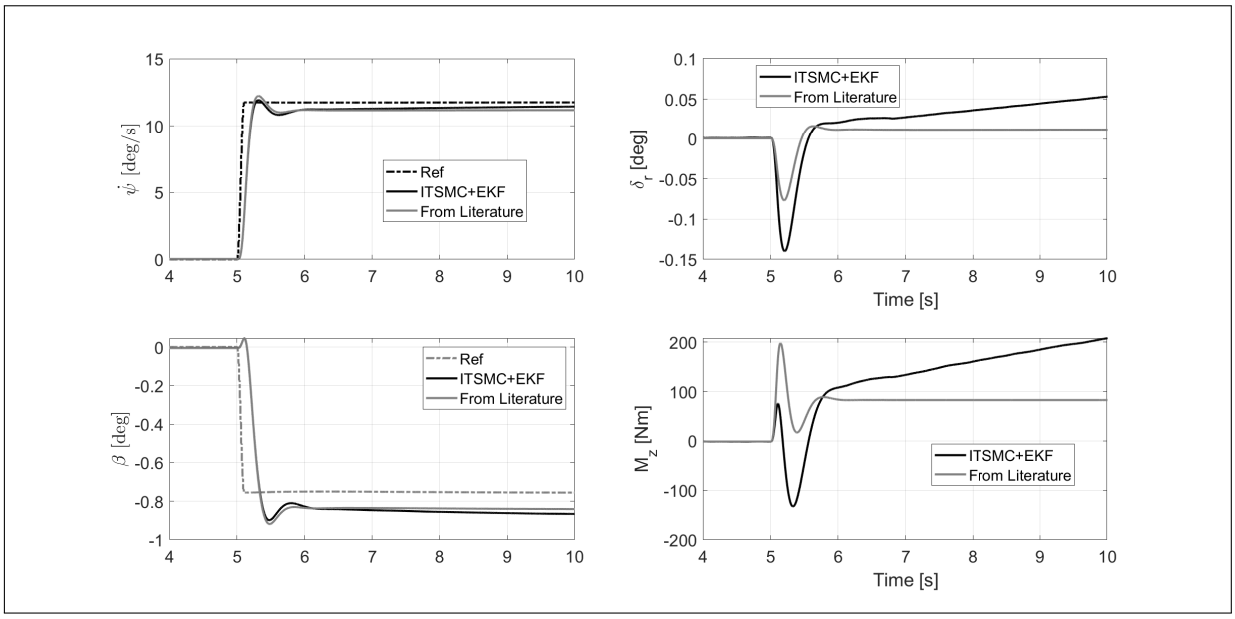

Figure 5.25: Comparison between a controller from literature and ITSMC with EKF for high speed step steer maneuver.

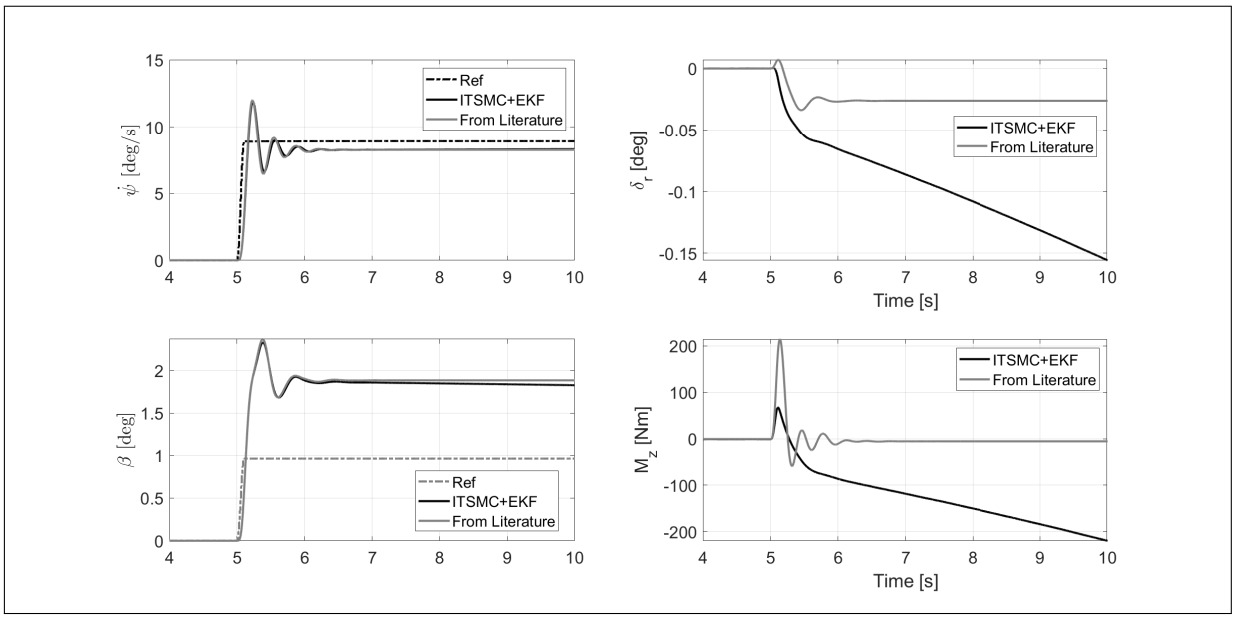

Figure 5.26: Comparison between a controller from literature and ITSMC with EKF for low speed step steer maneuver.

proper tuning of the parameters, ITSMC is able to track the reference yaw rate and achieve a 10% improvement without excessively increasing the magnitude of vehicle sideslip angle.

The controller with extended Kalman filter (EKF) as the observer has been implemented and tested using steady state and transient maneuvers performed with the VI-CRT model.

The controller with EKF is able to reduce the error between estimated and reference value. There can be significant estimation error during extremely low lateral accelerations maneuvers. The vehicle response in this case is smooth and may not require abrupt steering inputs by the driver.

The estimation errors are reasonably lower for moderate and high lateral acceleration and the controller with EKF responds similar to the one without EKF. At extremely high lateral acceleration (near the friction limit), some estimation error in β can be observed. However, this does not affect the controller's yaw rate tracking performance.

The ITSMC with EKF is also compared with a controller from literature. The controller from literature is also a sliding mode controller which does not have any integral terms in the definition of its sliding surfaces. The comparison of system response during all the maneuvers indicate that the ITSMC with EKF performed similarly or better than the controller from literature. The actuator inputs for the controller from literature are much lower as compared to those required by the ITSMC with EKF even with higher controller gains.

6 | Conclusions and future developments

In this thesis, a multi-input multi-output (MIMO) controller for improving vehicle lateral dynamics has been developed. The controller uses rear steering and torque vectoring as active systems. A linearized single track model has been derived for the vehicle with active rear steering (ARS) and torque vectoring (TV). Using the relevant parameters of the chosen VI-CarRealTime (VI-CRT) model, the effect of rear-to-front steering ratio and yaw moment on vehicle lateral dynamics is studied. From step response and frequency response functions, we can conclude that a suitable combination of ARS and TV is necessary to improve yaw rate while reducing vehicle sideslip angle.

Following this, two controllers are developed to improve vehicle lateral dynamics: a feed-forward controller and an integral terminal sliding mode controller. The controllers are derived and tested using open loop step steer maneuvers performed with the linearized single track model. The effect of reference sideslip angle (β_r) on the actuator inputs is also investigated. The actuator inputs when $\beta_r = 0$ are significantly higher when compared to β_r closer to the passive one. This observation can be helpful in setting reference values that are suitable for the sizing of available actuators.

The sliding mode controller is developed using integral terminal sliding surfaces. The controller is designed to be non-singular and is able to track the reference yaw rate and sideslip angle signals in real time. The sliding mode controller requires appropriate tuning of a large number of parameters.

A new method for generating yaw rate and sideslip angle reference signals is also explored. This method uses a logistic function fitted to the passive vehicle data. The parameters of the fitted function are then scaled to generate the reference signals. This ensures that reference signals are smooth and also account for the friction limit.

The two controllers are then tested by performing steady-state and transient maneuvers using the more realistic `CityCar_FullElectric` model of VI-CarRealTime software. The experimentation with VI-CRT model indicates that TV actuators (IWMs) are undersized.

This proves to be a major challenge for the feedforward controller. Due to IWM saturation, the feedforward controller is not able to track the reference yaw rate and can only track the reference sideslip angle. The integral terminal sliding mode controller (ITSMC), being a feedback controller, can track the reference yaw rate while achieving less than desired improvement on sideslip angle. The ITSMC prioritises yaw rate tracking due to particular tuning of controller parameters.

The ITSMC relies on real-time knowledge of sideslip angle value. Actually, sensors for measuring sideslip angle are too expensive and cannot be fitted in commercial vehicles. Thus, we use extended Kalman filter (EKF) as the state estimator to estimate vehicle sideslip angle using the data from available on-board sensors. The state vector is augmented to also include the friction coefficient. The EKF is able to estimate sideslip angle with reasonable accuracy for moderate to high lateral accelerations in real time. The filter convergence is found to be poor for low lateral accelerations where friction coefficient is non-observable. The ITSMC is tested with extended Kalman filter (EKF) added to the control loop. During transient maneuvers, a reduction in overshoots in both yaw rate and sideslip angle response can be noticed when simulating with EKF added to the control loop.

The ITSMC with EKF is then compared with another sliding mode controller from literature, which does not use integral terminal terms in sliding surface definition. The ITSMC tracked yaw rate better than the existing controller and also resulted in better sideslip angle response as compared to the existing controller.

6.1. Future developments

In this thesis work, the lower level controller allocating motor torques for the generation of yaw moment through torque vectoring (TV) follows a simple algorithm. This affects vehicle performance during high lateral acceleration maneuvers which are close to the friction limit. A more sophisticated controller which also takes the advantage of brake torque vectoring may further improve lateral dynamics near the friction limit.

During simulations with sliding mode controller, we had to remove the feedforward type part of the controller input in order to generate smoother vehicle response during steady state maneuvers. Here, the feedforward part relies on the linearised single track model. A more sophisticated approach could be used to generate the feedforward part using the nonlinear tyre force curve. This would reduce tuning efforts for the sliding mode controller as the major contribution for the calculation of controller inputs will come from the feedforward part.

Bibliography

[1] Wong J. Y. *Theory of ground vehicles / J. Y. Wong*. Wiley, Hoboken, 4. ed edition, 2008. ISBN 978-04-7017-038-0.

[2] Michele Vignati, Edoardo Sabbioni, and Federico Cheli. A torque vectoring control for enhancing vehicle performance in drifting. *Electronics*, 7(12), 2018. ISSN 2079-9292. doi: 10.3390/electronics7120394. URL https://www.mdpi.com/2079-9292/7/12/394.

[3] S Hegazy, H Rahnejat, and K Hussain. Multi-body dynamics in full-vehicle handling analysis. *Proceedings of the Institution of Mechanical Engineers, Part K: Journal of Multi-body Dynamics*, 213(1):19–31, 1999. doi: 10.1243/1464419991544027. URL https://doi.org/10.1243/1464419991544027.

[4] Dieter Schramm, Manfred Hiller, and Roberto Bardini. *Single Track Models*, pages 223–253. Springer Berlin Heidelberg, Berlin, Heidelberg, 2014. ISBN 978-3-540-36045-2. doi: 10.1007/978-3-540-36045-2_10. URL https://doi.org/10.1007/978-3-540-36045-2_10.

[5] Hans B. Pacejka. Chapter 1 - Tire Characteristics and Vehicle Handling and Stability. In Hans B. Pacejka, editor, *Tire and Vehicle Dynamics (Third Edition)*, pages 1–58. Butterworth-Heinemann, Oxford, third edition edition, 2012. ISBN 978-0-08-097016-5. doi: https://doi.org/10.1016/B978-0-08-097016-5.00001-2. URL https://www.sciencedirect.com/science/article/pii/B9780080970165000012.

[6] HB Pacejka and IJM Besselink. Magic formula tyre model with transient properties. *Vehicle system dynamics*, 27(S1):234–249, 1997.

[7] VI-grade GmbH. VI-CarRealTime 20.0. https://www.vi-grade.com/en/products/vi-carrealtime/.

[8] Shoichi Sano, Yoshimi Furukawa, and Shuji Shiraishi. Four wheel steering system with rear wheel steer angle controlled as a function of sterring wheel angle. *SAE Transactions*, 95:880–893, 1986. ISSN 0096736X, 25771531. URL http://www.jstor.org/stable/44725442.

[9] Edoardo Sabbioni and Michele Vignati. Torque vectoring control for different powertrain layouts of hybrid and electric vehicles. In *13th International Symposium on Advanced Vehicle Control (AVEC'16)*, pages 637–641. Taylor & Francis Group, 2016.

[10] Michele Vignati, Edoardo Sabbioni, and Davide Tarsitano. Torque vectoring control for iwm vehicles. *International Journal of Vehicle Performance*, 2(3):302–324, 2016.

[11] Heide Brandtstädter. *Sliding Mode Control of Electromechanical Systems*. Dissertation, Technische Universität München, München, 2009.

[12] Josef Zehetner and Martin Horn. Vehicle dynamics control with torque vectoring and active rear steering using sliding mode control. *IFAC Proceedings Volumes*, 40 (10):1–8, 2007.

[13] Vadim Utkin and Hoon Lee. Chattering problem in sliding mode control systems. In *International Workshop on Variable Structure Systems, 2006. VSS'06.*, pages 346–350. IEEE, 2006.

[14] Masato Abe. Vehicle dynamics and control for improving handling and active safety: from four-wheel steering to direct yaw moment control. *Proceedings of the Institution of Mechanical Engineers, Part K: Journal of Multi-body Dynamics*, 213(2):87–101, 1999.

[15] Leonardo De Novellis, Aldo Sorniotti, Patrick Gruber, and Andrew Pennycott. Comparison of feedback control techniques for torque-vectoring control of fully electric vehicles. *IEEE Transactions on Vehicular Technology*, 63(8):3612–3623, 2014.

[16] Suvansh Kasliwal. Development of active rear wheel steering and evaluation of steering feel. Master's thesis, KTH, Vehicle design, 2019.

[17] Lorenzo Tarsitano. Over-steering lateral dynamics control of an over-actuated vehicle. Master's thesis, Politecnico Di Milano, Ground Vehicles, 2018.

[18] Bin Li, Subhash Rakheja, and Ying Feng. Enhancement of vehicle stability through integration of direct yaw moment and active rear steering. *Proceedings of the Institution of Mechanical Engineers, Part D: Journal of Automobile Engineering*, 230(6): 830–840, 2016.

[19] Minh-Duc Tran and Hee-Jun Kang. Nonsingular terminal sliding mode control of uncertain second-order nonlinear systems. *Mathematical Problems in Engineering*, 2015, 2015.

[20] Liheng Shi, Hai Wang, Yunzhi Huang, Xiaozheng Jin, and Shuanglong Yang. A novel

integral terminal sliding mode control of yaw stability for steer-by-wire vehicles. In *2018 37th Chinese Control Conference (CCC)*, pages 7787–7792. IEEE, 2018.

[21] Lei Qiao and Weidong Zhang. Trajectory tracking control of auvs via adaptive fast nonsingular integral terminal sliding mode control. *IEEE Transactions on Industrial Informatics*, 16(2):1248–1258, 2019.

[22] Michele Vignati. *Innovative control strategies for 4WD hybrid and electric control*. PhD thesis, Politecnico di Milano, Italy, 1 2017.

[23] S. M. Blower and H. Dowlatabadi. Sensitivity and uncertainty analysis of complex models of disease transmission: An hiv model, as an example. *International Statistical Review / Revue Internationale de Statistique*, 62(2):229–243, 1994. ISSN 03067734, 17515823. URL `http://www.jstor.org/stable/1403510`.

[24] Lei Qiao and Weidong Zhang. Trajectory tracking control of auvs via adaptive fast nonsingular integral terminal sliding mode control. *IEEE Transactions on Industrial Informatics*, 16(2):1248–1258, 2020. doi: 10.1109/TII.2019.2949007.

[25] Lowell Jacob Reed and Joseph Berkson. The application of the logistic function to experimental data. *The Journal of Physical Chemistry*, 33(5):760–779, 2002.

List of Figures

List of Tables

List of Symbols

Variable	Description	SI unit
m	Vehicle mass	kg
A_x	Inertial acceleration in the vehicle longitudinal direction	m/s^2
A_y	Inertial acceleration in the vehicle lateral direction	m/s^2
J_z	Yaw moment of inertia	$kg\,m^2$
l_f	Distance between centre of mass and front axle	m
l_r	Distance between centre of mass and rear axle	m
$\ddot{\psi}$	Inertial yaw acceleration	rad/s^2
F_{xf}	Total longitudinal force at the front axle	N
F_{yf}	Total lateral force at the front axle	N
F_{xr}	Total longitudinal force at the rear axle	N
F_{yr}	Total lateral force at the rear axle	N
δ_f	Average steering angles of the front wheels	rad
δ_r	Average steering angles of the rear wheels	rad
M_z	Yaw moment generated by Torque Vectoring (TV)	Nm
α_f	Lateral slip angle for front wheels	rad
α_r	Lateral slip angle for rear wheels	rad
V_{xf}	Longitudinal velocity of wheel hub at the front axle	m/s
V_{yf}	Lateral velocity of wheel hub at the front axle	m/s
V_{xr}	Longitudinal velocity of wheel hub at the rear axle	m/s
V_{yr}	Lateral velocity of wheel hub at the rear axle	m/s
V_x	Longitudinal velocity of the vehicle centre of mass	m/s
V_y	Lateral velocity of the vehicle centre of mass	m/s
V	Vehicle speed	m/s
$\dot{\psi}$	Yaw rate of the vehicle	rad/s
β	Sideslip angle of the vehicle	rad

K_f	Cornering stiffness for the front axle	N/rad
K_r	Cornering stiffness for the rear axle	N/rad
$\vec{V}_G$	Velocity vector of the centre of mass in the moving reference system	m/s
$\vec{A}_G$	Acceleration vector of the centre of mass in the moving reference system	m/s^2
K_w	Rear to front wheel steering ratio	$-$
l	Wheel base of the vehicle	$[m]$
c_f	Front track width	$[m]$
c_r	Rear track width	$[m]$
μ	Coefficient of friction	$[-]$
g	Acceleration due to gravity	$[m/s^2]$

Acknowledgements

I am extremely grateful to Prof. Michele Vignati for giving me the opportunity to work on this beautiful and challenging problem. His suggestions and guidance have been extremely helpful throughout the course of this project. Discussion with him always helped in solving the problem at hand and deciding the direction for the thesis work. He always explained things patiently which was big help at times. I would like to thank Prof. Edoardo Sabbioni for his valuable inputs and supervision during the discussions. Finally, I would like to thank Ing. Michele Asperti. He cleared my initial doubts regarding modelling. He also helped in implementation and analysis of sliding mode controller for the vehicle dynamics model. Ing. Asperti provided valuable feedback on the thesis draft and helped in refining the text.

I would like to thank my parents and my sister for their unconditional support throughout the work. Their love, support and encouragement during the thesis was extremely helpful in successfully completing the work. I would like to extend my thanks to my friends Mangesh, Ganesh, Sumit, Giridhar, Ritesh, Akanksha for making my stay in Milan memorable. Their encouragement during the difficult times certainly helped.